ADDIS ABABA UNIVERSITY
SCHOOL OF GRADUATE STUDIES
SCHOOL OF EARTH SCIENCES

PETROGENETIC EVOLUTION OF THE MELKA WAKENA PYROCLASTIC DEPOSITS: IMPLICATIONS FOR THE DEPOSITIONAL HISTORY OF THE INTERCALATED VOLCANO-SEDIMENTARY ROCKS

BY
ANGESOM RESOM KIDANE

THESIS SUBMITTED TO THE SCHOOL OF EARTH SCIENCES OF THE ADDIS ABABA UNIVERSITY AS PARTIAL FULFILLMENT OF THE DEGREE OF MASTER OF SCIENCE IN GEOLOGICAL SCIENCES (PETROLOGY)

MAY, 2017
ADDIS ABABA

ADDIS ABABA UNIVERSITY
SCHOOL OF GRADUATE STUDIES
SCHOOL OF EARTH SCIENCES

PETROGENETIC EVOLUTION OF THE MELKA WAKENA PYROCLASTIC DEPOSITS: IMPLICATIONS TO THE DEPOSITIONAL HISTORY OF THE INTERCALATED VOLCANO-SEDIMENTARY ROCKS

By
Angesom Resom Kidane

Advisor: Prof. Asfawossen Asrat Kassaye

Thesis submitted to the School of Earth Sciences of the Addis Ababa University as partial fulfillment of the Degree of Master of Science in Geological Sciences (Petrology)

May, 2017
Addis Ababa

ADDIS ABABA UNIVERSITY
SCHOOL OF GRADUATE STUDIES
SCHOOL OF EARTH SCIENCES

PETROGENETIC EVOLUTION OF THE MELKA WAKENA PYROCLASTIC DEPOSITS: IMPLICATIONS TO THE DEPOSITIONAL HISTORY OF THE INTERCALATED VOLCANO-SEDIMENTARY ROCKS

By
Angesom Resom Kidane

Approved by Examining Committee:

Name	Position	Signature	Date
Dr. Balemwal Atnafu	**Head, SES**	_____	_____
Prof. Asfawossen Asrat	**Advisor**	_____	_____
Prof. Gezahegn Yirgu	**Examiner**	_____	_____
Prof. Dereje Ayalew	**Examiner**	_____	_____

May, 2017
Addis Ababa

Declaration of originality

I hereby declare that this is my original work prepared for the partial fulfillment of the Degree of Master of Science in the School of Earth Sciences, Addis Ababa University during 2017 under the supervision of Prof. Asfawossen Asrat Kassaye. In addition, I am assuring that this work is not presented and published anywhere else. All sources are well referenced and acknowledged.

	Signature	date
Angesom Resom Kidane	_____	_____

I hereby declare this is his original work as part of his Master of Science in Geological Sciences (Petrology).

	Signature	date
Prof. Asfawossen Asrat	_____	_____

ABSTRACT

The study area is located east of the Assasa town in the Arsi zone on the shoulder of the rift-plateau escarpment and close to the Gadeb archaeological sites. The main objective of the study was therefore to determine the petrogenetic evolution of the pyroclastic rocks using standard field (mapping and description), geochronological (stratigraphic logging, correlation and Ar-Ar dating of some selected samples), petrographic (thin section analysis) and geochemical (major and trace element geochemistry) methods, and constraining the depositional history of the intercalated volcano-clastic sediments in the area. A total of 26 samples were analyzed in this study: 9 for petrography, 13 for geochemistry and 4 for Ar-Ar dating. The pyroclastic rocks have been formed 1.617 to 0.696 Ma ago in a topographically complex area resulting in non-continuous and erratically distributed layers. They are generally of rhyolitic (the ignimbrite, ash fall and pumiceous ash units) and dacitic (the ash flow unit) composition. The geochemical characteristics and modeling suggest that the rhyolites were formed by fractional crystallization of basaltic magmas involving crustal input, while the dacites were formed by Assimilation Fractional crystallization followed by post depositional leaching of the mobile elements. The Melaka Wakena archaeological site was a geomorphologically active area during the Early to Middle Pleistocene where overbank sedimentary sequences (conglomerates and sands) formed by a big meandering river, dotted with possible temporary ponds and ox-bow lakes (depositing clays), have been covered by episodic volcanic eruptions and the products thereof. A dense network of channels and streams have been subsequently down cutting through the older volcanic and sedimentary sequences before the deposition of the younger volcanic and reworked volcaniclastic rocks. This episodic eruption of pyroclastic rocks on actively depositing and eroding sedimentary sequences containing cultural sequences allow constraining the age of the archaeological remains in the area as well as their depositional history.

Key words: **Melka Wakena, Petrogenetic evolution, Stratigraphy, Geochronology, Fractional Crystallization, Crustal contamination.**

ACKNOWLEDGMENTS

The Addis Ababa University and Aksum University are thanked for providing me the opportunity and necessary support to pursue my Masters studies. I am thankful to the "Melka Wakena Archaeological Survey Project" for allowing me to conduct my thesis in the project area.

I would like to express my deepest gratitude to Prof. Asfawossen Asrat for his endless support, starting from the pre-proposal formulation until the completion of the thesis. His scientific input and guidance, encouragement and moral support have been a great psychological boost for me to work hard and complete my thesis. I would also like to extend my gratitude to him for financially contributing and facilitating the geochronological and geochemical analysis of the samples. His critical reading and editing of the thesis has also contributed to the improvement of the thesis greatly. I have no enough words to express my gratitude.

I would also like to sincerely acknowledge Prof. Erella Hovers and Mr. Tegenu Gossa for their financial, material as well as moral support during the field season, for geochemical and geochronological analysis and throughout the progress of my thesis work.

In addition, I would like to thank my friends for their technical and material support and the people of Aluba village, my family and many more others for their unforgettable support.

TABLE OF CONTENTS

CHAPTER TWO

CHAPTER THREE

LIST OF FIGURES

LIST OF TABLES

LIST OF ACRONYMS

- ACs- Alder Creek Sanidine
- AFC- Assimilation fractional crystallization
- ALS- Australian laboratory Science
- ASS- Afar stratoid series
- ca- Circa age
- CIPW- Cross, Iddings, Pirrson and Washington
- CMER- Central Main Ethiopian Rift.
- DEM- Digital elevation model
- EAR- East African Rift
- EARS- East African Rift System
- EFB- Ethiopian flood basalt volcanism
- ESE- East South East
- ESE-WNW – East southeast – West northwest
- E-W- East west
- FC- Fractional Crystallization
- Fm- Formation
- GA- Gulf of Aden
- GCDKit- Geochemical data kit
- GGF- Gara Gumbi formation
- HT- High Titanium
- HT1- High Titanium one
- HT2- High Titanium two
- Ignimb- Ignimbrite
- ICP-MS81- Inductively coupled Plasma Mass spectrometry 81
- Km- Kilometer
- Kms - Kilometers
- LILE-Large ion lithophile elements
- LOI- Lose on Ignition
- LREE- Light rare earth elements
- LT- Low Titanium
- m- Meter
- ME-ICP06- Multi element inductively coupled plasma 06

- MER- Main Ethiopian Rift
- MEVD- Multi element variation diagram
- MSWD- Mean square weight deviation
- MW- Melka Wakena
- MW5N- Melka Wakena five north
- MW5-S- Melka Wakena five south
- MW7-S- Melka Wakena seven south
- MWNS- Melka Wakena new site
- MPx- Mega pixel
- NE- North east
- NE-SW – North east- South west
- NG- Nazreth Group
- NMER- Northern Main Ethiopian Rift
- NNE-SSW- North north east South south east
- N-S- North south
- NW- North west
- NW-SE- North west South east
- P- Primary magma
- PM- Partial melting
- PPL – Plane Polarized Light
- REE- Rare Earth Elements
- RS-Red Sea
- SA-NMERTZ- Southern Afar northern Main Ethiopian Rift transition zone
- SES- School of Earth Sciences
- SMER- Southern Main Ethiopian Rift
- SW- Southwest
- WFB- Wonji fault belt
- WGS- Wonji group silicics
- Wt%- Weight percent
- XPL- Cross polarized light
- YTVTL- Yerer- Tulu Welel volcano tectonic lineament

CHAPTER ONE

INTRODUCTION

1.1. Back ground

The project is conducted at the shoulder of the rift- plateau escarpment located at the Melka Wakena area, about 10 km east of the town of Assasa, in south central Ethiopia. "*Ecological perspectives on Hominin adaptation to highland environments in the Early Pleistocene: The case of the Melka-Wakena Acheulian site-complex, South-central Ethiopia"* Project, co-led by the supervisor of this Masters Thesis.

The main aim of this thesis work is to determine the petrogenetic evolution of the pyroclastic deposits constituting the archaeological site. In addition, geochronological and geochemical data on the volcanic sequences will help to constrain the depositional history of the intercalated volcano-sedimentary rocks containing cultural sequences (archaeological remains). Large igneous provinces are related to the composite effect of the continental break up and rising of hot mantle plume head (George at al., 1998). Ethiopian bimodal volcanic province is one of the youngest provinces related to the opening of the red sea and Gulf of Aden during 30Ma linked to the thermal influence of Afar mantle plume (Hoffmann et al., 1997; George et al., 1998; Dereje Ayalew et al., 2002; Kieffer et al., 2004; Kurkura Kabeto, 2010). Fissural flood basalt volcanics are transitional to theolitic composition (Mohr, 1983) in the northern Ethiopian and Somalian plateaus whereas the shield volcanoes are alkaline (Eberz et al., 1988; Tadiwos Chernet et al., 1998). These shield volcanoes are found on top of the plateau volcanics and erupted with in the 30Ma-10Ma time range (Kieffer et al., 2004).

The 1000km wide (Giday WoldeGabriel et al., 1990; Wolfenden et al., 2004) western and eastern Ethiopian plateaus are separated by 80 km wide (Mhor, 1983) Main Ethiopian Rift (Corti, 2009).The development of the Main Ethiopian Rift (MER) within the plateau after the eruption of voluminous flood basalt eruption is coherent with the thermal /mantle plume dynamics at or near the base of the lithosphere (Pik et al., 2006). The Main Ethiopian Rift (MER) (figure 1.1) is the key sector of East African Rift System (EARS) Connected with Red Sea Rift (RSR) and Gulf of Aden Rift (GAR) in the north and Kenyan Rift in the south (Corti, 2009). It is classified in to Northern (NMER), Central

(CMER) and Southern (SMER) based on morphology of the rift segments (Giday WoldeGabriel et al., 1990; Bonini et al., 2005; Kurz et al., 2007; Keranen and Klemperer., 2008; Corti, 2009). These different sectors reflect different stages of extension, fault architecture, timing of volcanism, deformation and lithospheric structures (Hayward and Ebinger, 1996).

SMER shows north ward propagation up to Goba Bonga transverse lineament whereas the northern sector of the rift start to develop by 11 Ma and propagates south ward until the BoruTura structural high (Bonini et al., 2005; Tsegaye Abebe et al., 2010). In the case of the CMER it was initiated at 9.7-8.3 Ma ago with significant rifting at 5-3 Ma ago and with the eruption of voluminous silicic eruptions and reactivation of SMER as the function of the counter clockwise rotation of the Somalian plate (Bonini et al., 2005). Moreover, the rift floor and adjacent escarpments are covered with plio-Pleistocene pyroclastics (Kazmin and Seife Michael Berhe, 1981; Gidey WoldeGabriel et al., 1990) intercalated with sedimentary sequences (Eberz et al., 1988).

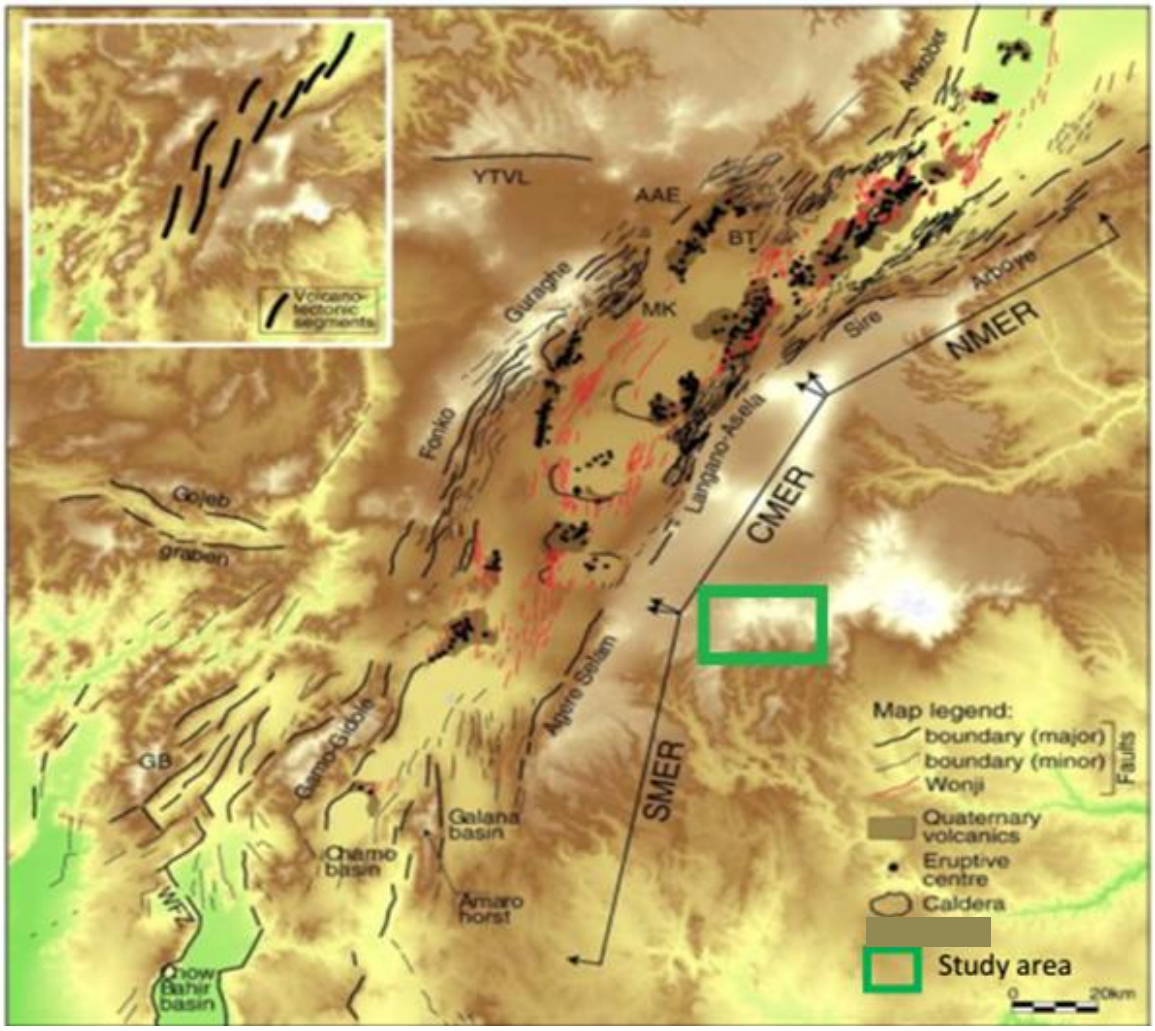

Figure 1.1. *Tectonic sketch map of the Main Ethiopian Rift (from Corti, 2009). Inset shows the en-echelon, right-stepping arrangement of the volcano-tectonic segments of the Wonji Fault Belt. AAE: Addis Ababa Embayment; BT: Boru Toru structural high; MK: Midre Kebd structural high; WFZ: Woito fault zone; YTVL: Yerer–Tullu Wellel volcano-tectonic lineament; GB: Gamo basalts. The black lines are major and minor boundary faults whereas the red lines are Wonji faults.*

1.2. Geographic Setting of the Study Area

The overall geographic characteristics of the study area and its surroundings is described below based on actual data collected in the field and data from previous works of Workineh Haro et al. (2014).

1.2.1. Location and Accessibility

The study area is located in the western Arsi Zone of Oromiya Regional state, Ethiopia near Asasa town which is the administrative center of Gadeb Asasa Woreda. It is particularly found at the eastern side of the Assela– Assasa- Dodola road (Figure 1.2). The study area is found at the average elevation of 2337m ranging between 2320 in the gorge to 2355 m above mean sea level in the flat land. The study area is easily accessible along dry-weather gravel roads and on foot.

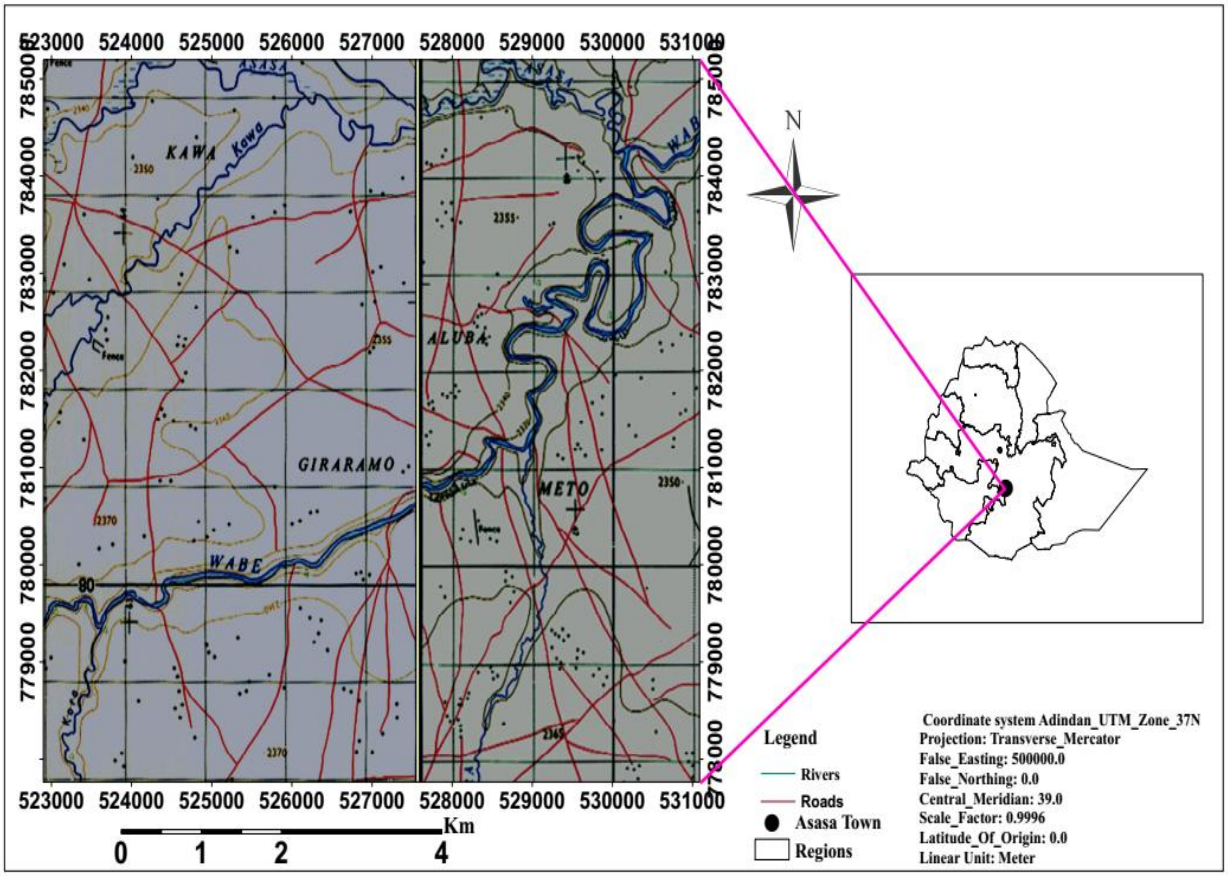

Figure 1.2. *Location map of the study area*

1.2.2. Physiographic and Drainage Characteristics

1.2.2.1.Physiography

The South eastern plateau is characterized by plateaus, high lands with mountain peaks, rugged terrains and low lands towards the east. The plateau starts from the rift escarpments and extends to Sagure, Bokoji, near Asasa and Melka Wakena areas. In addition it underlies the Arsi Robie, Adele, Bele and Seru areas. On the other hand,

mount Chilalo, Kaka, Bale and Galema range are considered as high lands with mountain peaks. In the Melka Wakena area Wabi River and its tributaries also dissect the terrain exposing a succession of volcanic and in its downstream sections sedimentary rocks, generally forming a rugged terrain. Moreover, low lands with flat surfaces are found in the north east of the area, where the Wabi River had eroded the overlying volcanic rocks forming flat terrains with minor volcanic remnants.

1.2.2.2. Drainage

The major river in the study area is Wabi Shebelle. This perennial river flowing to the east drains almost all the area. Other major rivers in the area include Robe, Elele and Hulul. Robe and Elele are tributaries of the Wabi River. Downstream of the MelkaWakena dam, Wabi River cut and flows in deep gorges. To the east of Wabi and its tributaries, the river wearied away the basalts of the region and exposed the Upper Sandstone and Upper Limestone. The upper course of the Wabi was dammed at Melka Wakena for the hydro-electric power generation. On the plateau, rivers flow in shallow wide valleys. The drainage type in these areas is dendritic to sub parallel. Drainages around the central volcanoes, like Kaka and on the Bale Mountain National Park form radial patterns. Drainage densities are high and intricate in such areas, but on the plateau of Bale drainages are scarce. Wabi Shebelle River drains to the SE crossing Somalia to Indian Ocean and exposes many of the sedimentary rocks in southeastern Ethiopia.

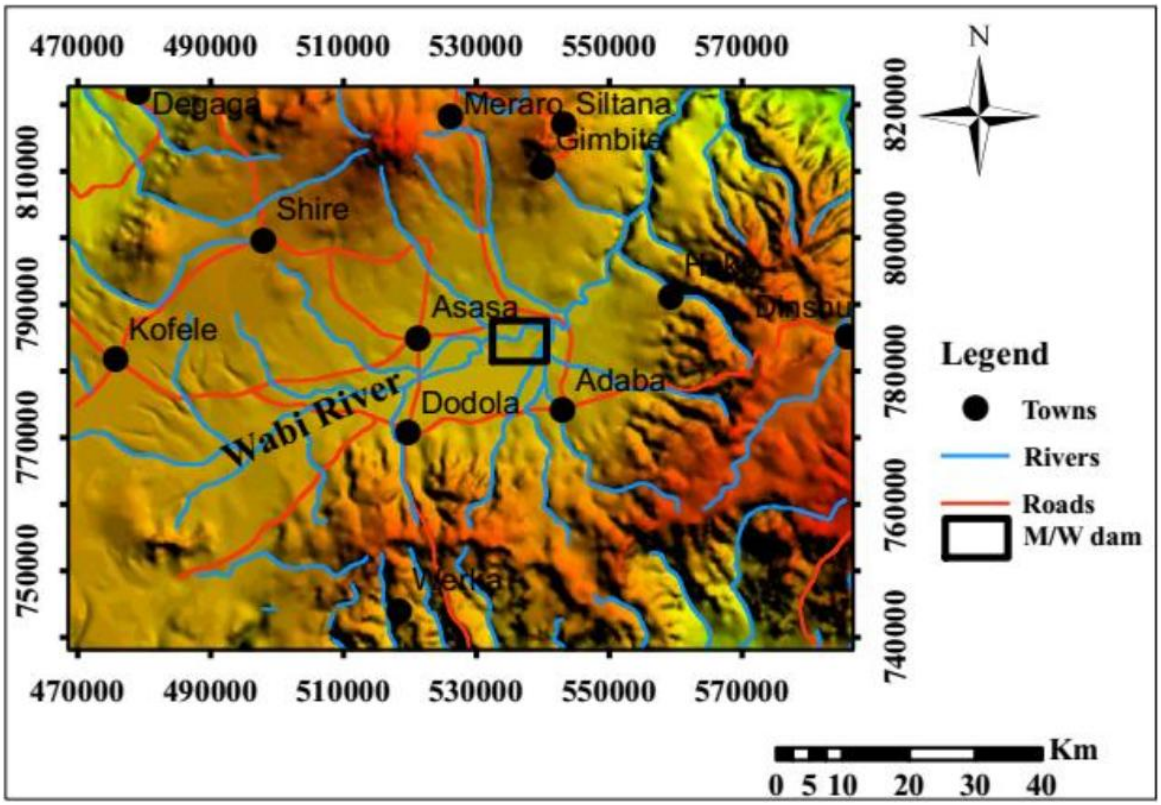

Figure 1.3. *Physiographic and drainage map of the study area; M/W dam refers for the Melka Wakena electric power generating dam.*

1.2.3. Climate and Vegetation

1.2.3.1. Climate

Tropical climatic condition prevails in the area with bi-modal rainfall season (the April to May is *Belg* and the June to September is *Kiremt* rain). The second major rainy season is summer. This begins in June and continues to September. The mean annual rainfall on the highland in the MelkaWakena area is relatively high (650ml) basically ranging 600-700ml. However, it can be lower in the northeastern parts along the Wabi Shebelle River gorge. The temperature in the Valley of Wabi Shebelle River is very hot and decreases in the mountains of Chilalo, Kaka, Galema and Dinsho with the annual temperature ranges 15-20^{0}C.

1.2.3.2.Vegetation

Vegetation and its distribution in the area vary with altitude, soil type and humidity and/or precipitation. Accordingly, there are areas of forest, woodland and savanna region.

Woodlands are common in the mid slopes of Bale Mountain National Park, the Galema mid slopes, Kaka and Chilalo Mountain. Forest cover mostly occurs along the middle Wabi River valley and its tributaries. The savanna region occurs along the lower course of Wabi. The plateau is mostly covered with grass land and scarce quarcetum mixtum vegetation. Afro-Alpine vegetation, partly savanna and grassland occurs on the summits of high rising mountains of Kaka, Chilalo and Galema whereas Bale is characterized by Afro and sub Afro-Alpine vegetation in areas above 3000m altitude, with mean annual temperature of less than 10ºc and average annual precipitation of 800 to 1600mm. Moreover, the savanna vegetation regions occur at altitudes ranging from 400 to 2000m above sea level with rainfall of 250 to 1300mm. On the other hand, the altitude range of 2300 to 3100m characterizes coniferous forest region with mean annual rainfall varying from 500 to1100mm.

1.2.4. Population and Settlement

The study area is mostly inhabited by Oromo nationalities speaking Afan Oromo language. They are mostly Muslims but some are Christians. Different ethnic groups live in the town. The rural area is unevenly distributed, primarily due to the differences in the suitability of environmental conditions for settlement and also due to socio-economic factors. Among the major environmental factors that influence population distribution in the area is the terrain characteristics (relief), and the suitability of the land for farming and livestock and pack animal breeding. Most of the people of the area live in the highlands and on the plateau suitable for farming and domestic animal breeding. They engage in agricultural practices cultivating different kinds of crops such as wheat, barley, teff, maize and sorghum. In addition, most of the rural dwellers engage also in breeding of domestic animals. Cattle, sheep and goat are common. Horses, mules and donkeys are also breed.

Lowland inhabitants live in scattered villages and are semi-pastoralists. Density of the population is rather scarce on the lowlands and highlands. Population density is higher on the plateau areas. The 2007 national census for Gadeb Asasa Woreda reported a total population of 186,907 of whom 92,471 were men and 94,436 were women; 20,667 or 11.06% of its population were urban dwellers. The majority of the inhabitants were Muslim, (80.68% of the population), while 17.89% of the population practiced Ethiopian Orthodox Christianity, and 1.31% of the population practiced Protestantism. With an

estimated area of 1,139.38 square kilometers, Gadeb – Asasa Woreda has an estimated population density of 149.2 people per square kilometer. The two largest ethnic groups reported in Gadeb are the Oromo (93.69%), and the Amhara (4.6%); all other ethnic groups made up 1.11% of the population. Oromiffa is spoken as a first language by 93.03%, and 6.51% speak Amharic; the remaining 0.46% speak all other primary languages

1.3. Statement of the Problem

This study investigates the pyroclastic deposits in the Melka Wakena area in terms of their petrogenetic evolution as well as their timing of deposition. These pyroclastic deposits are intercalated with cultural sequences within volcano-clastic and fluviatile sediments, which are currently under active archaeological investigation, allowing constraining the timing of deposition of the later. On the other hand, various petrological and geochemical studies in the region suggested that silicic volcanic rocks from the rift margin as well as the rift centers and adjacent plateaus are generated from fractional crystallization of basaltic magmas and variable degrees of crustal contaminations (e.g. Gasparon et al., 1993; Tadiwos Chernet and Hart, 1999; Peccerillo et al., 2003; 2007; Dereje Ayalew et al., 2006; Kurkura Kabeto et al., 2009; 2010; Rooney et al., 2012; Giordano et al., 2014). In contrast, Trua et al. (1999) and Deniel (2000) stated that the Asela–Ziway- pantellerite ignimbrite is formed from small degree partial melting of lower crust (10%) followed by low pressure fractionation (40%) of mostly Na-plagioclase. In the current study, the pyroclastic deposits in the Melka Wakena area are investigated in the context of their petrogenetic evolution in order to provide more field (stratigraphic), geochronologic, petrologic and geochemical data and interpretations, which will contribute to the larger discussion on evolution and petrogenetic modeling of these rocks.

1.4. Research Objectives

1.4.2. General objectives

The major objective of this study is investigating the petrogenetic evolution of the pyroclastic deposits in the Melka Wakena area using petrology and geochemistry approach as well as detailed field mapping, stratigraphic reconstruction, correlation and

determines using some Ar-Ar geochronologic data and investigating the depositional history of the intercalated volcano-clastic sediments.

1.4.3. Specific Objectives

The specific objectives of this research are

- To produce geological map and description of the area;
- To construct detailed stratigraphic logs of the localities in the study area and correlating them to develop composite stratigraphy of the area;
- To conduct petrological as well as geochemical analysis (thin section, major and trace element geochemistry);
- To determine age of the pyroclastic deposits
- To constrain the depositional history of the intercalated volcano-clastic sediments in the area.

1.5. Materials and Research Methodology

To achieve the objectives of the work the following methods were used. The research methodology focuses on collection of primary as well as secondary data, sample analysis, data synthesis and interpretation. The research was conducted in three stages: desk study, field work and post fieldwork. The desk study (pre-field work activities) required field planning and base map preparation, identification of resources relevant for the proposed study and secondary data collection. Following the initial stage, understanding of the methodology; literature survey and systematization of the results and, findings of previous research works in order to define the theoretical framework of the research work; and selecting analytical techniques for the research work have been conducted. In addition, practice on the softwares mentioned above was conducted. Appropriate traverses for field investigation were also selected before the actual fieldwork on the mosaic topographic map of the Asasa and Adaba sheets. The actual fieldwork was conducted during three field seasons: the first season (December 13-20/ 2016) for general appraisal of the area and sampling; the second season (February 10-20/2017) for further sampling and constructing detailed stratigraphic logs of the various localities) and the third season (March 23 – 25/2017) for verification. During the actual field work detailed lithological mapping and description of the various units was conducted. These included identification of the rock units; description of mineralogical and textural features;

delineation of both vertical and horizontal contact relationships; assessing degree of welding and fragmentation of the pyroclastic units, vertical as well as horizontal continuity of the rocks, and regularity/shape of the topography; and collection of structural data. Stratigraphic logs were also constructed in various localities of the study area, as well as sampling of rocks for petrological and geochemical analysis.

Sample preparation for petrological and geochemical analysis was conducted at the Sample Preparation Room of the School of Earth Sciences, AAU, where samples were cut, crushed and milled. Sample preparation included removal of some weathered surface and cutting to appropriate sizes. Thin sections from nine hard rock samples were prepared at the Geological Survey of Ethiopia. Thirteen powdered samples were sent to the Australian Laboratory Science (ALS) for geochemical (major and trace element) analysis, in Ireland. Major elements are analyzed using multi element inductively coupled plasma (ME-ICP06); trace elements are analyzed using multi element mass spectrometry (ME-MS 81) techniques. Previously, four volcanic ash samples were sent to the Berkeley Geochronology Center, USA for dating, where sample preparation for dating was also conducted (*Asfawossen Asrat, Pers. Commun*.). The prepared thin sections were studied using a standard petrographic microscope at the School of Earth Sciences of Addis Ababa University. The modal analysis of thin sections, petrological description of rocks, stratigraphic logs, along with the major and trace element analysis results, as well as geochronological data are then systematized and presented in appropriate formats. Finally, all the field and laboratory data as well as data from previous works have been integrated, synthesized and interpreted.

1.6. Expected Outcome and Significance of the Study

The expected outcomes of the research work are additional petrologic and geochemical as well as geochronological data which will help in further understanding of the petrogenetic evolution of silicic volcanics in Ethiopia, particularly the petrogenetic evolution of the silicic pyroclastic rocks widely distributed in the margins of the MER. In addition, the results of this research will help to constrain the timing and depositional setting of the archaeological layers as well as the stratigraphic significance of the area in detail will serve as geological input for archeology.

1.7. Previous Works in the Study Area

Except some regional works in the vicinity or incorporating the study area, there have not been many detailed studies. Some notable works include those of Eberz et al. (1988) and Corti, 2009) who described the Ethiopian plateau volcanism and evolution of the flood basalt volcanic province as well as rifting. The chemical composition of the flood basalt both in the north and southern sector of the Somalian and Ethiopian plateau have been discussed by Mohr (1983); Giday WoldeGabriel et al. (1990); and Kieffer et al. (2004), among others. Some detailed geological description of the Southeastern Ethiopian Plateau, including some stratigraphy, geochemistry and geochronology, as well as structural context has been given by Seife Michael Berhe et al. (1987) and Workineh Haro et al. (2014).

In addition, the geological setting and stratigraphy of Lake Gadeb, located some kilometers (kms) east of the Melka Wakena site (Williams et al., 1979), as well as the regional correlation, petrography, geochemistry, modes of eruption, fragmentation and deposition, and paleo-geographic implications of the inter-bedded ashes have been studied (Williams et al., 1979; Eberz et al., 1988). The Plio-Pleistocene volcanism and sedimentary facies changes in the Gadeb plain of Wabi Shebelle basin are also explained. Accordingly, volcanic ashes with compositional range from rhyolite to mixed scoria are regularly inter-bedded with fluvio- lacustrine successions. Positive correlation between incompatible trace elements showing co-genetic origin was used to conclude the cycles of increase followed by cycle of rapid decreasing in the amounts of the elements with respect to the stratigraphic positions (Eberz et al., 1988). This reflects the eruption of zoned magma in deep seated magma chamber followed by dormant stage of volcanism that builds up the incompatible elements and volatiles to rise for the next eruption (Eberz et al., 1988). In addition, the regressive - transgressive cycles of Lake Gadeb has been associated to climatic fluctuations (Eberz et al., 1988). On the other hand, Eberz et al. (1988) suggested the transition from lacustrine to fluvial deposition of Lake Gadeb to be due to regional volcano-tectonic conditions.

CHAPTER TWO

GEOLOGIC AND TECTONIC SETTING

2.1. Geologic Setting

Large igneous provinces are related to continental break up (Baker et al., 1996; Hofmann et al., 1997; George et al., 1998). It consists of huge volume of flood basalts and variable amounts of silicic products providing a Daly gap (Peccerillo et al., 2003 and reference therein). Two lines of evidence have been recognized for the existence of plume beneath the rift system, which has produced the earliest magmatism in southern Ethiopia (George et al., 1998; Rogers et al., 2000).

2.1.1. Ethiopian Plateau Volcanism

Ethiopian flood basalts (EFB) are the youngest major continental magmatism (Dereje Ayalew et al., 1999; Kieffer et al., 2004). It records magmatic events from initiation through high flux and shut down to the onset as well as initiation of sea floor spreading (Kieffer et al., 2004; Corti, 2009). It is developed through various stages of rift formation including from the Red Sea (RS), Gulf of Aden (GA), Afar and Main Ethiopian Rift (MER). Ethiopian volcanic event is classified into three main stages (Peccerillo et al., 2003; 2007). Accordingly, Most of the EFB are erupted during the first stage where voluminous eruption had taken place during short period of time (<1 Ma). Moreover, EFB volcanism covers 600, 000 m^2 volcanic plateaus (Hofmann et al, 1997) resulted from 350,000m^3 magmas (Mohr and Zanettin, 1988; Kurkura Kabeto et al., 2009). In contrast, Workineh Haro et al. (2014) suggest that magmatism in central Ethiopia did not commence and ended within short period of time. These Trap series are mostly theolitic flood basalts and alkaline shield volcanoes (Mohr, 1983; Giday WoldeGabriel., 1990; Kieffer et al., 2004). In addition, Pik et al. (1998) classified the Trap series basalts into High (HT) and Low Titanium (LT) types based on trace element and titanium concentrations. Accordingly, High Titanium (HT1) and (HT2) basalts are characterized by high concentration of incompatible elements and more fractionated rare earth element (REE) pattern. On the other hand, Low Titanium basalts have low concentrations of both incompatible trace elements and titanium producing smooth REE pattern. High Titanium

basalts are found in the south and east whereas Low Ti basalts are found in the north western plateau (Pik et al., 1998).

The Ethiopian plateau is made of flood basalts and shield volcanoes ranging from theolitic to alkaline (Kieffer et al., 2004). The overlying shield volcanoes, complex- time space in the evolution of magma, high proportion of pyroclastic rocks in the plateaus differentiates Ethiopian provinces from other monotonous, thick, nearly horizontal theolitic flows without shield volcanoes elsewhere (Kieffer et al., 2004; Gezahegn Yirgu et al., 2006). The nature of mantle plume responsible for the formation of Ethiopian plateau volcanics and its interaction with the continental lithosphere has been investigated by Baker et al. (1996), Hofmann et al. (1997) and Pik et al. (1998; 1999). These studies explained the relationship between theolitic and alkaline basalts specifically between mixed theolitic – alkaline basalts to exclusively alkaline magmatism (Kieffer et al., 2004). The studies also indicated that theolitic magmas were susceptible to crustal contamination whereas alkali magmas were unaffected. Kieffer et al. (2004) also used volatile content of the magma to describe the genesis of the two types of magmas and found out that the volatile rich alkaline magmas are formed without interaction with crustal rocks whereas volatile poor, high density theolitic magmas are formed by crustal contamination in large magma chambers.

Using K-Ar dating Seife Michael Berhe et al. (1987) also recognized that Ethiopian flood basalts were formed during three stages: at >40 Ma, 40-30 Ma and 30-21 Ma, though they are not the same in the NW and SW Ethiopian plateaus. This is also supported by Peccerillo et al. (2003; 2007). Seife Michael Berhe et al. (1987) suggests that stage one and stage three did not develop in the NW, while Tertiary volcanism develops during stage three in SE Ethiopia. The geology and geochronology of rocks in the SE plateau suggests the existence of flood basalt volcanism since the earliest eruption at 30- 22 Ma (Seife Michael Berhe et al., 1987). Accordingly, four units are recognized in the Bale area: 30-22 Ma lower stratoid basalts; Riera basalts (15-5 Ma); Dodola basalts (undetermined age) and 6-2 Ma Arorso trachyte (Merla et al., 1979) and 2.1 Ma Sante Basalts and Batu trachyte on the top. The lower stratoid basalts are overlain by 10-15m thick Damole ignimbrite in the east and by Riera basalts further to the west in the direction of the rift (Seife Michael Berhe et al., 1987). Riera basalts, pyroxene and plagioclase phyric basalt, form 600m thick succession of different units separated by

scoriceous basaltic horizons and paleo soils. This unit is unconfromably overlain by Dodola ignimbrite and Trachyte consisting of rhyolite ignimbrite, trachyte and ash flow tuff. The existence of intercalated volcano-sedimentary rocks is also recognized by Seife Michael Berhe et al. (1987) and all together is considered as the 6-2 Ma old Ghinir unit (Merla et al., 1979). Shield volcanoes of 2.1 Ma form the Sante and Batu trachytes forming large volcanic edifies. In addition, Workineh Haro et al. (2014) recognize various units in the Bale - Asela area: lower lava flows, middle lava flows, plateau basalts and upper pyroclastics to plateau basalts and Quaternary basalts, trachyte and scoria cones on the top. Workineh Haro et al. (2014) recognized fine to medium plagioclase phyric basalts, medium to course plagioclase phyric basalts, scoriceous basalts, as well as olivine-plagioclase phyric basalts, olivine-pyroxene-plagioclase phyric basalts and pyroxene-olivine-plagioclase basalts in the area.

2.1.2. Main Ethiopian Rift (MER) Volcanism

The Main Ethiopian Rift (MER) is a key sector of the East African Rift System (EARS) that records the history of episodic magmatic events throughout the rift (Giday WoldeGabriel et al., 1990) reflecting bimodal character (Tadiwos Chernet et al., 1998; Tadiwos Chernet and Hart, 1999; Peccerillo et al., 2007). Basalts and silicic products are characteristics of the rift floor whereas trachyte magmas evolved along the rift shoulder, for instance the Ziquala and Yerer volcanic centers (Gasparon et al., 1993; Peccerillo et al., 2007). Moreover, Peccerillo et al. (2003; 2007) attributed the occurrence of the majority of silicic products and subordinate basalts in MER during Pliocene to present times to the final stage of volcanic activity.

MER volcanic activities yielding 10-5Ma transitional and Na- alkaline basalts with minor trachyte shield volcanoes are considered as secondary phases (Peccerillo et al., 2003 and reference therein). In addition, Wolfenden et al. (2004) have found 10.5 Ma trachyte flows from the base of Megezez volcano. Further to the northern Main Ethiopian Rift (NMER), Kurkura Kabeto et al. (2009) dated 9-7Ma transitional–alkaline Addis Ababa basalts, suggesting the presence of volcanic gap between the two pre-rift volcanic activities (Tadiwos Chernet et al., 1998; Kurkura Kabeto et al., 2009). This shows southward migration and younging of volcanism following the rift shoulder (Dereje Ayalew et al., 2006 and reference therein). Bimodal volcanism in Southern Afar Rift floor close to SA-NMERTZ has taken place during the period 7Ma- recent, with the chemical

composition ranging from theolitic – alkaline basalts and basanites to trachyte and rhyolite (Tadiwos Chernet et al., 1998). The youngest rock of the Nazreth group in the NMER, for example is dated to 5.8 Ma (Tadiwos Chernet et al., 1998). Even though volcanic gap is reported between 6.6 and 3.5 Ma by Wolfenden et al. (2004) in the Adama basin, 7-5 Ma silicic rift margin transition zone magmas overlain by 5.6-4.5 Ma Afar Stratoid Series are recognized by Tadiwos Chernet et al. (1998). Using chrono-stratigraphic evidence it is followed by 4.5-3 Ma volcanic rocks of the Addis Ababa rift embayment (Tadiwos Chernet et al., 1998). Lastly young age rift floor basalts and Quaternary bimodal volcanic rocks (*ca*. 2 Ma) have formed (Tadiwos Chernet et al., 1998; Kurkura Kabeto et al., 2009). The 5.1-3.3 Ma Addis Ababa volcanics from the satellite of Wechacha give rise for the silicic rocks of Wechacha Formation, predominantly Benmoreite and trachytic rocks, on the flanks of the northwestern plateau (Tadiwos Chernet., 1998; Kurkura Kabeto et al., 2009). These units are consisting of volcanic products from Yerer, Furi, Wechacha and Menagesha volcanic centers formed near the intersections of major E-W trending Ambo Transverse Lineament and the Yerer – Gugu Lineament (Tadiwos Chernet and Hart., 1999; Kurkura Kabeto et al, 2009).

The upper Pliocene basalts of the rift are variously named as the Wolenchiti basalts, Bishoftu basalts and Rhyolite, and Bofa basalts (Tadiwos Chernet and Hart, 1999 and reference there in). In the NMER Bofa basalts and Melkasa units are considered as rift center basic volcanic centers, while the felsic rocks of Nazareth, Keleta, Boku –Tede and Dera – Sodere units are termed as Nazreth Group (Kurkura Kabeto et al., 2009). The Bofa basalts largely cover the northern and central sector of MER forming the barrier between ignimbrites of the Nazareth and Wonji group (Tadiwos Chernet et al., 1998; Tadiwos Chernet and Hart, 1999). The Nazreth Group volcanics consist of welded ignimbrite, pumice, ash, rhyolite flows and domes with minor intercalated basalts where the lower series are associated with earliest stage of rifting (Tadiwos Chernet and Hart, 1999). The ignimbrite of the Nazreth Group is formed from volcanic eruptions of the marginal centers (Peccerillo et al., 2003) covering large portions of rift margin and escarpments whereas basaltic magmas of this group are exposed along the fault scarps (Tadiwos Chernet et al., 1998). However, the formation of ignimbrite is not restricted to swelling fractures of the marginal centers, but could also be formed from central volcanoes, e.g., Fantale (Peccerillo et al., 2003).

Quaternary volcanism in the rift mainly occurred along the fractures of the Wonji Fault Belt (WFB) with series of scoria cones, peralkaline lavas and pyroclastics (Tadiwos Chernet et al., 1998; Peccerillo et al., 2003) and along the Butajira –Silti Fault Zone. The 1.6 Ma Boset trachytic flow is the earliest product of the Quaternary volcanism in the northern MER, followed by 0.6 Ma Harbona rhyolite dome and 0.11 Ma Bishoftu basalt (Tadiwos Chernet et al., 1998). Meseret Teklemariam (1996) reported felsic rocks dated 0.155 to 0.002 Ma at the Aluto-Langano complex.

Like the case of NMER, Corti (2009 and reference therein) recognizes rocks of different volcanic events in the central sector of MER having >5 Ma. The Butajira ignimbrite and Nazreth pyroclastics are grouped as syn-rift, while the remaining upper age volcanic rocks are formed after the onset of major rifting in the central sector of the rift (Corti, 2009 and reference therein). The ignimbrites in the rift floor are believed to be formed by the collapse of large caldera structures due to violent eruption such as the 3.5 Ma Munesa crystal tuff caldera buried beneath Lake Zway- Shala basin system (Le Turdu et al., 1999). Porphyritic, strongly welded ignimbrite unit (0.155 Ma) is recognized in the Aluto-Langano geothermal field (Meseret Teklemariam, 1996). Peccerillo et al. (2003) reported 0.32±0.02 Ma pre- and 0.26±0.02 Ma syn-caldera felsic products from Gedemsa volcano. These form pre-caldera lava domes, flows and pumice fallout deposits, syn-caldera ignimbrites as well as post-caldera dome, flow and pyroclastic fall deposits (Thrall, 1973; Peccerillo et al., 2003; Giordano et al., 2014). The felsic rocks, consisting of ash flow tuff, silicic tuff breccias, silicic domes and pumice flow, of Aluto- Langano overlay the 1.6 Ma, 800-1000m thick Bofa basalts (Meseret Teklemariam, 1996).

The Butajira ignimbrites and Nazreth pyroclastics are in places overlain by upper Pliocene basalts and pyroclastic deposits that characterize the western and the eastern plateaus near the rift margin analogues to those in NMER (Corti, 2009). The western margin volcanism of Tadiwos Chernet et al. (1998) and the Somalian plateaus Trachyte and basaltic central volcanoes of Zanettin et al. (1978) grew during Pliocene time giving off-axis volcanism (Corti, 2009 and reference therein). Subsequent volcanic activities have taken place during the Quaternary associated with oblique faulting of the WFB, which is characterized by bimodal volcanism (Corti, 2009). The major ignimbrite eruptions took generally at less than 1.6 Ma (Giday WoldeGabriel et al., 1990; Tadiwos Chernet et al., 1998; Meseret Teklemariam, 1996) related to the collapse of large calderas

at around 0.2-0.3 Ma (Le Turdu et al., 1999). Like in the case of NMER, the western margin volcanoes of CMER are dated to 4.6-3.3 Ma and gave rise to central volcanoes like Wechacha, Furi and Yerer which are aligned along an E-W trend related to the deformation along the transversal YTVL (Tadiwos Chernet et al., 1998; Mazzarini et al., 1999 as cited in Corti, 2009). This age is coincident with the age of the Addis Ababa Silicics of Tadiwos Chernet et al. (1998) and rift margin as well as rift center products of Kurkura Kabeto et al. (2009).

Peccerillo et al. (2007) attributed the predominance of felsic volcanic rocks over basaltic rocks of the sector (CMER) to the presence of a zoned magma chamber. Thus, the basaltic rocks erupted when the fractures intersect the lower portion of the magma chamber. Rooney et al. (2007) recognizes more complex parallel tectono-magmatic zones such as volcanic chains of Debrezeit - Butajira magmatic segments to the west and WFB belt in the east in the CMER. These complexes are differing from each other in the depth of magma fractionation reflecting different maturity of magma plumbing system and propagation of the rift (Rooney et al., 2007). Compositionally the Butajira ignimbrites and Nazareth pyroclastics are consisting of per alkaline pantellerite ignimbrites, rhyolite domes, rhyolite and trachytic lava domes associated with lava flows of 5.2-2.6 Ma with maximum concentration in 3.5 Ma (Corti, 2009 and reference therein). In addition, silicic volcanic rocks (Dino formation) constitute the basal portion of (1.5-0.8 Ma) rift floor of the Hosana area stratigraphy, also extensive to the escarpments and adjacent plateaus are reported as ignimbrite and pumiceous pyroclastics (Basalfew Zenebe et al., 2012). Accordingly it is mapped as Nazareth group and Dino formation together due to the insufficient data in rift escarpments to separate them. To both sides of the rift, this formation is characterized by lacustrine sedimentation correlated with young rift floor Silicics most probably the same age (Basalfew Zenebe et al., 2012). In addition to the idea of Basalfew Zenebe et al. (2012), Quaternary volcano clastic deposits are reported in the central sector of the rift and adjacent plateaus (Kazmin and Seife Michael Berhe, 1981; Seife Michael Berhe et al., 1987; Eberz et al., 1988; Williams et al., 1979; Giday WoldeGabriel., 1990; Basalfew Zenebe et al., 2012; Workineh Haro et al., 2014).

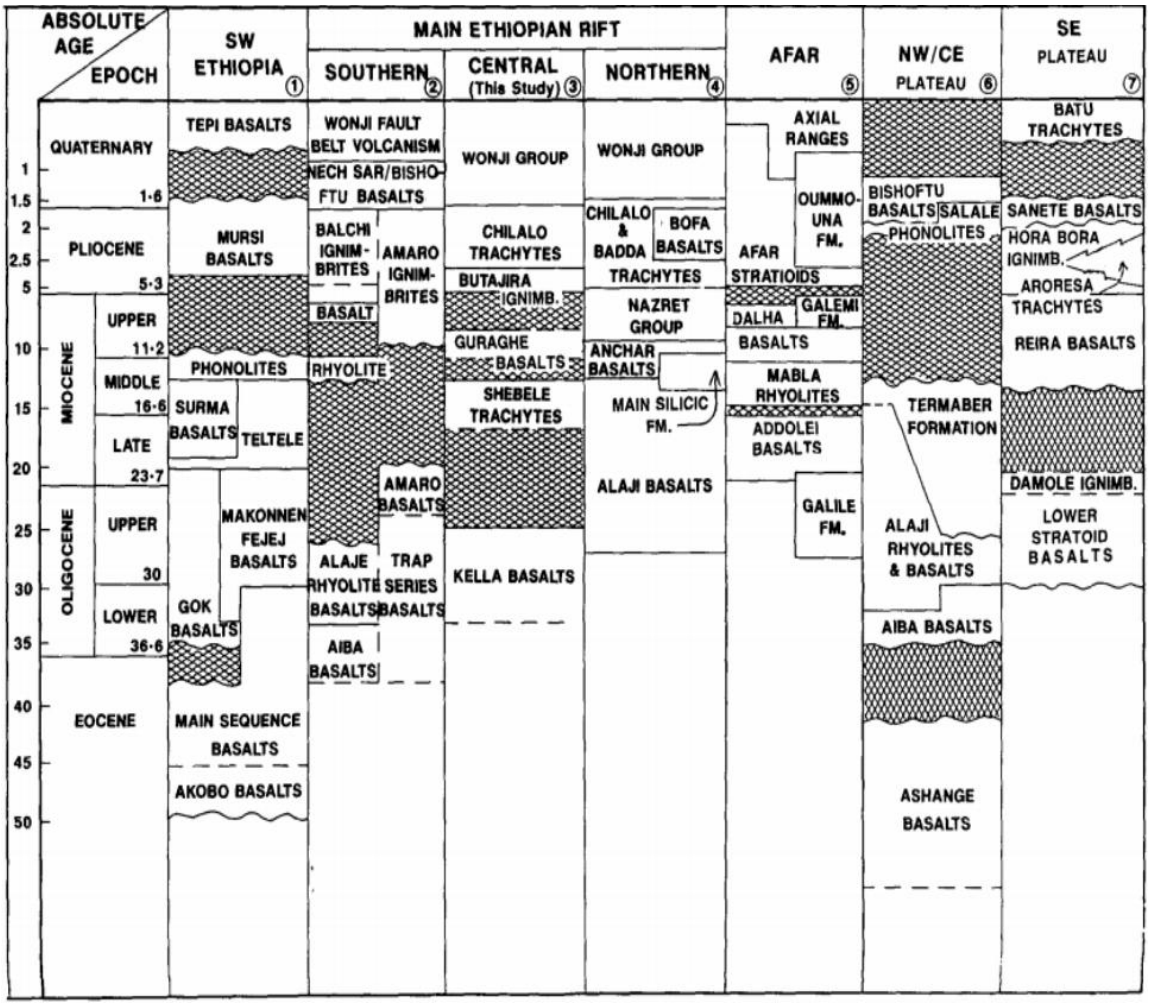

Figure 2.1*.Correlation charts of Cenozoic volcanic rocks in Ethiopia (Giday WoldeGabriel et al., 1990). Fm.: Formation; Ignimb.: ignimbrite*

In the case of SMER even though basalts older than 11Ma are reported (Davison and Rex, 1980; Ebinger et al., 1993; George et al., 1998) volcanism is then resumed during Pliocene-early Pleistocene (Zanettin et al., 1978) with bimodal volcanism in the rift floor started with ignimbrite volcanic eruptions (1.6-0.5 Ma), correlated with the Nazreth units of NMER (Bonini et al., 2005). The successions are followed by the Nechsar olivine basalt 1.34-0.77Ma (Ebinger et al., 1993), 0.66Ma old trachyte basalt of the Bobem volcano and pumiceous tuff, obsidian flows and basalts in the Bridge of God area (Ebinger et al., 1993; Bonini et al., 2005).

In conclusion, the Rift magmatism is characterized by bimodal volcanism. The existence of the Daly Gap and evolution of silicic products from basaltic magma has been controversial (Tadiwos Chernet et al., 1998; Peccerillo et al., 2003). According to Bocalleti et al. (1995) the coexisting silicic and basaltic magmas are different origin,

where the basaltic magma is generated from the mantle while the silicic magmas are generated from melting of under plated basalts. This contradicts with the curved trend of major and trace element diagrams suggesting continuous fractional crystallization of basalts to generate silicic magmas (Peccerillo et al., 2007). According to Peccerillo et al. (2007), the Daly Gap results due to fast cooling of residual liquids of intermediate composition crystallizing large amount of phases, at the same time suggesting the existence of zoned magma chamber with felsic magma at the top and basalts at the lower portion.

2.2. Tectonic Setting of the Region

Ethiopian and Somalian plateaus are dissected by the 80 km wide MER (Fig.1.1) forming large escarpments extending from the Red Sea and Gulf of Aden junction in Afar depression to the Turkana depression in the south (Mohr, 1983; Boccalleti et al., 1999; Corti, 2009). This rift system shows different stages of development from initiation through break up to oceanic spreading in the north (Hayward and Ebinger et al., 1996). Though Ethiopian rift system is classified in to Afar and MER (Corti, 2009) it is consisting of three rift segments reflecting different orientation of the fault boundaries (Giday WoldeGabriel et al., 1990; Bonini et al., 2005; Kurz et al., 2007; Keranen and Klemperer, 2008; Corti, 2009).

Basically NMER, CMER and SMER are the segments of MER reflecting different timing of volcanism, fault architecture, stages of extension deformation and lithospheric structure (Hayward and Ebinger, 1996). Boccalleti et al. (1999) classified the Ethiopian rift as the northeastern sector characterized by recent volcanism and the southwestern sector with abundant older volcanic products. Transverse structures such as Boru-Tura structural high located at Lake Koka separating NMER and CMER as well as the Goba-Bonga transverse lineament of Lake Hawassa between CMER and SMER are recognized by Bonini et al. (2005). According to Bonini et al. (2005) MER is the roughly NE trending rift system where rifting starts in SMER (21- 20 Ma) due to northward propagation of the Kenyan rift. SMER shows northward propagation up to Goba-Bonga transverse lineament whereas the northern sector of the rift start to develop by 11 Ma and propagates southward until the Boru-Tura structural high (Bonini et al., 2005; Tsegaye Abebe et al., 2010). The CMER developed at 9.7-8.3 Ma with significant rifting at 5-3 Ma accompanied by eruption of voluminous silicic magmas and reactivation of SMER as

a function of the counter-clock wise rotation of the Somalian plate (Bonini et al., 2005). Tadiwos Chernet et al. (1998) and Kurz et al. (2007) described the NMER as oriented NE in the Afar depression where as both the CMER and SMER orient along NNE-SSW direction. On the other hand, Corti (2009) suggest that MER extends along NE-SW direction at the Red Sea – Gulf of Aden triple junction in the Afar depression and N-S in the south at the Turkana depression. The NMER is oriented N40°E where it is bounded by the Arboye and Sire boundary faults in the southeastern and by the Ankobor and Boru-Tura structural high in the Northwest side (Wolfenden et al., 2004).

In the case of CMER, the boundary faults are oriented at an average trend of N30°E, where the western margin is well expressed by the N25°E–N35°E trending and ESE-dipping Guraghe and Fonko faults, whereas the eastern margin is well represented by the N30°E trending and WNW-dipping Asela–Langano fault system (Corti, 2009). The border fault is characterized by minor transverse structures in which the NE-SW trending structure meets the NW-SE trending structure near Langano resulting in the 'S' or 'Z' morphology (Le Turdu et al., 1999). In the DebreZeyt area, the NE–SW trending rift margin and the N–S Boru-Tura structural high give rise to the major Addis Ababa rift embayment (Corti, 2009). The direction of stress field for extension in the CMER was oriented roughly along ESE-WNW with local variations to E-W and NW-SE (Bonini et al., 2005). This gives the oblique slip pattern on NE-SW trending fault pattern. According to Bonini et al. (2005) the rift margin in the CMER is formed around 6 Ma but Giday WoldeGabriel et al. (1990) proposed that it is formed at 8Ma. Most of the active strain in the CMER is localized within the WFB (Bonini et al., 2005).

In the SMER the boundary faults are oriented N0°E to N20°E due to rotation of the rift valley from N20°-35° to N 5°-20° (Corti, 2009). It is characterized by the Chencha major fault in the west, which is curvilinear in shape oriented N–S and N40°E and the Agereselam linear shaped NNE–SSW trend boundary fault in the east (Corti, 2009). According to Giday WoldeGabriel et al. (1990) the Agereselam boundary fault was formed at 10Ma whereas south of Lake Abaya extensional deformation initiated at 20-21 Ma ago (Bonini et al., 2005).

The rift floor of the MER is affected by widespread deformation related to faulting along the Wonji Fault Belt (WFB) formed at 2 Ma (Bonini et al., 2005; Kurz et al., 2007). It is oblique to the direction of main rift margins forming 'S' shaped curvature resulting in

sigmoidal geometry (Corti, 2009). N-S trending Kenyan rift gives rise to the development of SMER at about 20-21 Ma and lasted up to 11Ma in which the northward propagation of the Kenyan rift is hindered by Goba Bonga transverse lineament (Wolfenden et al., 2004; Bonini et al., 2005). Accordingly, this propagation is due to the combined effect of mantle plume movement and the existence of pre-existing structures (Bonini et al., 2005 and reference therein). In addition, southward migration of deformation from Afar (Bonini et al., 2005) is evident from the existence and re-activation of pre-existing tectono-magmatic structures in southern Afar at around 10-11 Ma (Wolfenden et al., 2004).

Basically faults, fractures, shear zones, joints, dike swarms of Bale mountain, micro folds and deformed fiames are reported in tertiary rocks of highland and plateaus of Arsi and Bale areas with columnar structure in the lower lava flows of Wabi gorge and other highlands (Workineh Haro et al., 2014). In the Bale area Lake Gadeb is developed due to the composite effect of local faulting during Mio- Pliocene and topographic increase from local shield volcanism (Eberz et al., 1988). In addition primary structures such as bedding and lamination are reported in Mesozoic sediment in the north eastern part of Asela sheet (Workineh Haro et al., 2014).

CHAPTER THREE

GEOLOGY OF THE STUDY AREA

The area was investigated along selected traverses mostly following the river gorges (Fig. 3.1). Various rock layers were accordingly identified and they are classified based on their stratigraphic positions as well as field and petrographic characteristics.

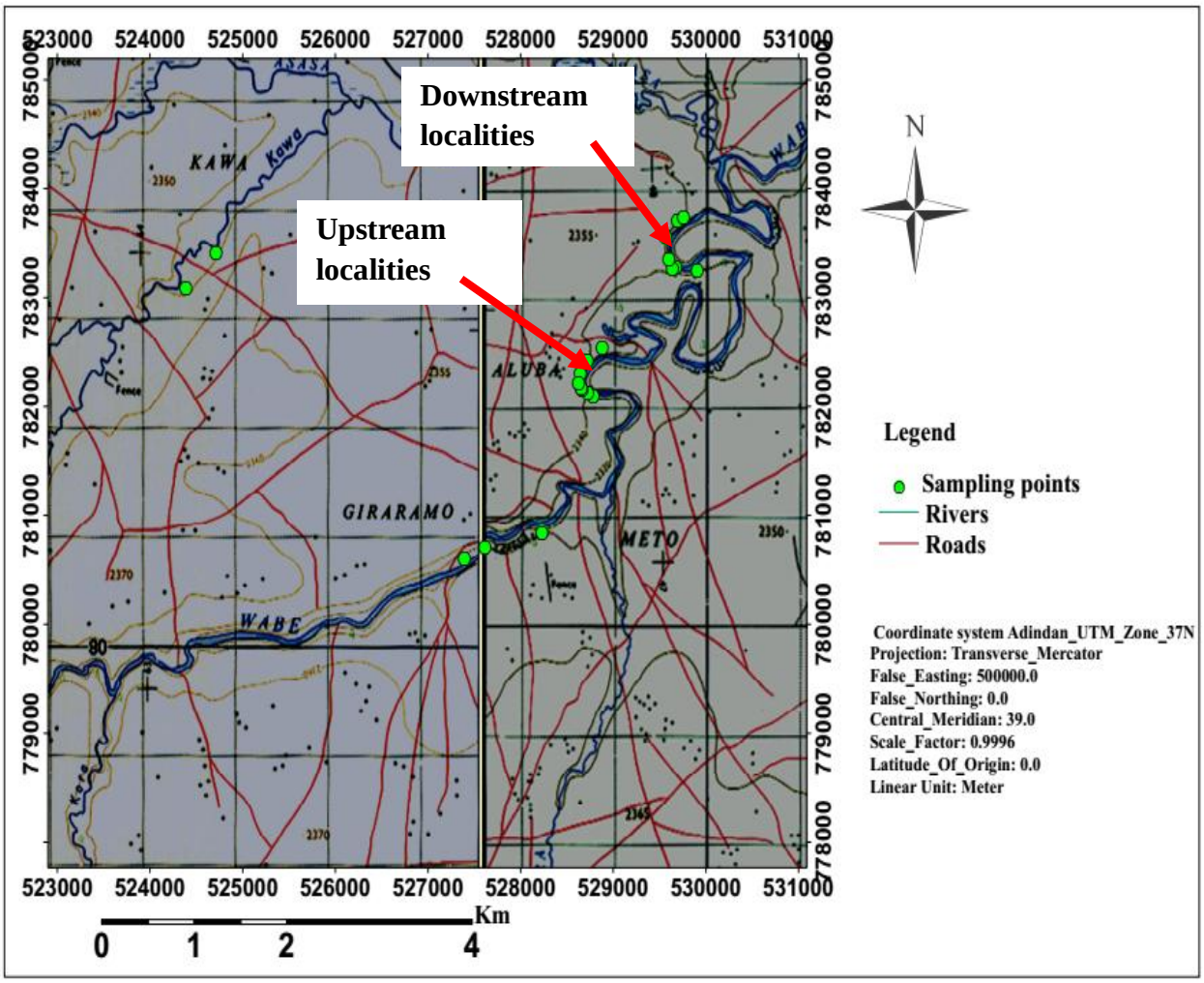

Figure 3.1. *Sampling locations in the study area at the scale of 1:25,000 showing the site of stratigraphic logs and data points following the river gorge; Two sampling points are along the Kawa River, whereas the rest are along the channel of the major Wabi River.*

3.1. Lithology and Petrography

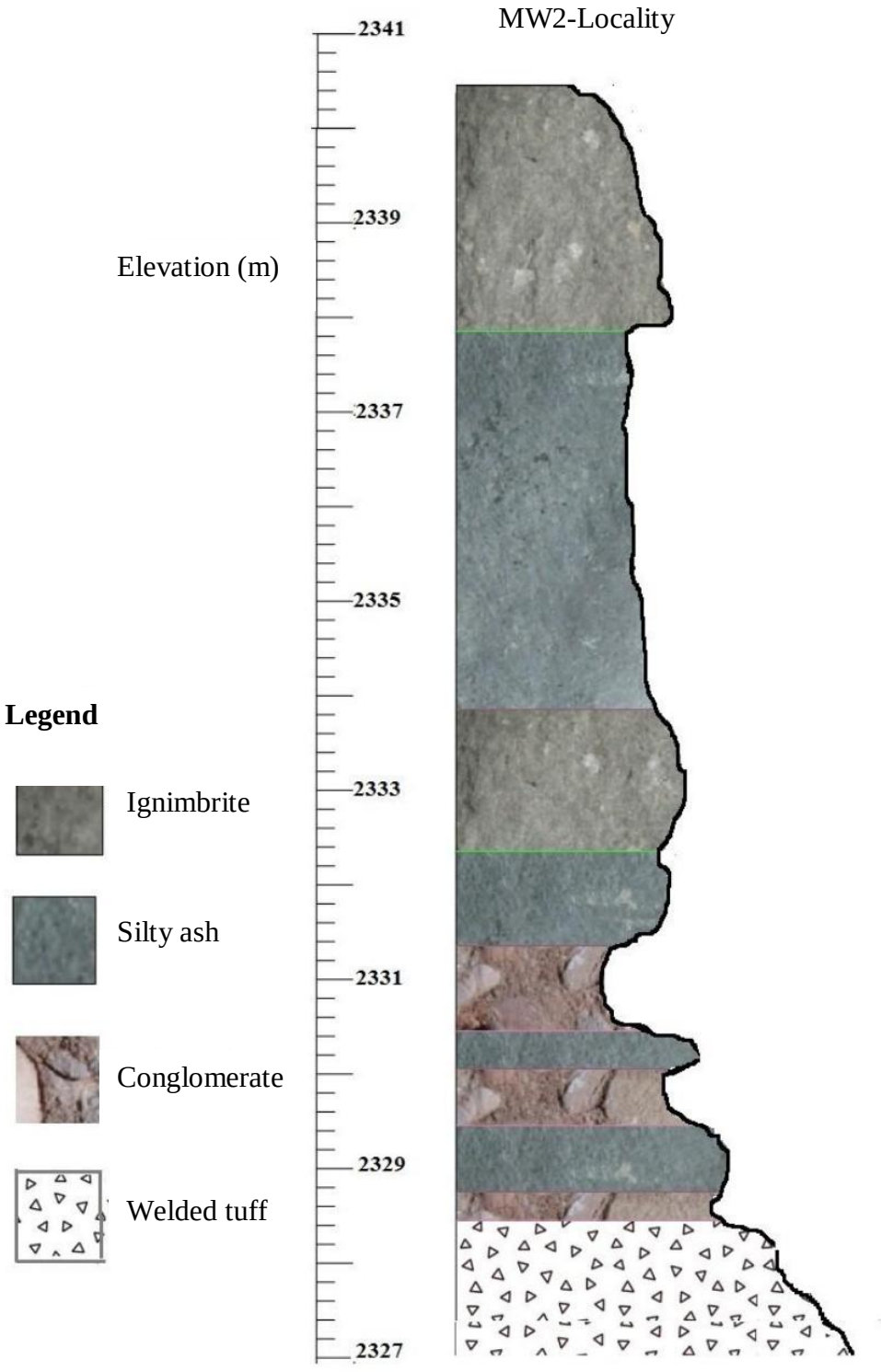

Figure 3.2. *Stratigraphy of the relatively complete section consisting of dated layers.*

3.1.1. Glassy and Crystalline Ignimbrite

Glassy ignimbrite is exposed along the Kawa River, a tributary of Wabi River. Upon breaking, it produces sharp edge with dark brownish color (Fig. 3.3.). It is characterized by big phenocrysts of alkali feldspar with in a glassy matrix and minor quartz crystals visible both in hand specimen as well as in thin section. Two thin sections from this unit show porphyritic texture with phenocrysts ranging from <1mm up to 8mm big, euhedarl to sub-hedral, preferred and elongated orientation of fiammes and rock fragments, and horizontal flattening of the phenocrysts. In addition, the petrographically uniform orthoclase phenocrysts themselves contain crystals of quartz, and minor accessory minerals forming pokiolitic texture. The preferred orientation and elongation of the fiammes, as well as rock fragments and the structurally deformed flow banding suggest one directional flow during rapid cooling and welding of the flow. The presence of inclusions in the phenocrysts with different characteristics suggests they are older and included at depth prior to the crystallization of orthoclase during the way of the magma to the surface.

On the other hand crystalline ignimbrite is exposed at the Wabi River gorge mainly at the upper portion of the study area. At hand spacemen scale, they differ in color and in texture from those of the Kawa River ignimbrites. Accordingly, the Wabi River ignimbrites are light bluish, light brownish and grayish, and porphyritic while the Kawa River ignimbrites contain abundantly glassy. Both ignimbrites contain fiammes, though these are very small in size in the crystalline ignimbrites, and slightly elongated in one direction.

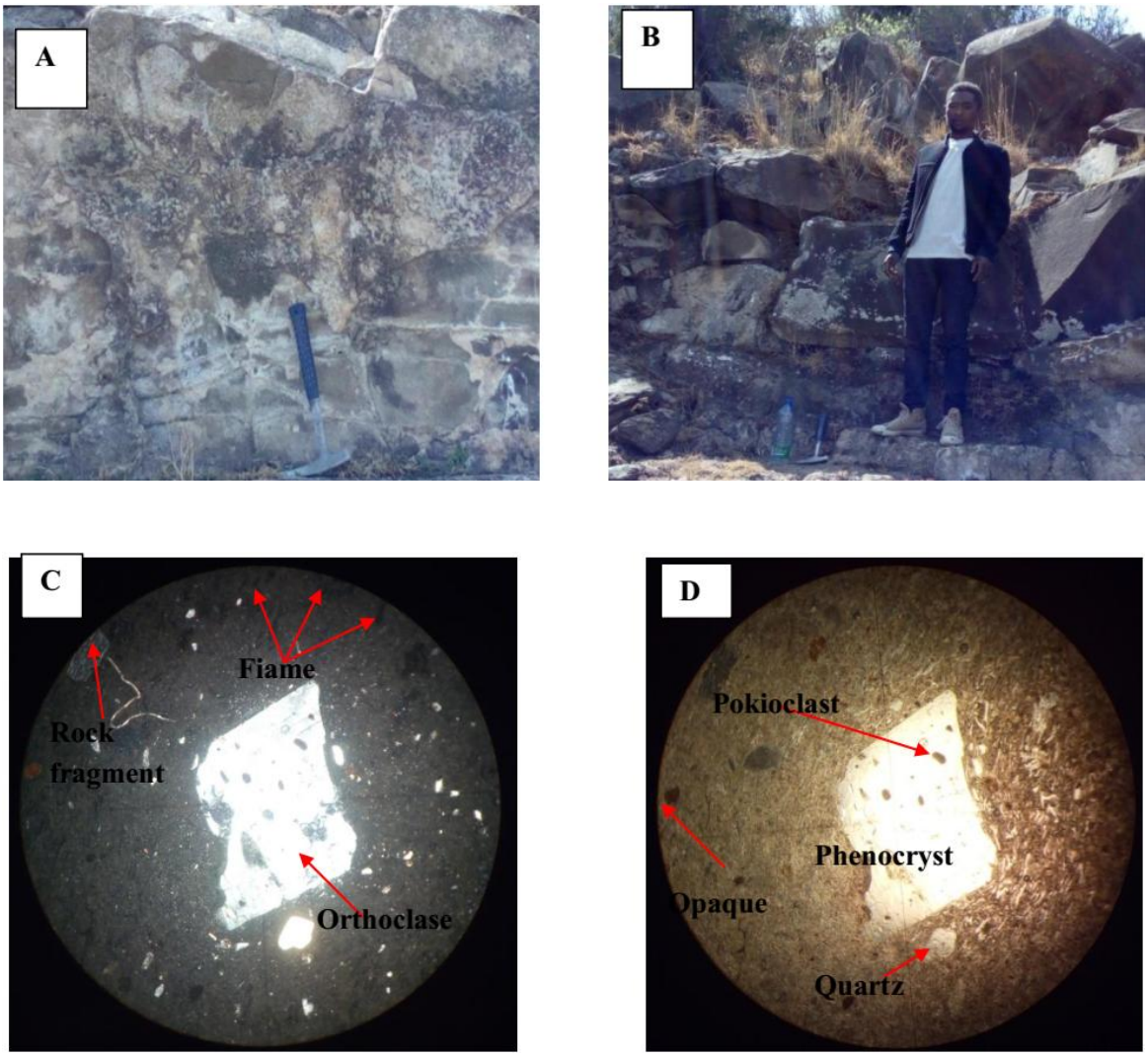

Figure 3.3. *Ignimbrite layers exposed along the Wabi River channel separating the loose pyroclastic rocks and the massive ignimbrite flow in the upper stream portion of the study area:(A) Glassy ignimbrite from MWD1 (X-0528232 Y-0780848 Z-2324); B. Crystalline ignimbrite from MWD2A (0527615 Y-0780707 Z-232349); (C) Glassy ignimbrite under XPL; (D) Glassy ignimbrite under PPL; Thin section photos are with 10x magnification. Where X- is Easting and Y- is Northing and Z- is Elevation in meters throughout the chapter.*

The modal composition of the ignimbrites is 65-70% ground mass, 5-10% orthoclase, 5-10% quartz, 5-10% fiammes, 5-10% rock fragment <3% opaque together with minor sanidine, zeolite, opaque and muscovite crystals. The dominant phenocrysts are flattened to elongate orthoclase crystals.

3.1.2. Volcanic Ash/ Unwelded Tuff

This ash layer is composed of light grayish to light yellowish ash exposed at the base of the sections immediately above the ignimbrite flows. Currently, most of these layers are

covered under the water of the Wabi River and the lower contact is invisible. Where it is exposed, it is highly weathered possibly due to the fluctuating level of the River water. This unit is generally horizontally layered except in the upper stream portion of the study area (MW2 and MW8 localities), where the unit pinches out forming an unconformity below the welded tuff unit. These layers show minor sign of vesiculation, randomly oriented tiny fractures and the effect of grass roots on their top levels suggesting strong post-deposition weathering and erosion. A thin, highly weathered, laterally non-continuous diatomite layer is also found on top of this section in some localities (MW9). Some fragmented travertine on top of this unit also suggest that this unit might have been strongly eroded and weathered and covered by some water body before the eruption and deposition of the next layer.

3.1.3. Volcanic Tuff

The welded tuff unit is exposed at two localities forming the bottom of the sections. 1.5m thick, highly vesiculated, welded, dark to brownish (white to buff when fresh) tuffceous materials and poorly sorted pumice fragments characterize this unit (Fig. 3.4.). The unit contains primary tuff beds with no sign of reworking. The degree of welding decreases from bottom to top. The pumice fragments are <1cm to 15cm-sized clasts showing random orientations. In addition the vesicles show random orientation throughout the layer. Generally circular bombs with small sized angular basaltic blocks are observed and the numbers of clasts are increasing up ward forming two distinct layers, where the clast-rich layer is near the top. The clasts are held together dominantly by ash sized materials (matrix), rarely lapilli, with few shiny crystals. This unit is devoid of archaeological remains. The welded tuff is separated by a 20 cm thick layer of angular basaltic gravel fragments (breccias) arranged in a preferred orientation.

Figure 3.4. *Welded tuff layer at the base of MW2 log section (X- 0528885 Y- 0782535 Z-2314). showing non-sorted, welded, fining up ward primary fall deposits (it is devoid of any rock fragments, fossils, sediments and artifacts).*

3.1.4. Conglomerates and Breccias

Conglomerates and breccias set in a reworked volcanic ash, silt, and fine sand matrix, and ranging in thickness from 0.20m to 1m, are found intercalated with the pyroclastic layers (Fig. 3.5.). These layers generally thin out laterally and pinch out in places. These layers consist of sediments ranging from granules to large pebbles of 10-30 mm diameter, sub-angular, sub-rounded and rounded grains, poorly sorted, and moderately packed and with preferred orientation in the direction of decreasing slope of the basin. The sub-rounded to rounded materials are basalts whereas ignimbrite materials are angular.

Figure 3.5. *Thin layers of conglomerates from MW5 –E (X-529904 Y-783250 Z-2322) showing highly compacted, generally rounded conglomerates in the matrix of ash, silts and fine sands at the base of lower stream portion of the area; the conglomerates get finer in the NNE direction suggesting the flow direction of the former river and its relative loading capacity.*

3.1.5. Volcano clastic Sediments and Sandstone

Loose, reworked volcano clastic sediments are observed in MW1 and MW2 localities (Fig.3.6.). This layer is composed of gravel size, sub-angular to sub-rounded conglomerates, breccias, pumice, as well as sand, silt and reworked ash matrix. The sediments are poorly sorted with poor fabric. Overlying the light brownish ash in MW2, about 50 cm thick, moderately compacted brownish layer of volcano clastic sediment is exposed containing gravels with in a reworked ash matrix. This layer shows gradational contact with the lower ash unit while it becomes richer in conglomerates towards the top. The conglomerates and breccias are randomly oriented sub-angular to sub-rounded ignimbrites and rounded pumice. This unit is missing in the lower and middle portions of the study area.

At MW3 locality, fine to medium grained, well-sorted, layered sandstone, with some fragile conglomerate layer near the top of the succession is exposed. This layer is not continuous laterally within the sequences.

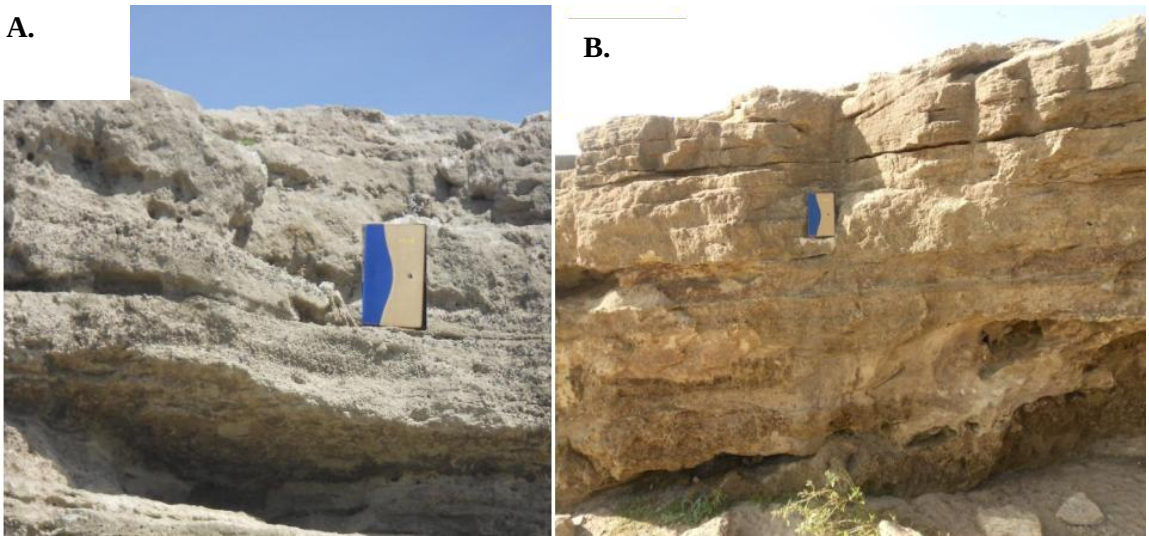

Figure 3.6. *Reworked volcanoclastic sediments and fluvial deposits: (A) Loose volcanoclastic sediments at MW2 locality (X- 0528885 Y- 0782535 Z-2317); (B) Sandstone beds at MW3 locality (X-528979 Y-782900 Z- 2336).*

3.1.6. Vitric Ash

Fine-grained bluish ash forms laterally non-continuous, non-compacted thin layer at the top of the upper stream localities and at mid sections at the downstream localities. This layer is characterized by the existence of shiny crystals suspended in the ashy matrix. Two varieties are recognized in which the deep blue ash shows relatively uniform thickness with comparatively continuous lateral extension whereas the light blue lapilli ash does not possess uniform thickness. Besides, theses layers show sign of intercalation within the sequence. Toward the top in the sequence this layer shows gradation in texture with sign of weathering on the top.

Figure 3.7. *Fine grained light bluish ash from MW5-N1 (X-529640 Y-783267 Z-2332) showing intercalation between lapilli ash and fine ash.*

3.1.7. Fractured Ignimbrite

A layer of strongly fractured and weathered ignimbrites in places forming separate sub-rounded to sub-angular 10-70cm sized blocks is exposed mainly at MW9-S, MW9 and MW7 localities (Fig. 3.8.). They show moderately packed and E-W oriented fabric. The interstices of theses boulders are filled by fine-grained reworked ash. These boulders are similar to those crystalline ignimbrite exposed in the upper Wabi River localities. Rock falling due to gravitational effect also accumulates, some blocks from this layer at the foot of the slope and the river. Three thin sections from various parts of these units show porphyritic texture in which orthoclase phenocrysts are set in fine-grained quartz and ashy matrix. Unlike the glassy ignimbrite there are less fiammes and non producing of the sharp edge when break indicating less welding. In addition, the phenocrysts are smaller in size than those in the glassy ignimbrite. Some minor reddish minerals in one sample indicate slight alteration due to weathering.

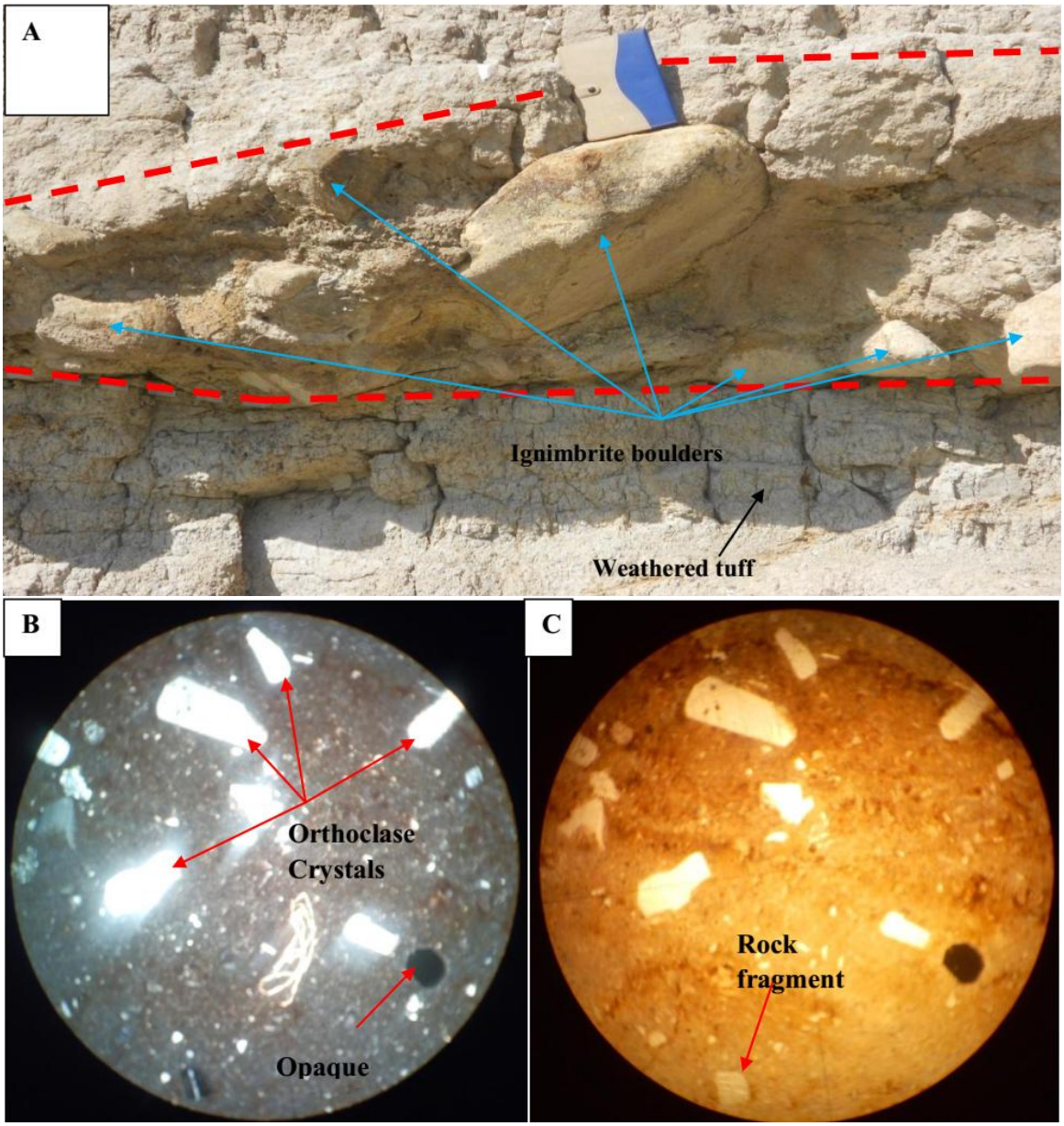

Figure 3.8. *The Fractured Ignimbrite: (A)Ignimbrite boulders interbeded within the weathered ash (X-0528624 Y-782220 Z-2320); (B)Petrographic observation under XPL; (C) Petrographic observation under PPL;. It is observed using 4x magnification of the standard petrographic microscope.*

The modal composition of the ignimbrites is 70-75% groundmass, 5-10% orthoclase, 5-10% quartz, 10-15% rock fragments <5% fiammes, opaque, pyroxene and sanidine crystals. Even though three of the ignimbrite boulders are observed with different color, their mineral constituents as well as their modal composition is similar (See appendix II).

3.1.8. Pumiceous Ash

Pumiceous ash layer is exposed only in the upper stream localities. This layer is consisting of grayish pumice fragments in which the size of the clasts range from <1cm to 20cm set in fine-grained, grayish ash. It is moderately compacted and relatively thick (3.3m), and occasionally forms small caves (Fig. 3.9). The pumice clasts have variable size, varying degree of vesiculation, random orientation, spherical shape, and no fiammes, indicating that they are primary fall deposits.

Figure 3.9. *Pumiceous ash layer from MW12 locality (X- 528655 Y- 782172 Z- 2328).*

3.1.9. Moderately Welded Ignimbrite

Moderately welded ignimbrite layer is exposed in the upper stream localities and rarely in the downstream area (Fig. 3.10.). This unit is 1.5-2m thick but horizontally non continuous throughout the study area except in the upper course of the river. It is fine-grained, and contains some small, slightly vesiculated pumice clasts. It is weathered at its upper surface. This unit is found at different positions in the sequence separated by inter bedded weathered unwelded ash and may be trachytic layer.

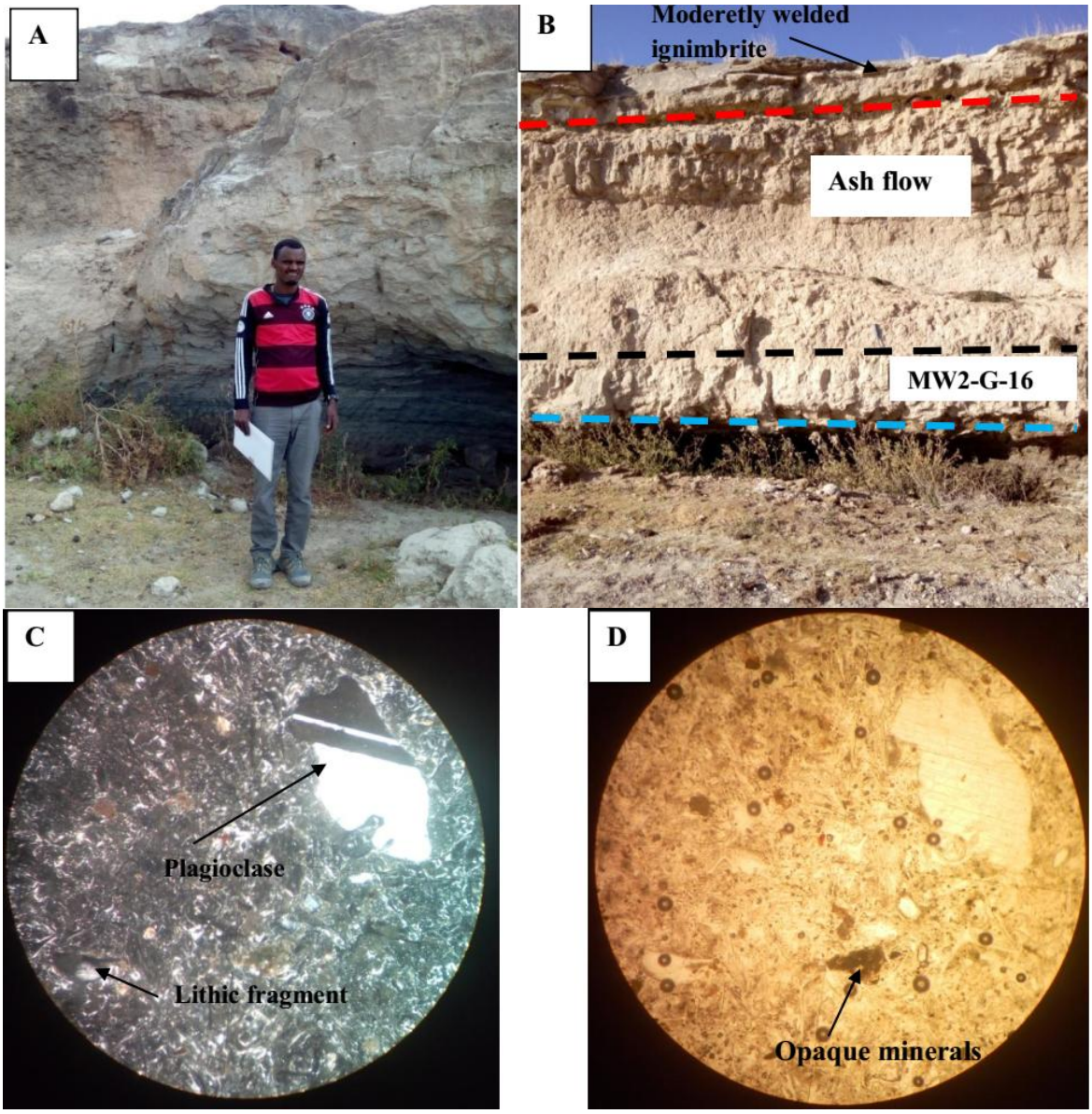

Figure 3.10. *The moderately welded ignimbrite at MW2 (X- 0528885 Y- 0782535 Z-2317); (A) position of both moderately welded ignimbrites in the sequence; B. position of only the upper ignimbrite layer (C) thin section under XPL (D) thin section under PPL. The broken lines are the contacts between the layers.*

Table 3.1. Compiled thin section analysis results and descriptions summarized from the values in the appendix II. It represents the summary of all thin sections

Components	**Descriptions**
Orthoclase	Light color, euhedarl to subhedral in shape; elongated and rectangular shaped crystals are also observed. Size ranges from <1mm to 8 mm along the maximum length and <1mm to 2mm width. Generally the samples show minor sign of alteration along the margins and sparsely within the Phenocryst itself. In some cases the cleavage direction are not clearly visible due to the composite effect of included lithic fragments and alteration effect. Oscillatory zoning is also observed in one thin section (MWNS1). In addition, pokioclasts of pyramid shaped zeolite mineral with 2mm diameter is observed.
Quartz	It is generally fine grained in size, generally unhedral in shape, showing light color and randomly oriented, served as Pokioclast within the lithic fragments.
Rock fragments /Lithic fragments	These vary in shape and size with numerous included crystals of orthoclase, quartz, minor sanidine and opaque. Theses crystals serve as pokiolites. It shows irregular to sub-rounded and occasionally elongated shape; no deformed lithcs. It ranges from <1mm to 4mm in size; with sign of alteration along the boundaries.
Volcanic glass	Volcanic glass is the matrix in which the large alkali feldspar grains, quartz, opaque minerals as well as minor constituents and lithic fragments are set. It shows flow banding structures elongated along one direction. It is devoid of pokioclasts. It is light color in PPL and dark under XPL. The fiammes show sigmoidal geometry. In addition, the directional arrangement of fiammes indicates post-eruptive welding effect during pyroclastic flow.
Plagioclase	Light in color, shows multiple twinning, perfect cleavage, subhedral in shape, 4mm along the longest dimension and 2mm width, no fracture and shows oscillatory zoning.
Zeolite	Small in %, light green in color, shows radiating pattern starting from one center/apex and rounding in the base with 2mm basal diameter. It is unaltered and not common.
Microcline	Light in color, small in size and elongated in shape, perfect cleavage, crosshatch twining and slightly altered.
Opaque	Are minor constituent in the samples, <1mm in length, some of them are irregular in shape, and dark in both XPL and PPL.
Others	In addition to the above components minor amount (2%) of pyroxene and hornblende are observed.

3.1.10. Clay

Primary clay deposits are exposed in the upper part of the study area forming laterally non continuous 0.3m thick layer found interbeded between moderately welded ignimbrite layers and underlying weathered ash layer. This layer contains fine grained and well-sorted clay. Generally similar but with slight reworking is found below the uniformly sorted clay layer at the lower stream localities. This layer contains some basalts and ignimbrite clasts with random orientation. This layer is found near the base in MW5, MW5-N and in MW5-E but it is deposited below the cap layer of the relatively thicker section exposed in MW5-N3, indicating layers between the grayish ash and the reworked clay are missed before deposition of this layer.

3.1.11. Reworked Pyroclastic Products

Reworked pyroclastic deposit is exposed only in the lower stream localities (Fig. 3.11). This unit consists mainly of pumice clasts ranging in size from <1cm to 20cm, together with generally less sand grains, silts and minor basaltic as well as ignimbrite pebbles. The pumice clasts are sub-angular to sub-rounded, non-sorted. In addition, specific dense accumulation of large pumice clasts is observed in particular sites. The field evidences, including the mixed-up nature of the constituents of the unit suggest that this layer is formed from re-deposition of transported pumice fragments as well as other rock fragments and sediments. In addition, cross bedding structures are observed in two parts of MW7-S locality forming angular unconformities reflecting the pumiceous reworked layer is deposited at different stages of deposition. The non-welding, laterally non-uniform thickness and the non-sorting of the clasts in this layer indicates the absence of primary depositional magmatic process, and confirms the reworked nature of this unit.

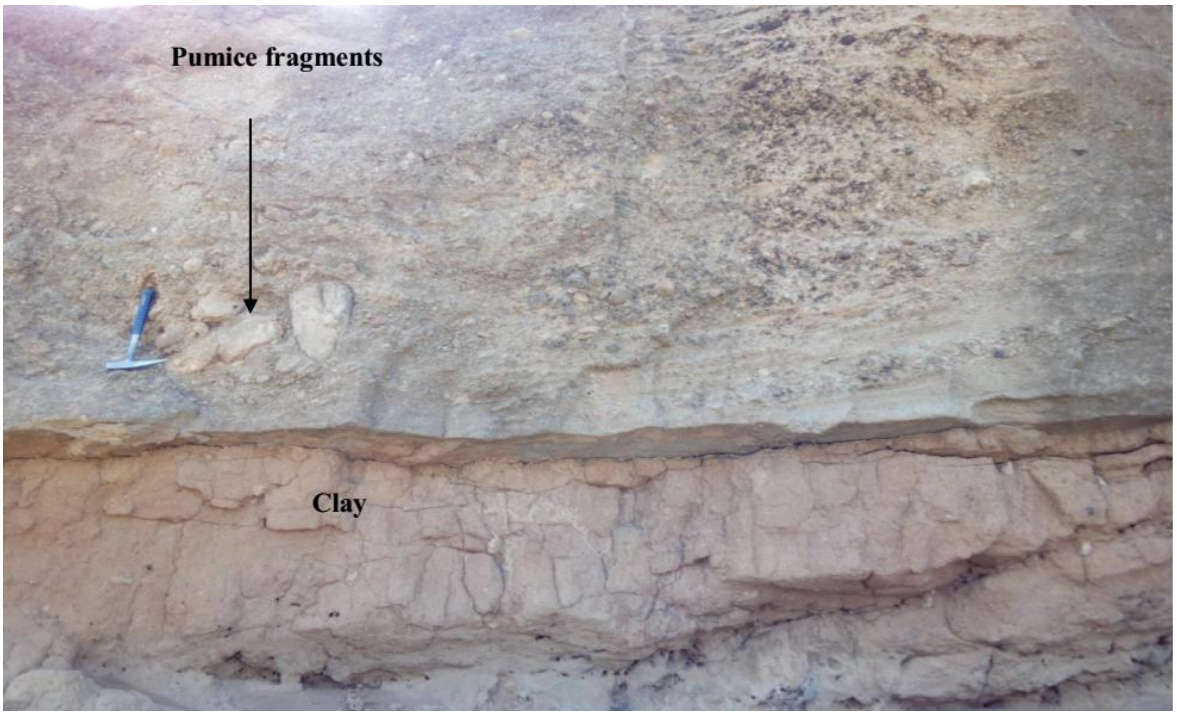

Figure 3.11. *Pumice rich reworked layer and clay (X-529569 Y-783561 Z-2330). Pumice clasts are showing high concentration in specific points suggesting the separation of theses light density materials from the crystal rich ash either during reworking.*

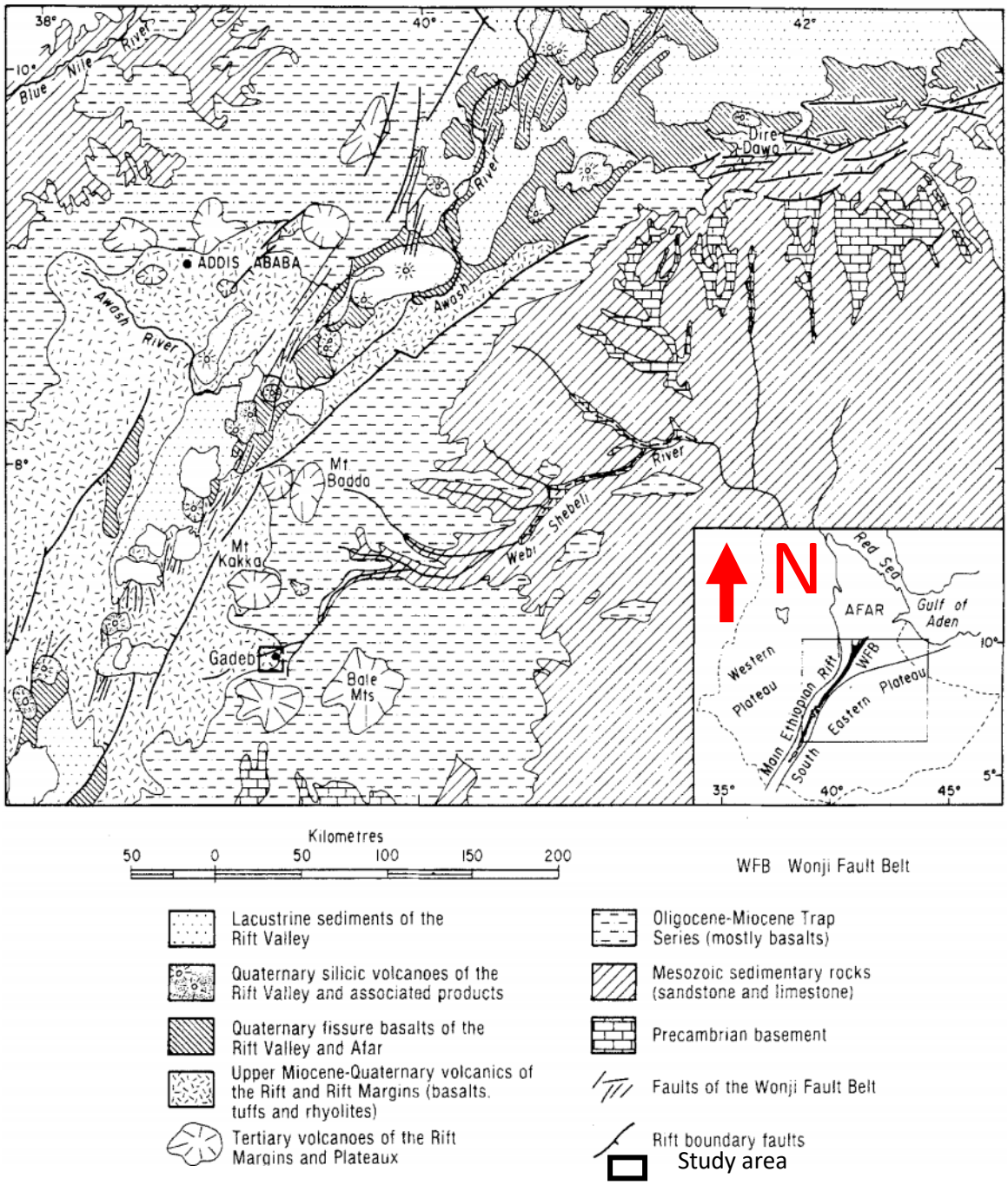

Figure 3.12. Geological map of central main Ethiopian rift after Eberz et al. (1988).

3.2. Contact Relationships

The sedimentary and volcanic layers show different types of contact relationships reflecting complex depositional histories.

Sharp/Abrupt contact: In the upstream locality, the contacts between the bluish, light grayish weathered ash, moderately welded ignimbrite and ignimbrite boulders are sharp.

The bluish ash is interbeded between fine-grained unwelded ash layers forming abrupt contact. But this relation is laterally extended for short distances of ~10m. In addition, both moderately welded ignimbrite layers show abrupt contact with both the overlying and underlying layers. In this case upper ignimbrite layer is separated from the underlying thin grayish ash layer without any gradation or intercalations. Moreover, the lower ignimbrite layer found between the clay and ash layers even clearly shows abrupt lithological (compositional and textural) changes. The layer of ignimbrite boulders is interbeded between ashes layers of separate textural as well as compositional characteristics and show sharp contacts. In the downstream locality, the light bluish, deep blue ash layers, conglomerates as well as reworked sediments and fine grained clay show sharp contacts, where the layers are also relatively laterally extensive.

Gradational contact: The volcano clastic sediments, pumiceous ashes, light bluish lapilli ash and the unwelded ash layers show gradational contacts (Fig. 3.13). The sandy layers on MW2 show fining upward whereas the conglomerates are consisting of grains in a disturbed orientation. Pumiceous ash exposed only at the upstream locality also shows gradation in the distribution of pumice grains with fining upward in the sequence. In MW5-N1, the smoky lapilli ash grades to the silty ash and finally to more compacted ashy layer with weathered upper surface.

Figure 3.13. *Gradational contact relationship exposed on MW5-N1 section (X-0529603 Y-783356 Z-2328).*

Intercalation: In some of the localities, particularly in MW2 locality, fine-grained sandy conglomerates and the breccias layers are alternating with the ash deposits (Fig.3.2). In addition, ash layers in MW5-N, MW5-N1, and MW5-N2 consist of very fine ash and light bluish lapilli ash intercalations (Fig. 3.14).

Figure 3.14. *Intercalation of lapilli and smoky ash layers from MW5-N1 (X-0529603 Y-783356 Z-2328).*

Pinch outs: In the upstream locality, the light bluish ash, welded tuff and unwelded ash layers, and in the downstream locality, the different ash verities forming cross beds in the reworked pumice rich cape layer show some angular contact relationships due to some pinching out features (Fig. 3.15).

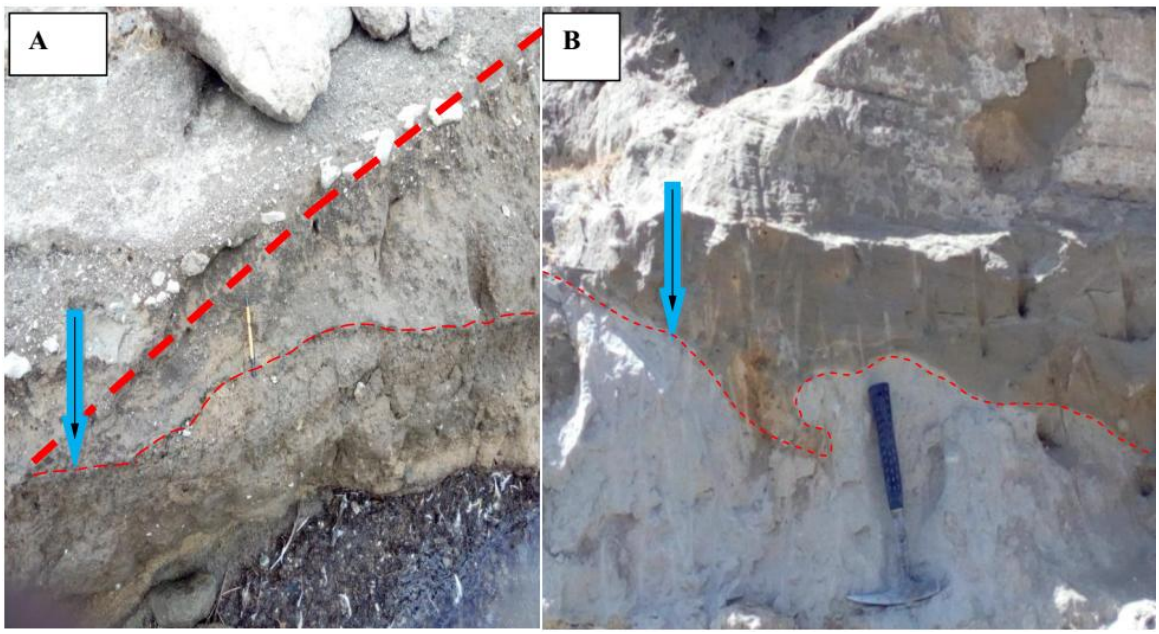

Figure 3.15. Pinch out contacts; (A) Pinch out in the ash layers of different varieties (X-0528726 Y-0782120 Z-2321). (B) Pinch out between slightly reworked lapilli ash and fine grained smoky ash (X- 0528667 Y- 0782148 Z-2326).

Erosional contact: Many layers are absent laterally indicating significant post-depositional erosion. Erosional contact is observed between the basal welded tuff and the underlying fine-grained light grayish unwelded ash layer. This layer is overlain by ignimbrite pebbles, cobbles and boulders having different shape and fabric and on top of a conglomerate layer. In the downstream locality ignimbrite boulders having similar characteristics are also dislodged from the layer in the stratigraphy and transported as well as deposited at the base of the stratigraphy. At MW2, lower ignimbrite, weathered ash and upper ignimbrite layers are missing suggesting their post-depositional erosion.

Figure 3.16. *Welded tuff and unwelded ash with an erosional contact.*

3.3. Geological Structures

The major structures observed in the area are primary depositional (bedding, cross-bedding, lateral pinch outs) as well as erosional.

3.3.1 Primary Horizontal Bedding

Most of the units are horizontally bedded, except some units at the top of the section, which show some dipping and irregular, non-continuous layers (Fig. 3.17). More specifically, the unwelded ash layer at the bottom of the sections and the crystalline ignimbrite layer in the Dodola area (MWD) and glassy ignimbrite in the Kawa River are perfectly horizontally layered though the overlying layers show less irregular morphology due to post-depositional erosion. The unwelded tuff at the base of the section is used as marker horizon to correlate the sections and interpret the depositional history of the deposits. The fact that the conglomerate, reworked clay and reworked pumice rich layers are dipping have a direct contact with the bottom layered light grayish un welded ash suggest the removal by erosion of the intermediate layers. The lateral non-continuity of many of the layers in the studies localities makes the correlation and interpretation of the depositional history complicated.

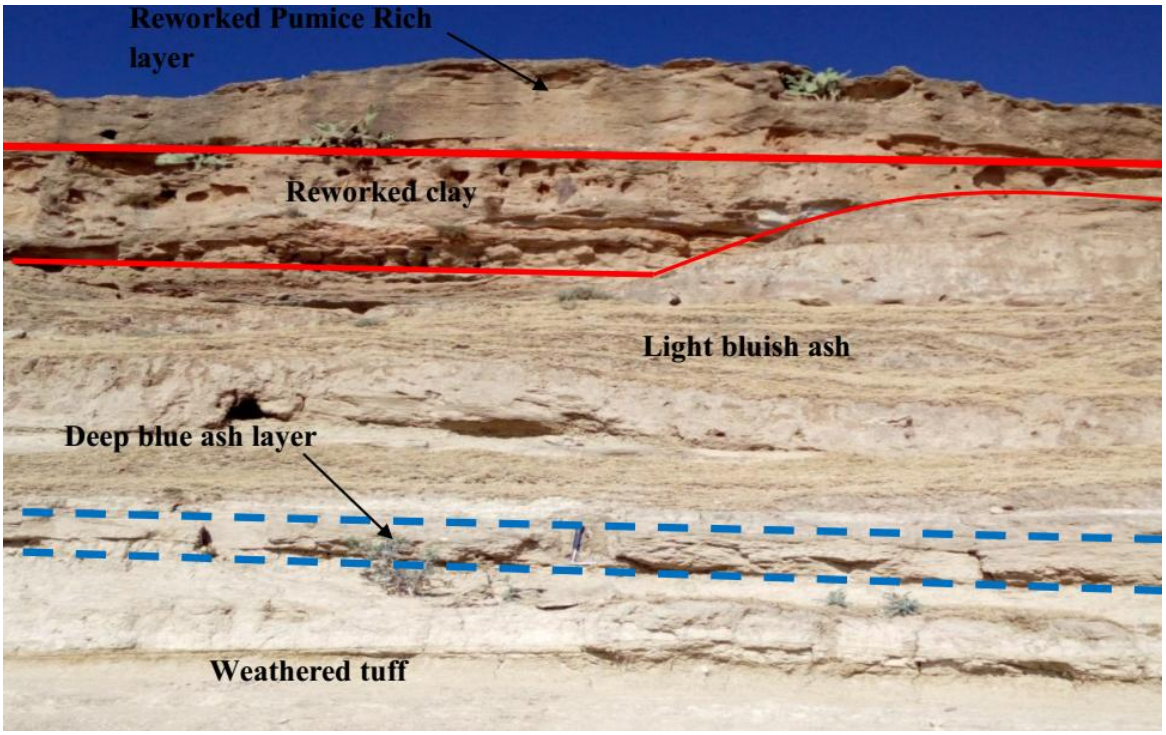

Figure 3.17. *Horizontal beddings from MW5-N3 (X-0529569 Y- 0783561 Z-2330) exposed in the downstream localities showing horizontal layering of the reworked as well as primary fall deposits except dipping of the upper most layers.*

3.3.2 Cross Bedding

Cross bedding structures are visible on the top layer of downstream localities particularly at MW7-S section in which pumice fragments and sandy grains are common (Fig. 3.18). These structures observed at two parts of the upper layer dip towards NW. The sharp contrast between the cross-bedded and the horizontal pumice rich layer might indicate deposition of these materials on an erosional surface of the horizontally bedded layer. The cross bedding at MW7-S1 is oriented at N255E/60NW, while the one at MW7-S2 is oriented at N330E/45SW.

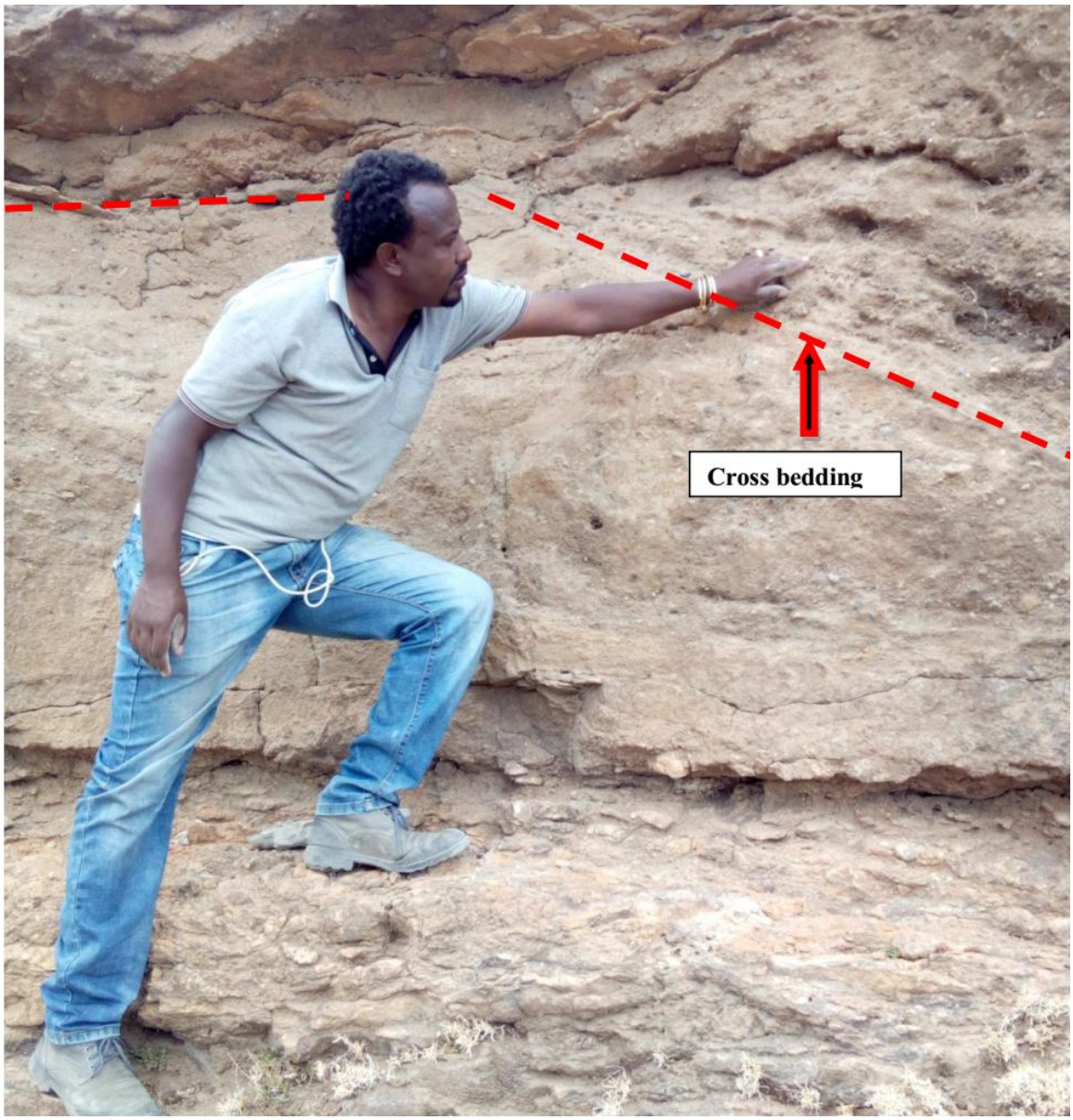

Figure 3.18. *Cross bedding structure at MW7-S (X-0529695 Y- 783700 Z-2325) on pumice rich reworked layer.*

3.3.3 Structural Pinch Outs

This structure is observed in MW8 locality between the welded tuff and underlying light grayish weathered ash as well as in MW11 between light grayish and light brownish ash (Fig. 3.19). These structures are erosional surfaces formed on underlying layers before the deposition as well as subsequent erosion of the top layer, subsequent to former river flows orthogonal to the layers. The pinch out in MW11 is described by N210E/25NW. In addition, in MW8 locality, the pinch out is oriented at N320E/35SE. The pinch outs are observed only on the upper stream localities (See fig.3.15.).

3.4. Stratigraphic Logs and Local Correlation

Stratigraphic logs were constructed in localities where clear exposures and relatively thicker sections are available. Seventeen lithologic/stratigraphic logs were constructed in the field. As the area is characterized by significant lateral variability (non-uniform thickness varying from 0.05 to 3.5m, pinching out features, non-continuity of units, etc.) the sections were constructed at about 10 to 20m distance from each other in order to account for the complex depositional history of the area. The area is further sub-divided in two localities: Locality 1 (upstream locality) where logs MW1, MW2, MW3, MW8, MW9, MW9-S, MW10, MW11 and MW12 are constructed (Fig.3.20.) and Locality 2 (downstream locality) where logs MW5, MW5-E, MW5N, MW5N1, MW5-N2, MW5-N3, MW7-S and MW7 are constructed (See Fig. 3.21).

3.4.1. Upstream Locality

In this locality the constructed stratigraphic logs are correlated based on textural and compositional similarity and their relative position in the sequence, though the complex depositional history of the basin as manifested in the significant lateral and vertical variability of the sequences makes correlation difficult. This section is consisting of different units ranging from weathered unwelded ash at the base overlain by welded tuff and 0.7m thick fine grained blue ash at the top, with numerous volcanic, volcanoclastic, and sedimentary units in between (Fig. 3.20.).

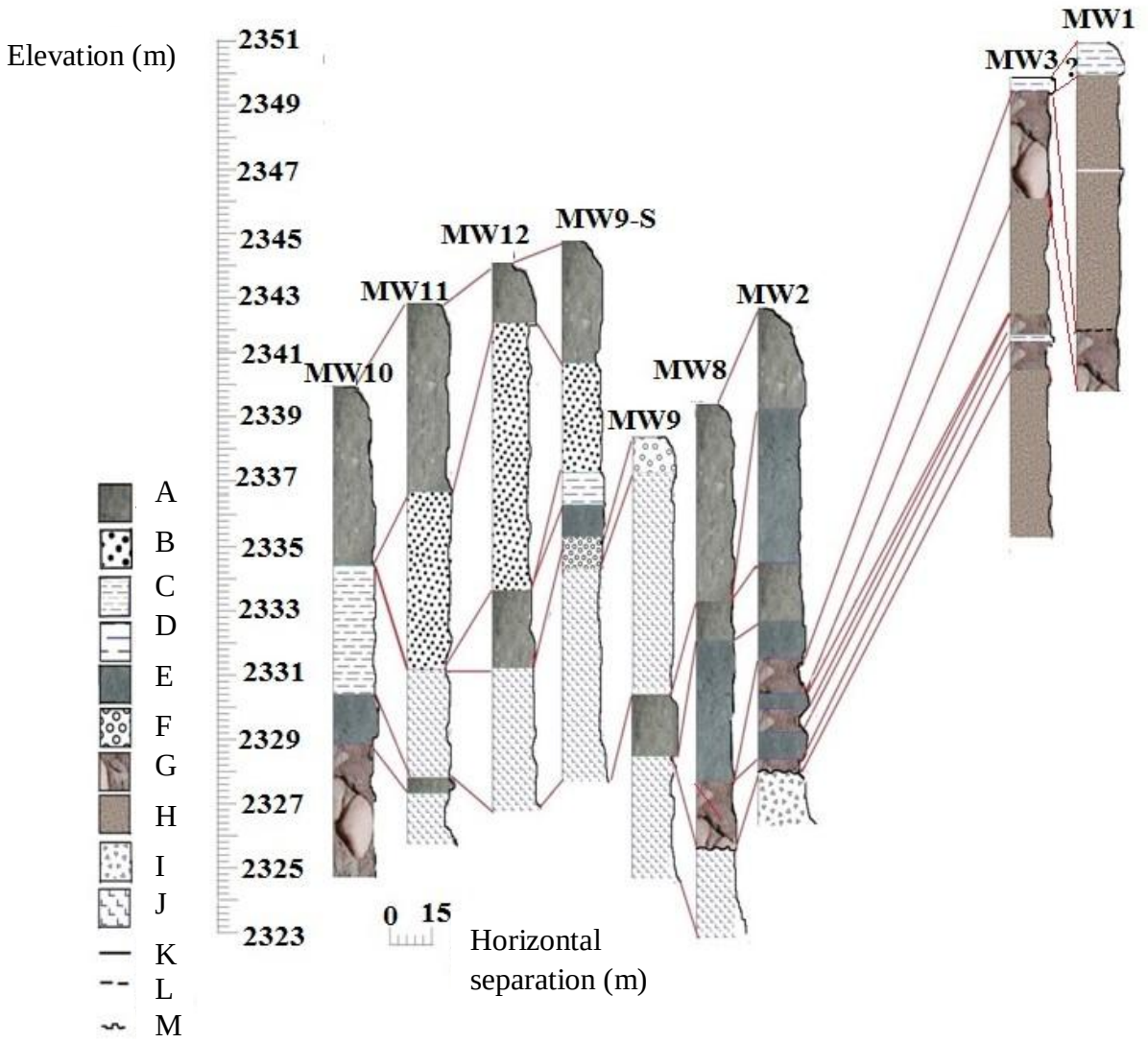

Figure 3.20. *Correlation chats of the stratigraphic logs in the upstream localities: (A) Moderately welded ignimbrite;(B) Pumiceous layer; (C) Clay (D) Blue ash layer;(E) Ash flow;(F) Ignimbrite boulders; (G) Conglomerate; (H) Sand; (I) Welded tuff and (J) Unwelded ash; (K) sharp contact;(L) Gradational contact; (M) Erosional contact. Vertical scale is elevation and horizontal scale represents lateral separation among the log locations.*

3.4.2. Downstream Locality

The downstream locality stratigraphic logs were correlated similarly. In this locality, the succession is about 25m thick above the River water level (Fig. 3.21). The composite section shows succession of conglomerates and breccias, thin layer of light yellowish relatively weathered ash (unwelded tuff), ignimbrite boulders, deep blue as well as light blues ashes of different verities, reworked clay with numerous conglomerates, fine grained non reworked clay and thick reworked pumice rich layer.

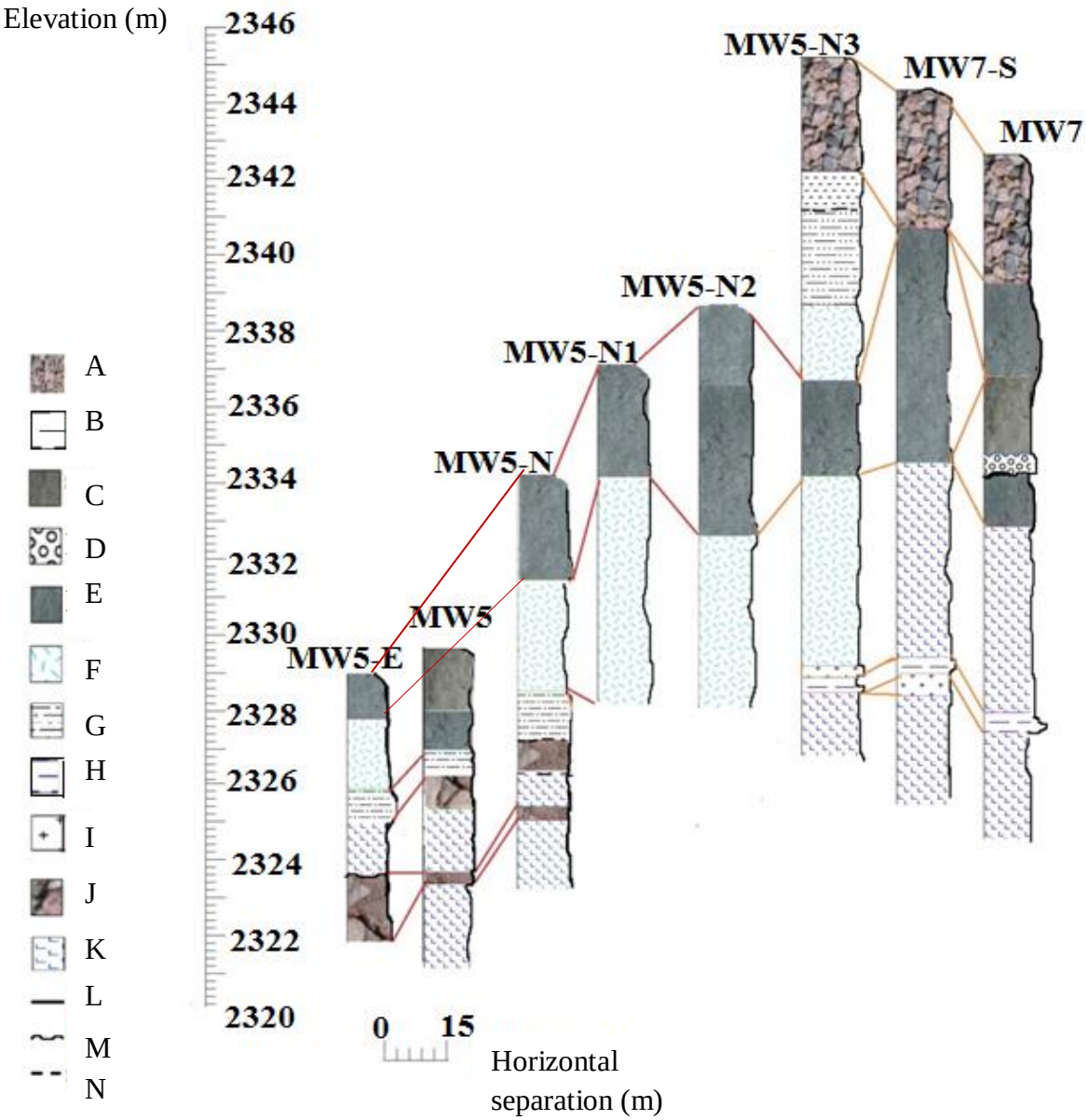

Figure 3.21. *Correlation charts of the stratigraphic logs in the downstream localities :(A) Reworked pumice rich layer ;(B) Clay; (C) Moderately welded ignimbrite; (D) ignimbrite boulders; (E) Silty ash;* (F) Lapilli ash; (G) Reworked clay; (H) deep blue ash; (I) Weathered ash; (J) Conglomerate (K) Unwelded ash; (L) Sharp contact; (M) Erosional contact; (N) Gradational contact.

CHAPTER FOUR

GEOCHEMISTRY

4.1. Introduction

Many petrogenetic studies in the rift as well as adjacent plateaus involve the use of geochemical data to discriminate the petrogenetic processes (e.g., Gasparon et al., 1993; Dereje Ayalew et al., 1999; 2002; 2006; Tura et al., 1999; Dereje Ayalew, 2000; 2011; Giordano et al., 2014). Major elements, trace elements and isotope data as well as volatile behavior in magmas have been used for petrogenetic studies (Rollinson, 1993; Trua et al., 1999; Dereje Ayalew et al., 2006). In this study only major and trace element data as well as volatile contents (as inferred from Loss on Ignition; LOI) have been used to understand the evolution of the pyroclastic rocks.

4.2. Methodology

A total of thirteen samples (Four ash flow, five ash fall, three ignimbrites and one pumiceous ash) were selected for whole rock geochemical analysis based on their stratigraphic position, physical properties and based on hand specimen as well as petrographic description. These samples largely represent the lithological distribution in the study area. Sample preparation has been conducted in Addis Ababa University School of Earth Sciences crushing and milling room and gets analyzed in the Australian laboratory Science (ALS) in Ireland. Major elements were analyzed using Multi-Element Inductively Coupled Plasma06 (ME-ICP06) whereas trace elements were analyzed using Multi-Element Mass Spectrometry81 (ME-MS 81) techniques. The detection capacity of the method ranges between 0.01 and 100% for major elements and generally 0.01 to 10,000ppm for trace elements except for Cr (10-10,000ppm) and V (5-10,000ppm). In addition, the instruments are also sensitive for lose on ignition ranging between 0.01 and 100%. The used standards are lithium borate fusion for resistive elements, four acid digestions for base metals, and aqua regia for volatiles. Here only Cr in the rhyolites is reported less than the detection limit (<10ppm) whereas the others are above the sensitivities of the instruments. TAS classification, K_2O vs SiO_2 classification, feldspar classification, REE spider plot and multi element variation diagram is constructed using geochemical data kit (GCDKit version 3.2.0) software (*http:// www. gsdkit.org*) whereas

the Major and trace element Harker diagram, subalkaline-peralkaline and pantellerite–comendite classification diagrams are plotted using Microsoft excel 2007. Besides, mass balance calculation, and modeling operations are facilitated using Petrographic 2 beta software version 1.0.2 (see Fig.6.1.).

4.3. Results

The analysis results are given in Table 4.1. Three rhyolitic ignimbrite samples have < 5% LOI, four rhyolitic ash, one pumiceous ash and four dacite ash flow samples have 5 - 10% LOI, and one dacite sample has a high LOI value (13.5%). Following these results the data is recalculated, structured and presented on volatile-free base required for interpretation. Hence, the calculation is conducted by normalizing the values of the oxides to 100% after removing the volatiles. All diagrams, descriptions and interpretation are according to the recalculated results presented in Table 4.1. The empty spaces represent values below the sensitivities of the instruments (below the detection limit).

Table 4.1 Geochemical data for thirteen samples (13) recalculated by removing lose on ignition values required for volatile free base interpretations.

	MW2-G10	MW2-G16	MW2-G19	MW3-G3	MW3-G7	MW5-5	MW5-7B	MW7-4	MW9-S7	MW9-S9	MWD2-D	MWNS-1	MWNS-5
SiO_2	70.98	66.65	75.14	75.61	75.4	70.94	69.55	71.51	74.29	70.76	73.47	73.34	73.9
TiO_2	1.14	0.92	0.22	0.43	0.27	1	0.89	0.35	0.44	0.35	0.41	0.41	0.34
Al_2O_3	13.01	16.92	11.74	10.45	8.86	14.18	14.89	11.94	10.15	13.94	10.34	10.23	11.32
Fe_2O_3	5.5	8.06	4.11	6	7.87	6.33	5.97	6.28	6.42	4	5.68	5.85	5.09
MnO	0.17	0.25	0.15	0.19	0.28	0.9	0.13	0.67	0.25	0.11	0.23	0.24	0.17
MgO	0.44	1.95	0.2	0.14	0.11	0.89	0.87	0.12	0.21	0.72	0.16	0.15	0.17
CaO	1.44	1.3	0.38	0.46	1.05	1.14	1	0.73	0.43	1.41	0.32	0.31	0.52
Na_2O	3.13	1.17	2.91	2	1.49	2.28	3.02	2.1	2.21	2.97	4.69	4.41	3.02
K_2O	4.14	2.68	5.13	4.68	4.65	3.09	3.56	6.28	5.54	5.69	4.65	5.02	5.42
P_2O_5	0.04	0.08	0.02	0.04	0.02	0.08	0.13	0.02	0.06	0.05	0.05	0.04	0.04
Total	99.99	99.98	100	100	100	100.83	100.01	100	100	100	100	100	99.99
LOI	6.82	13.5	6.1	6.75	8.46	10.55	7.65	7.37	7.2	6	0.88	3.02	5.74
Sc	4	11	5	1	1	8	7	1	7	3	5	5	6
V	19	66	7	10	12	57	43	16	17	13	9	6	8
Cr	10	70				30	20				10		
Ni	9	57	5	2	2	16	16	5	3	10	4	3	3
Rb	76.7	100.5	105	113.5	147.5	77	79.8	140.5	91.5	83.3	113.5	112	137.5
Sr	105	120.5	24	46.8	41.4	138.5	186.5	19	22.1	122	16.7	11.6	59.6
Y	84.6	68.2	112.5	112	193	81.8	83.8	119.5	117	118.5	123	135.5	110
Zr	926	662	1050	1040	1850	854	882	1250	961	979	1180	1190	127
Nb	130	87.2	124.5	136.5	225	97.2	102.5	157	125	127	149	151	142
Cs	259	157.5	210	252	402	186	196.5	269	293	246	276	273	272
Ba	659	321	38.2	272	242	342	452	239	80.7	678	163.5	93.4	160.5
Hf	21.2	15.7	24.2	26.1	43.9	18.6	20.2	28.7	22.6	24.3	28.8	27.8	27.3
Ta	7.1	5.8	8.2	9.1	15.7	6	6.5	10	8.2	8	10.3	10.4	9.2
La	130.5	77.5	99.9	120.5	188.5	90.3	103	134.5	122	136.5	133.5	133	132

Ce	259	157.5	210	252	402	186	196.5	269	293	246	276	273	272
Pr	30.2	18.3	25.3	29.2	47.9	21.3	23.9	30.5	30.1	33.2	33	32.3	30.8
Nd	130	87.2	124.5	136.5	225	97.2	102.5	157	125	127	149	151	142
Sm	21.3	13.45	20.7	23.6	38.2	16.7	17.7	22.9	22	26.1	26.3	25.7	21.5
Eu	3.39	1.95	1.77	3.62	5.97	2.76	3.07	2.08	3.7	3.71	3.63	3.84	2.67
Gd	17.6	11.75	18.4	21.7	34.8	14.25	15.6	20.3	19.25	22.1	23	23.8	18
Tb	2.62	1.96	3.06	3.5	5.56	2.35	2.46	3.35	3.15	3.58	3.75	3.93	2.99
Dy	15.35	11.75	18.45	20.6	33.8	14.35	14	20.4	19.7	21.6	23	24.1	18.5
Ho	3.08	2.41	3.81	4.17	6.82	2.81	2.81	4.2	3.92	4.21	4.33	4.7	3.83
Er	9.17	6.94	11.8	11.95	19.8	8.32	8.1	12.4	12.1	12.15	13.75	14.05	11.4
Tm	1.3	1.08	1.67	1.84	3.02	1.28	1.24	1.99	1.92	1.85	1.97	2.18	1.76
Yb	8.14	6.85	10.9	10.9	18.4	7.82	7.69	11.6	11.65	11.6	12.5	12.5	11.15
Lu	1.28	1.1	1.69	1.63	2.73	1.19	1.2	1.83	1.8	1.78	1.86	1.97	1.72
Pb	21	23	20	22	26	20	15	29	15	12	24	24	25
Th	11.9	13.55	15.2	16.4	25.9	11.75	11.8	18.5	12.65	12.4	16.1	15.5	18.1
U	2.45	1.64	4.12	4.61	7.26	2.13	2.77	4.54	3.88	3.16	2.7	4.32	5

4.3.1. Major Element Variations

Major oxides in wt % are plotted versus SiO_2 in wt % as the index of differentiation on Harker diagrams. This helps to visualize the property of those oxides as the function of the greater silica variability in felsic magmas (Rollinson, 1993). As shown in Table 4.1 and Fig. 4.1, the rhyolite ignimbrite samples have comparatively low concentration of Al_2O_3 (8.86-11.74 wt%) and CaO (0.31-1.14 wt%). Generally Al_2O_3 and MgO show decreasing trend with increasing silica content whereas an increasing trend is observed in K_2O from 2.68 wt% in dacite to 6.28 wt% in rhyolite. Al_2O_3 decreases from 16.92-13.01 wt % in dacite samples to 8.86 wt % in rhyolite ash fall and ignimbrite samples. MgO decreases from 1.95 wt% in dacite to 0.11 wt % in the rhyolite. On the other hand, CaO, MnO, and Fe_2O_3 display scattered distribution. Na_2O increases from 1.17-3.56 wt % in dacite to 4.68 wt % in rhyolite ignimbrite and decreases until 1.49 wt % in rhyolite ash fall deposit. Even though, Fe_2O_3 generally shows scattered values it reflects decreasing trend in a separate dacite as well as rhyolite ignimbrite samples and increasing in the rhyolite ash fall products. The Harker diagrams also show the range of clustered concentration in TiO_2 (0.89-1.14 wt % to 0.22- 0.44 wt %) and MnO between 0.13-0.0.9 wt% in dacite to 0.15-0.67 wt% in the rhyolite. The concentration of TiO_2 shows comparatively higher values (0.89- 1.14 wt% in the dacite ash flow) and markedly decreases (0.2-0.44 wt %) in the rhyolite ash as well as ignimbrite samples. The concentrations of P_2O_3 through the entire samples generally show systematic variation from 0.13wt% in dacite ash flow to 0.02 wt% in rhyolite ash.

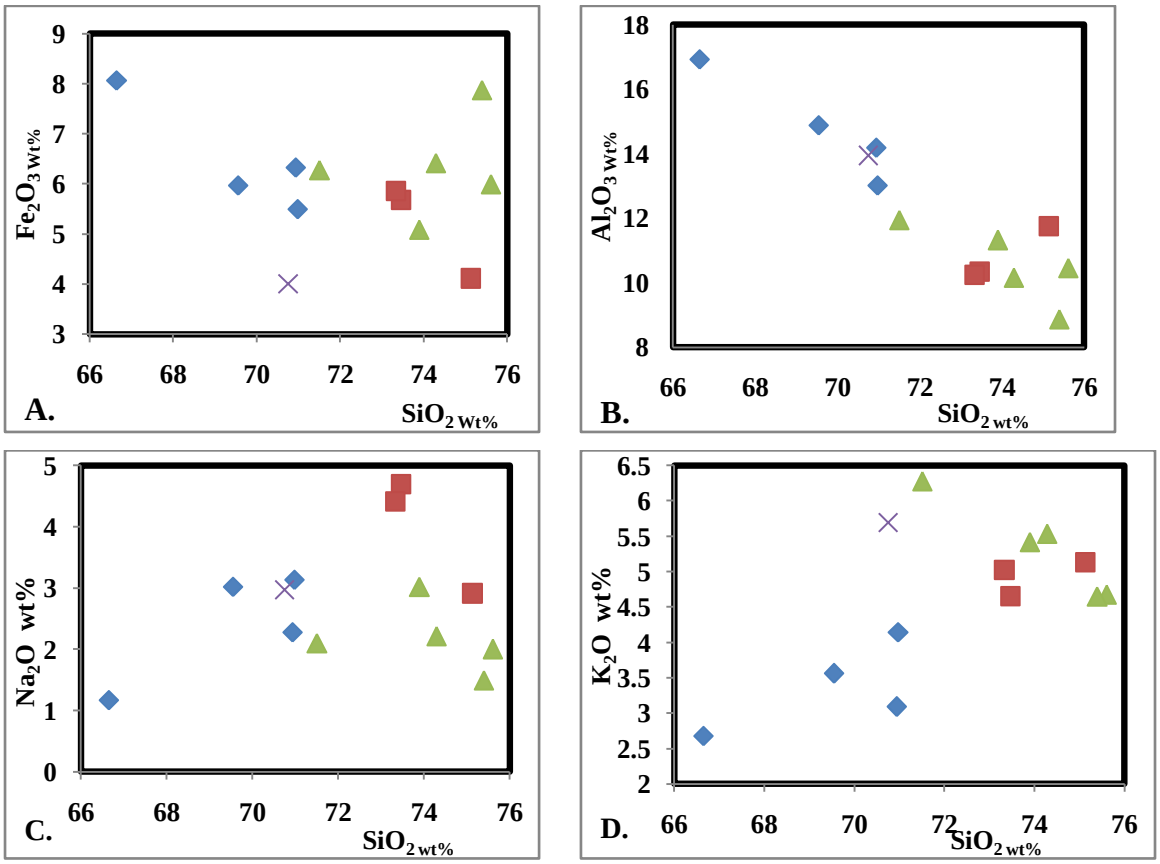

Figure 4.1. *Weight percent (wt %) of major oxides vs SiO_2 suggesting the behavior of major oxides during magmatic process. Vertical axis represents wt % of major oxides where as wt% of silica in the horizontal axis is used as differentiation index. P/ash refers to pumiceous ash.*

4.3.2. Classification using Total Alkali Silica (TAS)

Based on TAS classification scheme adopted from Le Bas et al. (1986) all the samples constitute > 66 wt % of SiO_2 in which ten samples (K_2O+Na_2O= 6.68-9.48 wt%) fall in the rhyolite field whereas the remaining three (K_2O+Na_2O= 3.85-6.58 wt%) are dacite (Fig. 4.2A). Even though, all the samples are plotted below the line separating sub-alkaline from alkaline series rocks, pumiceous ash and rhyolite of two of the welded ignimbrite samples are close to the transition line where as the moderately welded rhyolite ignimbrite is entirely below the line (Fig. 4.2).

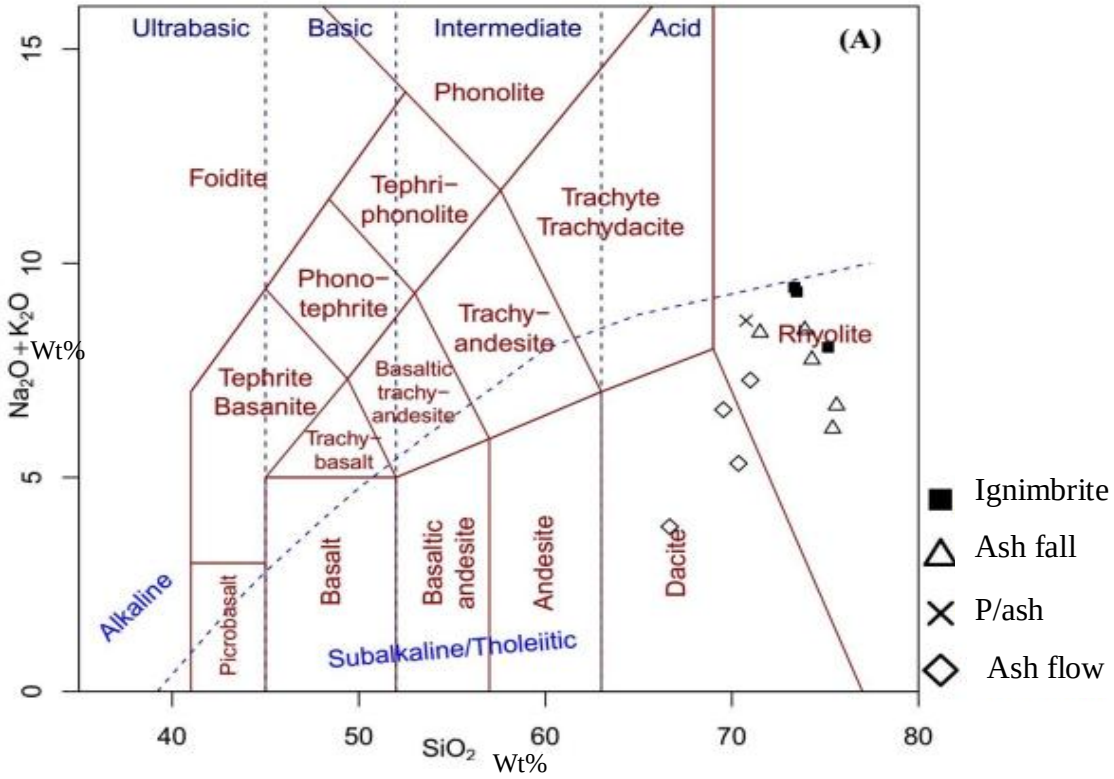

Figure 4.2. *TAS classification diagram showing classification of Melka Wakena silicic rocks based on their total alkalinity and silica variation (LeBas et al., 1986);*

Agpaitic plots based on the molecular ratio of Al_2O_3 to the sum of total alkalis vs SiO_2 shows most of the samples fall within the peralkaline field (1.04-3.51), in which two of the ignimbrite samples (0.805-0.811) values are plotted in the subalkaline field close to the line (Fig 4.4A). Even though most of the samples are plotted in the peralkaline field, the dacite samples are comparatively highly peralkaline with high agpaitic index values compared to the other samples. Additional classification is performed to understand the entire chemistry of the subalkaline- peralkaline rhyolite and dacite samples as the function of their Al_2O_3 and Fe_2O_3 contents (wt%). Accordingly, one ignimbrite rhyolite sample is pantellerite trachyte and three dacite samples are comendite trachyte. In addition, one dacite and one rhyolite ash fall samples are comendite whereas the remaining two rhyolite ignimbrites and four ash fall rhyolite samples are entirely pantlleretic rhyolite (Fig 4.3B).

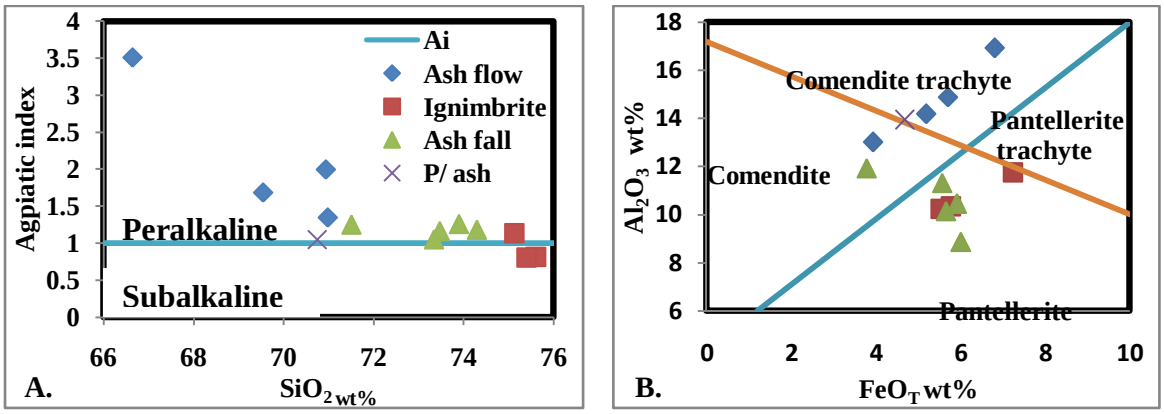

Figure 4.3. *Binary classification plots: (A) classification of the rocks based on agpaitic index (molecular proportion) as the function of wt% of SiO_2 (LeBas et al. 1986); (B) Classification of rhyolite and dacite rocks based on their proportion of Al_2O_3 and Fe_2O_3 (Mac Donald, 1974); L1-line separating the field of pantellerite from comendite and comendite trachyte; L2-line separating comendite trachyte as well as pantellerite trachyte from comendite and pantellerite fields; Ai - Agpaitic index line separating the field of subalkaline from peralkaline field.*

Agpaitic index is calculated using the formula {molecular (Al_2O_3/Na_2O+K_2O)} Boccalleti et al. (1999). Hence, the plot is conducted based on Agpaitic index versus silica following LeBas et al. (1986). Normative calculation is also conducted using CIPW (Cross, Iddings, Pirrson and Washington) norm to constrain the normative and volumetric composition of the samples in the TAS classification scheme. Thus, the major normative minerals are quartz, plagioclase, and orthoclase with accessory minerals such as corundum, hypersthene, rutile, and hematite. The normative analysis for all samples give 15.85-46.5 normative wt% values and 18.18-43.99 wt% volumetric modal ranges and generally less than 10 % normative values for the accessory minerals in the case of dacite. On the other hand, ignimbrite rhyolite samples are consisting of compositional ranges of 24.6-37.39 normative wt% and 25.67- 37.87 volumetric percentage for the normative minerals and with less than 6 wt% in accessory phases. In the pantelleretic ash, it ranges from 16.25 to 44.69 normative wt% and 16.8-45.9 volumetric percentages with generally less than 8 wt% of accessory minerals. Besides, the comendite to comendite trachyte ash flow samples are within the range of 15.83-43.83 wt% of the normative minerals and less than 8 % accessory phases. The normative mineralogy is used to classify the rocks based on the normative minerals. Accordingly, in a feldspar classification diagram (Fig 4.4) two of the dacite flow and all of the rhyolite deposits fall in the rhyolite field representing more than 50% orthoclase feldspar, agreeing with the dominance of orthoclase phenocrysts observed on thin sections.

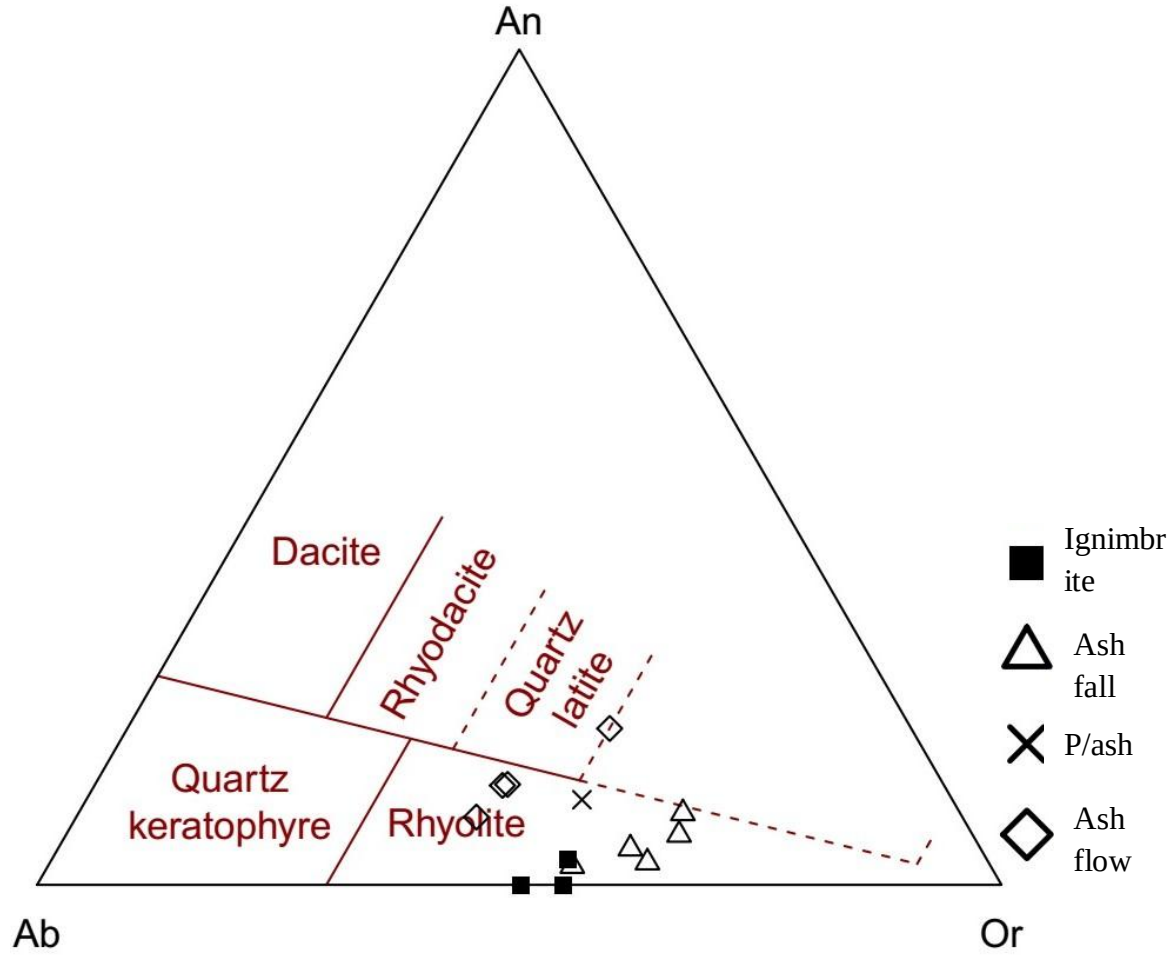

Figure 4.4. *Feldspar classification scheme based on O'Connor (1965). P/ash represents pumiceous ash.*

4.3.3. Trace Element Variations

The compatible element versus silica plot is constructed taking compatible elements (Ni, Cr, Sc, V and Sr) on the vertical axis and silica as index of differentiation. Accordingly, all of the compatible elements except Sr show decreasing trend although minor dispersion is observed in Sc vs silica plot. Sr versus SiO_2 Harker plot shows systematic variation. In the case of Ba it shows increasing trend until 69.55 wt% of SiO_2 in the dacite and sharply decreases until 73.4 wt% of SiO_2 in the rhyolite ignimbrite as well as ash fall deposits. Even though an inflection trend is obvious in two ash fall and flow deposits, one ash flow layer and the pumiceous layer do not fit to the inflected trend.

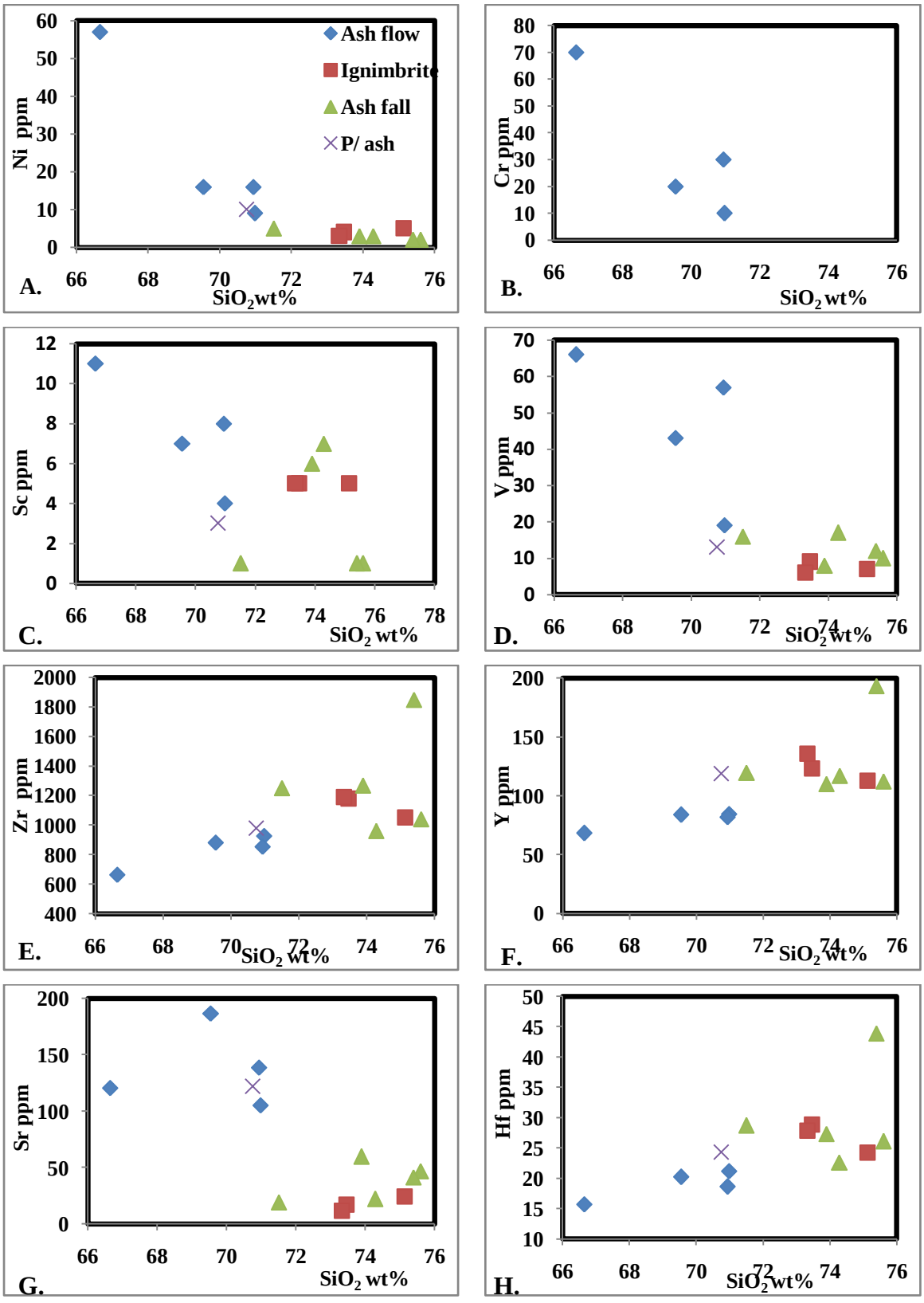

Figure 4.5. *Trace element Harker diagrams showing the variation of compatible and incompatible elements as the function of silica variation. All trace elements are in parts per million (ppm) and silica is in wt %.*

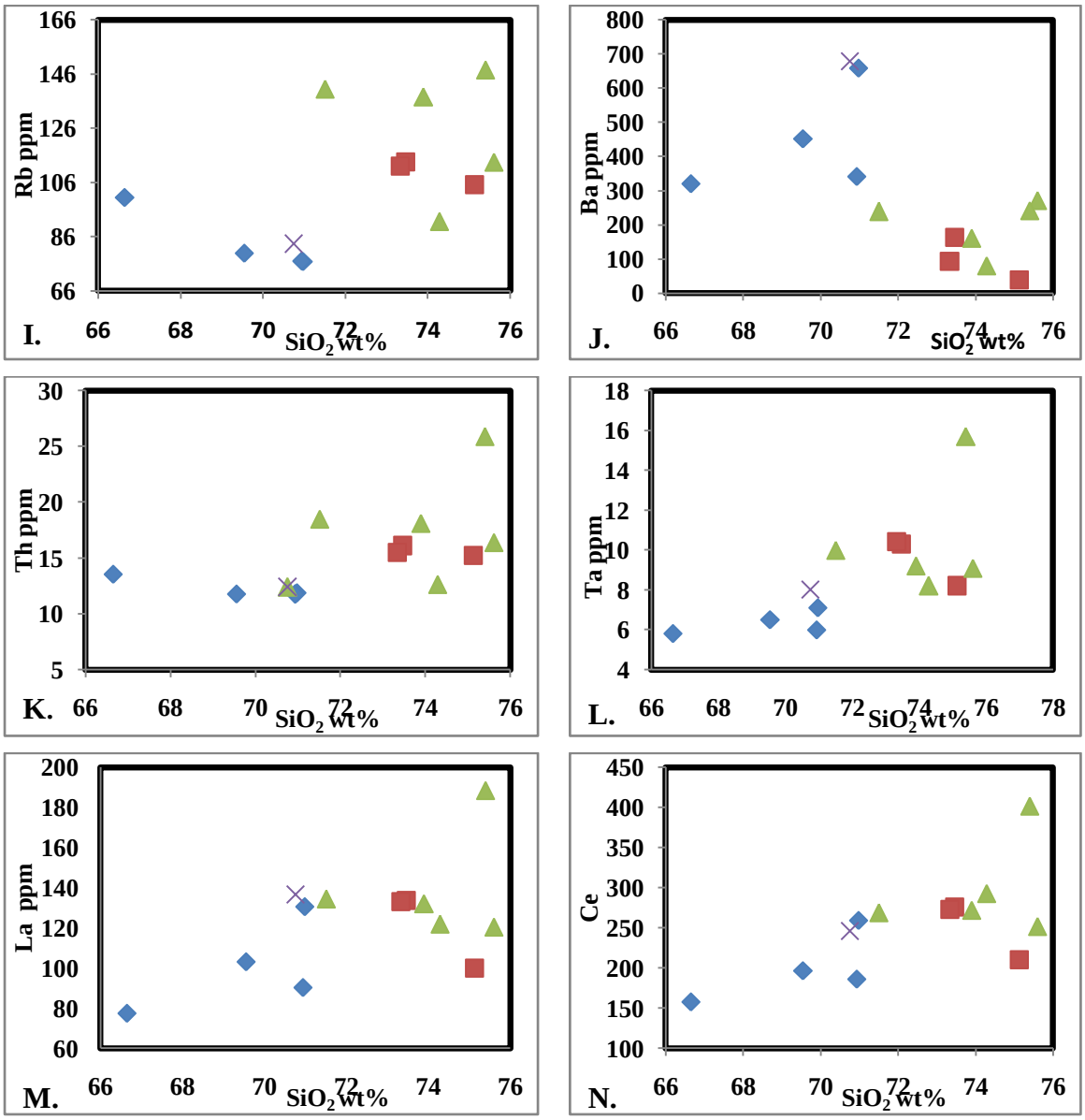

Figure 4.5. *Trace element Harker diagrams showing the variation of compatible and incompatible elements as the function of silica variation. All trace elements are in parts per million (ppm) and silica is in wt %.*

Moreover Zr, Y, La and Ce also shows inflected trend but unlike Ba theses start with relatively lower values constituting ash flow concentration and increases until about 74 wt% of SiO_2. It does not show sharp decrease toward rhyolite ash and ignimbrite as shown in (Fig 4.5 E, F, G, L, M and N). Unlike in the case of Ba one rhyolite ash sample shows anomalous value in all cases and the trend is not perfectly smooth. On the other hand, scattered plots are reflected in the case of Rb and Sc.

Incompatible vs compatible element plot (Fig.4.6.) is used to understand the differentiation mechanism (Peccerillo et al., 2003). Variation diagrams of the compatible elements Sr, V, Ni and Cr versus the incompatible element Zr (Fig. 4.7) show generally decreasing trend from the ash flows to the ash fall samples with an indication of nearly uniform in the rhyolite ignimbrite and minor scatter in rhyolite and dacite ashes.

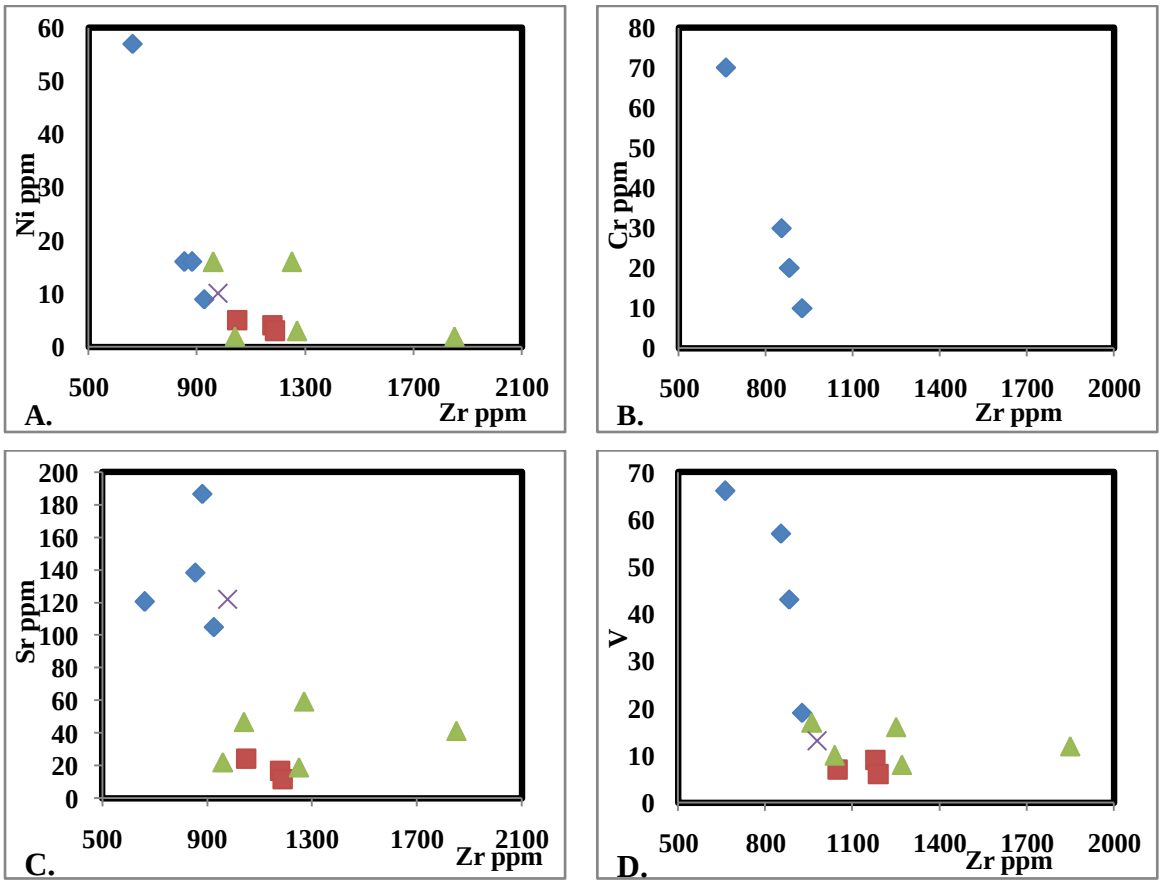

Figure 4.6. *Incompatible vs compatible element variation diagrams with compatible element on the vertical and incompatible elements on the horizontal axis, constraining magmatic differentiation mechanism for the genesis of felsic pyroclastic products.*

In addition, the samples are clustered in to two groups in the Sr vs Zr binary diagram, except one anomalous sample, while sigmoidal pattern is observed in the Zr vs V plot. In the Zr vs Ni plot all samples are clustered except two anomalous samples. On the other hand, all of the rhyolite ash, pumiceous ash and three of the ignimbrite samples have Cr values below detection limit (<10ppm).

Incompatible vs incompatible element binary plots (Fig. 4.7) show simultaneous increase (positive trend) in the residual liquid generally passing through the origin. Minor

dispersion is observed in U vs Zr plot, while Nb vs Zr plot show perfect positive correlation

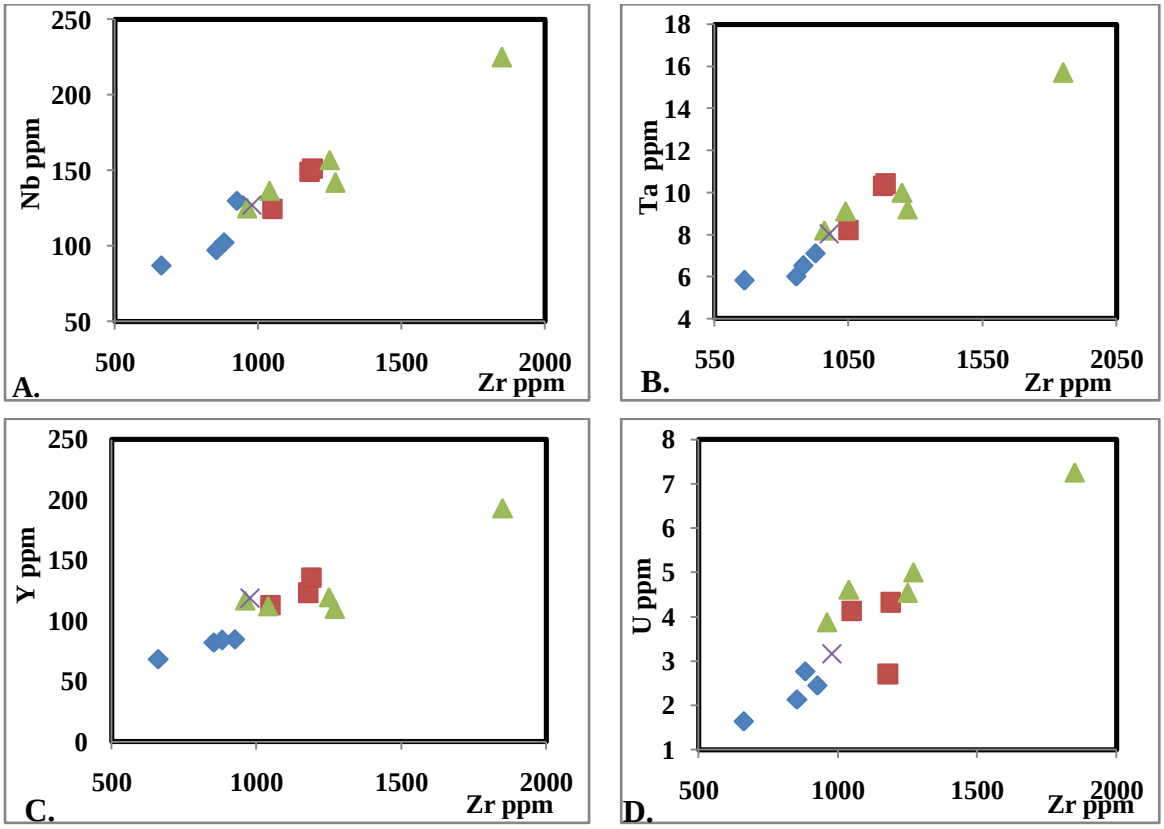

Figure 4.7. *Highly incompatible trace element bi-variant plots in which Zr is used as index of differentiation in the horizontal axis and Nb, Ta, Y and U vary positively with Zr during magmatic differentiation.*

4.3.4. Rare Earth Element (REE) and Multi-element Variation Diagrams

The REE variation diagram (Fig. 4.8) shows a significant decreasing trend from La to Sm (LREE) with minor spike in Nd. In addition high negative anomaly (trough) is observed in Eu in which (Eu/Eu*) ranges from 0.28 to 0.56 (calculated using the ratio of normalized Europium (Eu_N) to the square root of the product of normalized Samarium ($Sm_{N)}$ and Gadolinium(Gd_N) (Rollinson, 1993)). Moreover, heavy REE (HREE) from Gd to Lu excluding Er and Tm show gently sloping trend. The REE/Chondrite normalized plot also shows the ash flow layers to have relatively lower position, with alternative rhyolite and ignimbrite trends forming wider gap between the two rhyolites at the top part of the trend (Fig. 4.8).

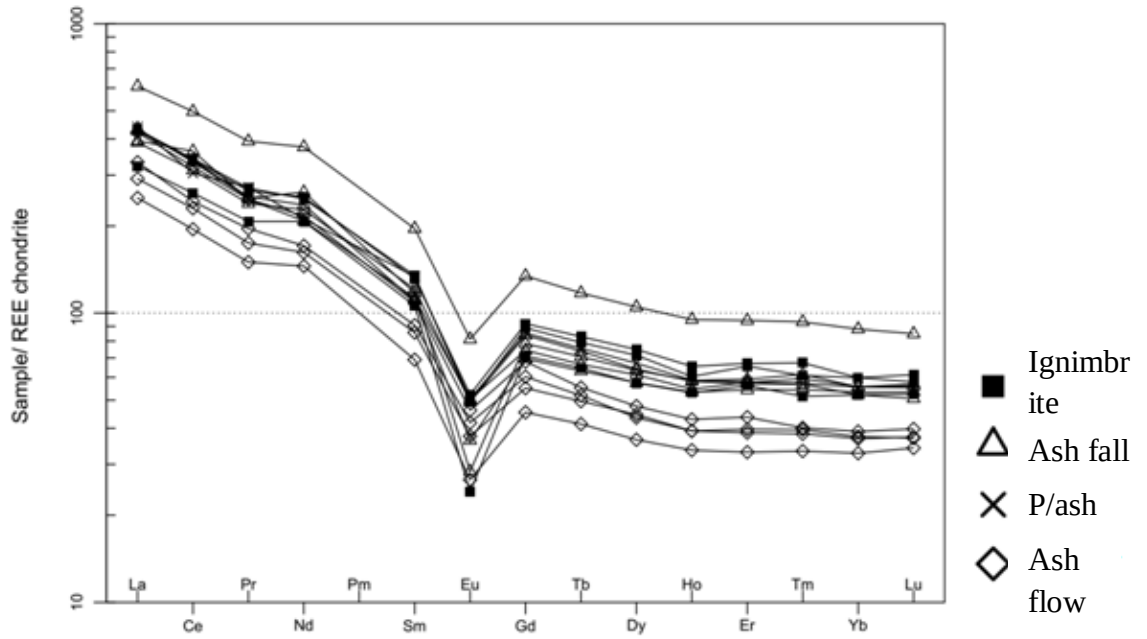

Figure 4.8. *Chondrite normalized REE patterns (Boynton, 1984) for the Melka Wakena pyroclastic rocks. The plot shows decreasing trend from La to Sm (LREE) with high negative anomaly in Eu and generally horizontal trend from Gd to Lu (HREE) in both the dacite and rhyolite samples.*

Multi-element variation diagram (MEVD) (primordial mantle normalized spider diagram) displays the property of selected trace elements together with REE arranged in an increasing degree of compatibility from the left to the right (Fig. 4.9). The spider diagrams show negative anomaly for Ba, U, Sr, P and Ti whereas La, Ce, Sm, Y and Rb show small degree of decreasing pattern although one rhyolite ash fall sample shows flat trend in U and decreasing trend in K. On the other hand, there is small spike in K, Ta, Nb, and Zr for almost of the samples. Generally decreasing trend is observed in the case of light lithophile elements comparing to the high field strength elements. Hence, the rare earth elements, other high filed strength elements except P and Ti in the multi element variation diagram shows almost uniform trend except the minor spikes. On the other hand, the LILE marks generally anomalous value and comparative enrichment than the high field strength elements. Moreover, the comendites shows comparatively lower values in Y, Zr, Nb and LREE compare to the corresponding pantellerites and generally uniform HREE pattern.

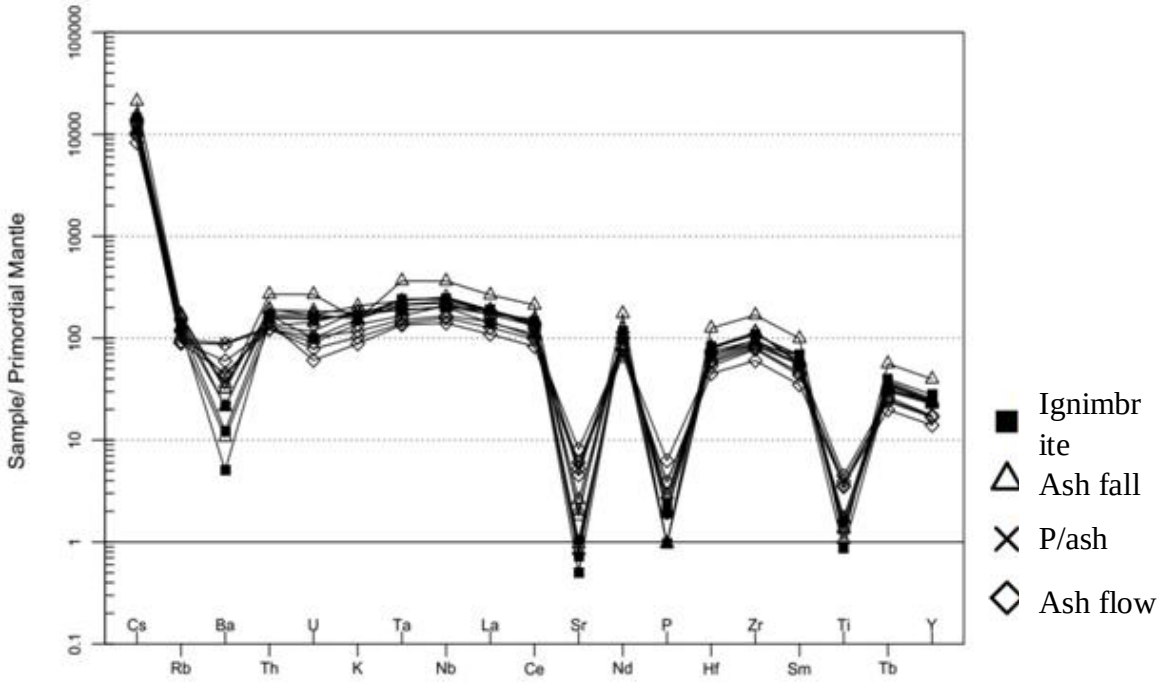

Figure 4.9. *Multi-element variation diagram according to Wood et al. (1979). Spider diagram showing the variation of trace elements during magma evolution; strong negative anomaly is observed for Ba, Sr, P and Ti, and decreasing trend for Ce to Rb and Tb to Y with generally horizontal to slight increasing trend for the remaining the elements.*

Even though negative anomaly is observed in the elements listed in the caption of Figure 4.9., throughout the samples the greater negative anomaly of the elements is pronounced in the ignimbrite samples. Moreover, one rhyolitic ash fall layer shows exceptional trend in K. It reflects negative anomaly in the K concentration while the others show increasing amount in K.

CHAPTER FIVE

GEOCHRONOLOGY AND STRATIGRAPHIC CORRELATION

5.1. Ar-Ar Dating

5.1.1. Introduction

Four tephra/pyroclastic rock samples (MW2-G3, MW2-G10 and MW2-G16, MW1-G9 collected from the bottom to top of the stratigraphic section in that order) were collected for dating in 2015 from the MelkaWakena area, under the MelkaWakena Archaeological Project, which is co-led by the supervisor of this thesis. Three samples are collected from MW2 locality (X- 0528885 Y- 0782535) and one sample from MW1 locality (X-0528972 Y-0782975) See Figure 3.1 for locations. Samples were sent to the Berkley Geochronology Center, USA and were dated using standard Ar-Ar method. Here, X- represents Easting, Y- is Northing and Z – is elevation (m).

5.1.2. Results

The measured ages were interpreted and calculated based on Niespolo et al. (2016) published on the inter calibration of Alder Creek Sanidine (ACS) standard comparing an astronomically tuned calibration of ACS to an optimization calibration after Renne et al. (2011). The result of the dating (Table 5.1) suggest that at the base of the succession (represented by the welded tuff layer, MW2-G3) is dated to 1.617±0.003 Ma, while the youngest age reported is from MW1 at 0.696 ± 0.002.

Table 5.1. Ar-Ar dating results of the MelkaWakena samples.

Sample number	**Calibration of alder creek sanidine from Niespolo et al.(2016)**								
	Astronomical Age (ACs=1.1848 ±0.0006Ma)	**±1σ linear**	**± 2σ**	**Optimization age (ACs=1.1891±0.0008Ma)**	**± 1σ Linear**	**± 2σ**	**n/N**	**MSWD**	**P value**
MW-1-G9	0.696	0.002	0.005	0.698	0.003	0.005	7/33	1.543	0.15
MW-2-G16	1.227	0.014	0.029	1.232	0.014	0.029	44/71	0.45	0.99
MW-2-G10	1.337	0.003	0.007	1.341	0.003	0.007	16/62	0.71	0.78
MW-2-G3	1.617	0.003	0.006	1.623	0.003	0.006	32/33	1.32	0.11

These ages constrain the possible major eruptions of pyroclastic rocks as well as the volcanic quiescence periods during which the volcano-clastic sediments and sedimentary rocks were deposited. The dated samples perfectly agree in terms of their successive ages with their stratigraphic positions. The welded tuff at the base of the section in locality MW2 is the oldest unit in this section, while the youngest dated sample is higher up in the stratigraphic column. However, the presence of xenocrysts of significantly older ages (up to 3.5 Ma) along with the juvenile population suggests the presence of older unexposed volcanic sequences in the vicinity, which is also evidenced by the presence of the unwelded weathered ash layer in the upstream localities. This has also been verified by the presence of some older crystals from MW2-G10 at the tail end of MW2-G16 (MW2-G10 underlies MW2-G16, both separated by a succession of sediment layers and another intermediate tephra).

5.2. Composite Stratigraphy and Unconformity

5.2.1. Composite Stratigraphy

Two separate composite Stratigraphic sections are produced during the study after 17 detailed graphic logs are constructed and then correlated. This is purposely done to solve the complexity of the area. Accordingly, it is classified as upper and downstream side stratigraphy as discussed below.

5.2.1.1. Composite Stratigraphy of the Upstream Localities

This area is consisting of different layers with variable thickness as well as lateral extensions. Moreover, the rock layers represent complex depositional history. This section is consisting of different unites with unwelded and weathered ash overlain by 1.67 Ma welded tuff at the base and 0.67 Ma and 0.05m thick fine grained blue ash at the top as shown in the given log below. This succession shows the former alternative depositional and erosional activities observing its contact relationship and over all geomorphology. Here, most of the layers are not continuous and sometimes missed within the sequence.

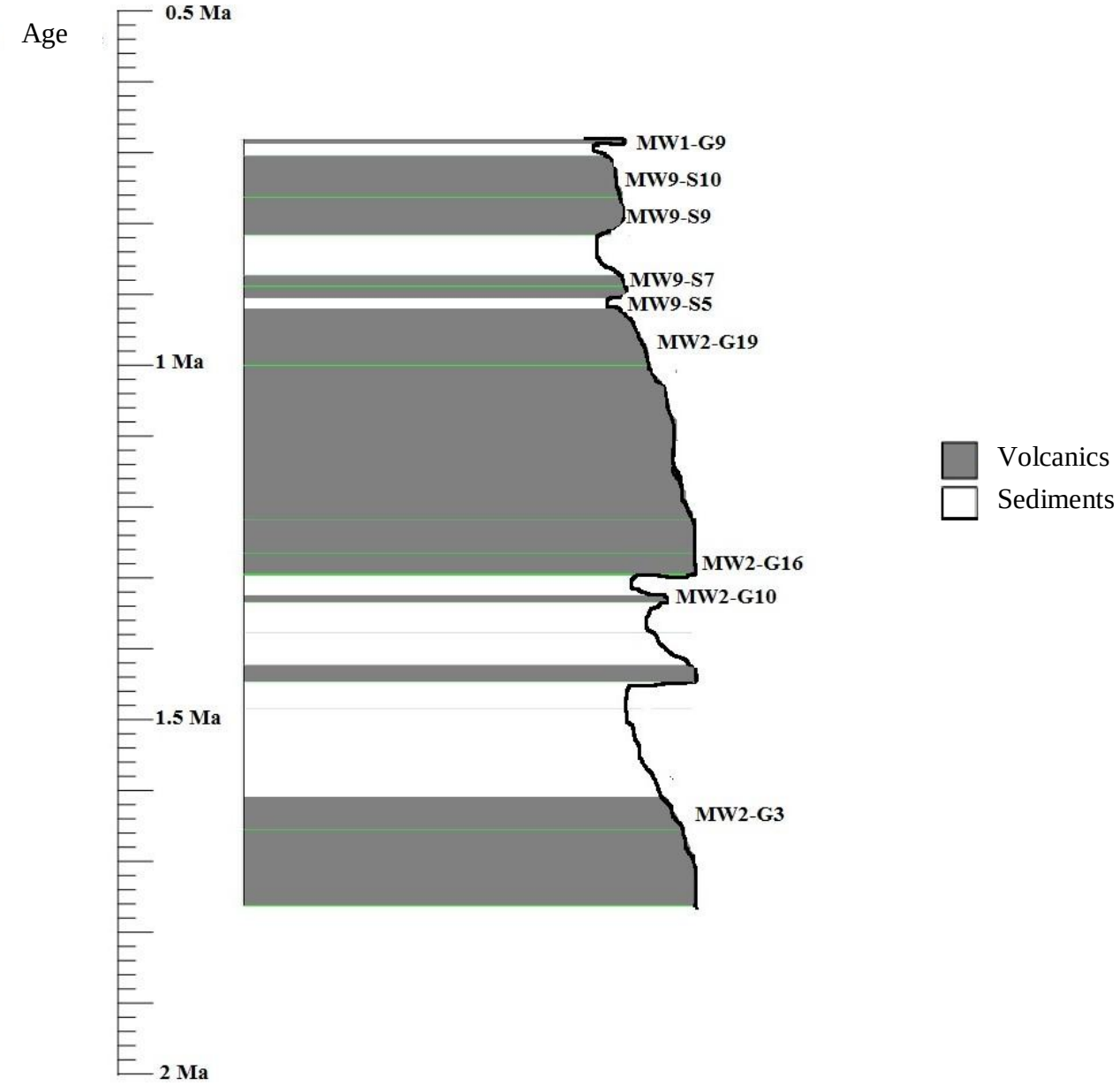

Figure 5.5. *Composite stratigraphy of upper stream portion of the study area produced after correlation of each of the graphic logs from separate localities. It is constructed using Strater4 software (http://www.goldensoftware.com/guidespurch/st4ugpd.shtml). Codes are the layers where samples are taken for petrography, geochemistry and geochronology.*

5.2.1.2.Composite Stratigraphy of the Downstream Localities

Downstream portion of the study area is consisting of about 25m thick rock successions using water level as a reference frame. This section is compiled from the textural as well as compositional information gained in each log section together with geochemical data. As far as the field observation as well as stratigraphic correlations of the eight localities the composite section is consisting of conglomerates and breccias, thin layer of light yellowish relatively weathered ash, ignimbrite boulders, deep blue as well as light blues

ashes of different verities. Besides, light grayish ash, reworked clay with numerous conglomerates overlain by fine grained non reworked clay with thick pumice enriched, sand, silt and conglomerate constituting upper reworked layer. Unlike in the upper stream stratigraphy, uniformly sorted as well as non reworked clay, lapilli tuff and reworked pumice rich layer is observed.

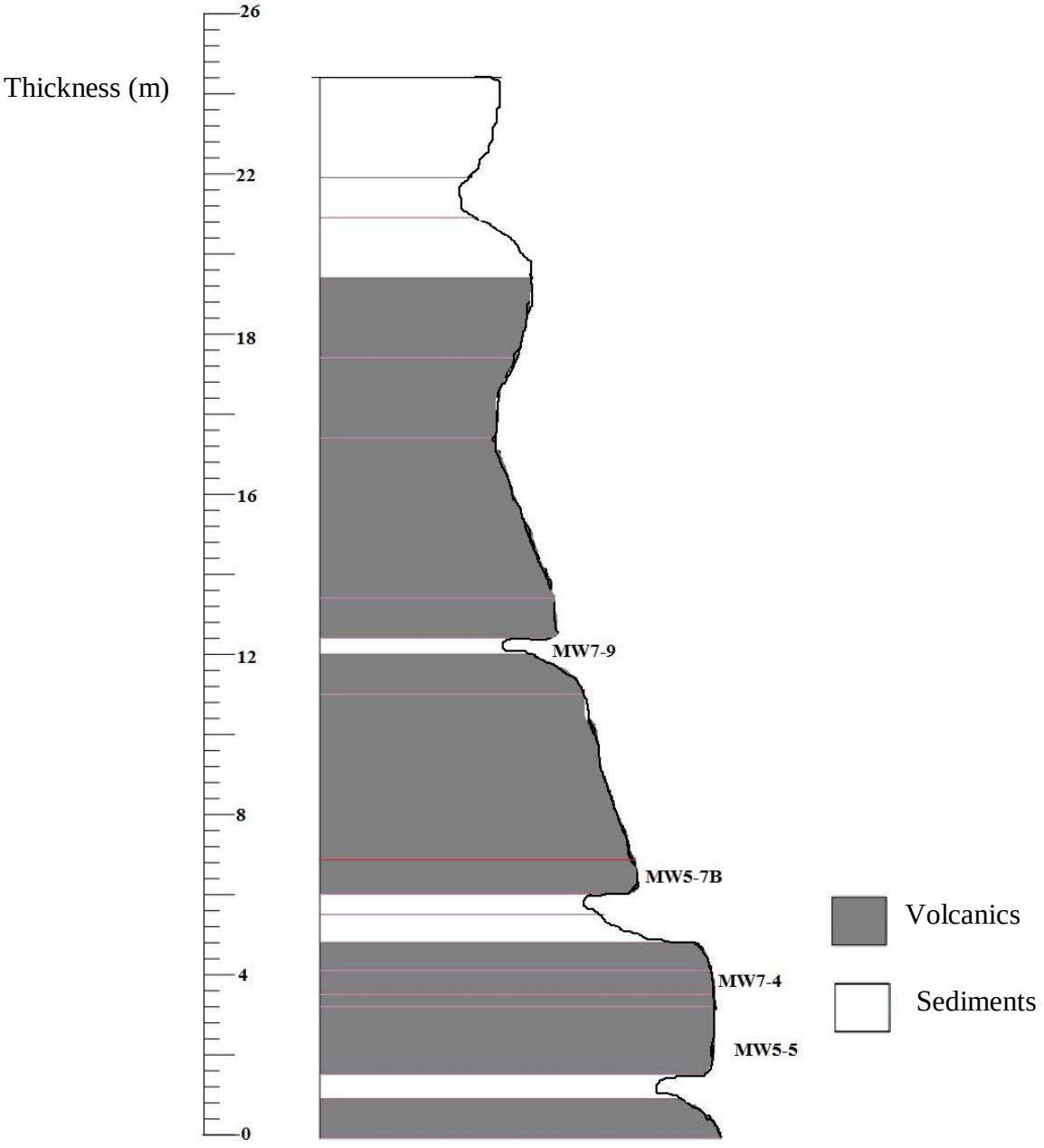

Figure 5.6. *Composite stratigraphy of downstream portion of the study area produced using Strater4 software (http://www.goldensoftware.com/guidespurch/st4ugpd.shtml) after correlation of each of the graphic logs from separate localities; Codes are where samples are taken for petrography and geochemistry.*

CHAPTER SIX

DISCUSSION

6.1. Quaternary Volcanic Events

Wide spread basalts and silicic products ranging in age from 2-0.6 Ma are recorded in the central and northern sectors of the rift with 1.95 ± 0.3 Ma basalts and agglomerates from the base of Asela escarpment and 1.3± 0.3 silicic domes and calderas close to the eastern margin near Asela area (Bekele Abebe et al., 2007). Tadiwos Chernet et al. (1998) reported Quaternary bi-modal volcanism along the WFB including the 1.6 Ma trachyte flows from Boset volcano and 0.66 Ma rhyolite from Harbona volcano, suggesting the presence of active volcanic centers until late Pleistocene. In addition, 1.66 Ma vitric tuff in the Munesa- Asela eastern escarpment (Giday WoldeGabriel et al., 1990), younger 1.3± 0.3 Ma silicic domes and 0.65 Ma ignimbrites are reported from near the Asela area (Bekele Abebe et al., 2007). Bimodal volcanism during 1.6-0.5 Ma also characterizes the rift floor of SMER (Zanettin et al., 1978).

The pyroclastic rocks in the study area were successively deposited during the early Quaternary (early to middle Pleistocene), interspersed with sedimentation events, which deposited fluviatile and reworked volcaniclastic sediments. The 1.617 ± 0.003 Ma welded tuff layer from the MelkaWakena area is similar in age to the 1.66 Ma vitric tuff in the Munesa- Asela eastern escarpment, while the 0.65 Ma ignimbrite of Asela area is of similar age to and compositionally coincident with the 0.696 ± 0.002 Ma rhyolite ash layer of the study area. The 1.33 ± 0.3 Ma silicics from Asela area shows similar age with the 1.337 ± 0.003 Ma of the rhyolite layer in Melka Wakena. These all suggest that the Quaternary volcanism in the WFB, whose axis is very close to the eastern escarpment, is the likely source of the volcanic products in the study area (the whole Gadeb plain), an assertion also supported by earlier works (e.g., Giday WoldeGabriel et al. 1990; Giday WoldeGabriel et al., 2000; Giday WoldeGabriel, 2009).

Integration of the petrographic and geochemical results with field data suggests that three of the ash flow layers are dacitic whereas one ash flow layers, the ignimbrite and ash fall as well as the pumiceous ash layers are rhyolitic in composition. On the other hand, the chemical signatures indicate that the pyroclastic rocks are almost peralkaline pantellerites

and comendites except the two subalkaline ignimbrites (Fig.4.3A).The tuff and ignimbrite units consist of alkali feldspar phenocrysts, lithic fragments, plagioclase, minor pyroxene, amphibole and opaque minerals set in vitric matrix. Based on their compositional similarity, these units may correspond to the upper pyroclastics of Workineh Haro et al. (2014). The well-sorted ash sample of rhyolitic composition is comparable with the vitric tuff of Eberz et al. (1988). Tura et al. (1999) reported comendite to pantellerite rhyolites and ignimbrites in the Asela -Ziway area, which also incorporates the current study area. The pyroclastic rocks in the study area could therefore be compared with those reported from the vicinity by Eberz et al. (1988), Giday WoldeGabriel et al. (1990), Giday WoldeGabriel (2009), Trua et al. (1999) and their age and chemistry allows comparing their evolution with the Plio-Pleistocene Asela-Ziway felsic products.

6.2. Petrogenetic Evolution of the Pyroclastic Rocks

It is suggested by the fact that the pyroclastic products of the Gadeb plain, which also includes the pyroclastic deposits in the current study area, were deposited by plinian eruption (Eberz et al., 1988) from the rift related to Plio-Pleistocene large calderas such as Aluto, Gademota, Hawasa and Shalla (Eberz et al., 1988; Gidey WoldeGabriel, 2009). In addition Giday WoldeGabriel et al. (2000) reported that large sized calderas such as Aluto, Bora, Corbetti, Gedemsa, Gademota and Shalla were active during the Pleistocene. The current study area is located at the eastern shoulder of the rift where unsorted rhyolite pumice rich ash layers, unsorted welded tuff and younger moderately welded ignimbrites are exposed. These rock units extend to the rift suggesting that they are sourced from the rift (Seife Michel Berhe et al., 1987; Eberz et al., 1988; Giday WoldeGabriel et al., 1990; Giday WoldeGabriel, 2009; Trua et al., 1999). Even though, fractional crystallization of basaltic magmas could possibly explain the origin of the pyroclastic products in the area, the textural and geochemical variability and their age difference suggest separate chronozones, as well as eruptive and crystallization histories. Hence, the well sorted; generally uniformly thick ash layers probably suggest pyroclastic fall products from a distant source. On the other hand, the ignimbrite, welded tuff and ash flow materials are indicator of pyroclastic flow deposits of proximal source, although this contradicts the suggestion that all the pyroclastic products are sourced from the rift (e.g., Giday WoldeGabriel, 2009).

The major element Harker diagrams show clustering of the results with respect to TiO_2 and MnO, probably suggesting some mantle plume input as suggested by some (e.g., Dereje Ayalew et al., 2002). On the other hand, crystallization of Fe-TiO_2 minerals (may be ilmenite, hematite or titanomagnetite) at depth and rapid ascent of the least evolved magma followed by fractional crystallization plus assimilation in the shallow magma chamber producing Fe-TiO_2 cumulate could also be the possible reason.

The positive and negative correlations in the Harker diagrams reflect either the entry of new phases during partial melting or removal of phases during fractional crystallization (Rollinson, 1993). Accordingly, the positive correlation in K_2O versus SiO_2 may be an evidence for the breakdown and addition of alkali feldspar as assimilant to the melt. Hence, the most probable reason could be the composite effect of dominant fractional crystallization of Ferro-magnesian minerals leaving subalkaline-peralkaline evolved magma involving minor degree of crustal contamination. On the other hand, the negative correlation in MgO, Al_2O_3, Ni, V and Cr against silica suggests the removal of Ferro-magnesian minerals (Rollinson, 1993; Dereje Ayalew et al., 2002). Hence, this result together with mass balance calculation reflects removal of olivine, plagioclase/ apatite and pyroxene or spinel during the course of the process.

Scattered plots in the Harker diagrams could result from different cases like different magma source, different differentiation mechanism, changing in the crystallization phases, assuming that contamination during sample preparation as well as analytical uncertainties are ruled out (Rollinson, 1993). In the current study, CaO and Fe_2O_3, Rb and Sc show scattered plots, which could be due to either different source or different degree of differentiation. On the other hand, mobility of the elements, and oxidation of iron during weathering and alteration could also lead to scattering of data in the Harker diagram (Rollinson, 1993). The analyzed samples generally show high LOI and field observations indicate that some of them have been weathered due to the rapidly fluctuating river water, suggesting that some of the scattering could be attributed to this. Secondary hydration of glass produces removal of alkaline elements (Eberz et al., 1988; Dereje Ayalew et al., 2002). Hence, the cyclic pattern in Na_2O and Sr may suggest post depositional removal of these elements or magma zonation in the magma chamber in the case of Na_2O.

The inflection trend observed in Ba, Zr, La, Ce and Y reflects the concentration of the elements in the liquid during the initial stage of fractional crystallization followed by the involvement of alkali feldspar, zircon, and accessory phases**.** Besides, decreasing slope in case of highly incompatible REE trend reflects fractionation of these elements in the residual melt due to the crystallization of olivine, and possibly clinopyroxene and othopyroxene, whereas the minor spike in Nd could be due to monazite effect. Low concentration in Eu as well as its negative anomaly in the spider plot could be related to the integrated effect of oxygen fugacity (Dereje Ayalew et al., 1999; Ronga et al., 2010) as well as Eu oxidation state, hence Eu^{2+} shows negative anomaly at higher oxygen activity with the reverse condition in Eu^{3+} (Rollinson, 1993). In addition, negative anomaly in Eu results due to the fractionation of Eu in the crystal structure of plagioclase substituting Ca/alkali feldspar substituting K (Rollinson, 1993). Shallow caldera source of these products (Giday WoldeGabriel, 2009) together with the ideas of Rollinson (1993) and Dereje Ayalew et al. (1999) suggests these products are probably formed at relatively low oxygen activity so that it leads for the negative anomaly in Eu whose $(Eu^{2+}/Eu^{*})_N$ is <1. On the other hand, the existence of plagioclase and alkali feldspar phenocrysts in the rhyolite ignimbrite samples and in the compacted ash thin section together with abundant volumetric proportion of plagioclase feldspar in the normative calculation could be evident for the fractionation of Eu in the crystal structure of plagioclase/alkali feldspars.

Fractionation of middle REE depends on the crystallization of amphibole whereas ferromagnesian minerals are responsible for light REE enrichment and garnet for heavy REE fractionations (Rollinson, 1993). However, Trua et al. (1999) suggests neither amphibole nor garnet was involved in the fractionation of the samples from Asela – Ziway. The generally gentle trend with respect to middle and heavy REE in the samples from Melka Wakena agrees with the conclusion of Trua et al, (1999). Besides, light REE are fractionated in the residual liquid during fractional crystallization due to removal of olivine, clinopyroxene, orthopryroxne and spinel (Rollinson, 1993). Hence, the enrichment of highly incompatible elements in the samples of the study area could be due to the increasing degree of fractional crystallization of the parent magma producing highly evolved magma contributing small amount of assimilation. This is supported by mass balance calculations of Stromer and Nichols (1978) where 85.74% of fractional crystallization of primitive magma plus minor assimilation is required for the observed incompatible REE enrichment.

The multi element variation diagram (MEVD) shows negative anomaly for Ba, Sr, P and Ti, which could be due to the removal of alkali feldspar, plagioclase, apatite and Fe-Ti oxide, respectively. On the other hand, the minor spike in the concentration of Ta, Nb and Zr could probably be due to the fractionation of these elements in the residual liquid during fractional crystallization process or non/minor involvement of crustal materials in the liquid. The minor decrease in Rb, La, Ce, Sm, Y and Lu could reflect the fractional crystallization of alkali feldspar, and accessory phases probably at the end of magmatic differentiation. Positive correlation between incompatible trace elements is used to constrain the magma co genetic origin producing the samples (Eberz et al., 1988). Hence, the binary Harker diagram (Fig. 4.8.) shows positive correlation probably indicating co genetic origin of the magma.

6.2.1. Petrogenetic Modeling

The results of various petrological and geochemical studies imply silicic magmas are generated from fractional crystallization of basaltic magmas with variable degrees of crustal contaminations (Gasparon et al., 1993; Tadiwos Chernet and Hart, 1999; Dereje Ayalew, 2000; 2011; Dereje Ayalew et al., 2002 and reference therein; 2006; Dereje Ayalew and Gezahegn Yirgu, 2003; Peccerillo et al., 2003; 2007; Kurkura Kabeto et al., 2009; Kurkura Kabeto, 2010; Rooney et al., 2012; Giordano et al., 2014). In contrast, it can also form from small degree of partial melting producing least evolved magma followed by fractional crystallization of the least evolved magmas leaving highly evolved magmas (Boccalleti et al., 1999; Trua et al., 1999; Deniel, 2000). Tadiwos Chernet and Hart (1999) suggested that the Wonji Group Silicics (WGS) are generated from differentiation of transitional to calcalkaline basalts and the more evolved Wonji Group Basalts (WGB) whereas the Gara Gumbi Formation (GGF) of southern Afar margin is associated with sub-alkaline to theolitic flood basalts of the Afar Stratoid Series (ASS). On the other hand, rift shoulder felsic rocks of Addis Ababa area are associated with differentiation of sub alkaline to per alkaline Bofa Basalts (Tadiwos Chernet et al., 1999). The distribution of the Melka Wakena samples in the dacite and rhyolite fields in the TAS classification system of Le Bas et al. (1986) and in the high K calcalkaline field in the Peccerillo and Taylor (1976) diagram might suggest fractional crystallization of sub alkaline basaltic magmas as the probable origin of the felsic rocks in the study area. This has also been suggested by Trua et al. (1999).

Major oxides (elements) did not differentiate fractional crystallization from partial melting during magmatic differentiation unless the process happens in different physical settings (Rollinson, 1993). To solve this situation, binary plots involving incompatible versus compatible trace elements are required for modeling the responsible differentiation mechanism (Rollinson, 1993; Peccerillo et al., 2003). According to Peccerillo et al. (2003), partial melting leads to enrichment of incompatible elements with moderate depletion of compatible elements whereas fractional crystallization involves high depletion of compatible elements compared to the enrichment of incompatible elements. Among the felsic rocks in the study area, the rhyolites show low values of Ni, Cr, Sc and V and are negatively correlated with Zr implying the fractionation of these elements in crystal structure of olivine, pyroxene and Fe-Ti oxides. On the other hand, the concentration of the elements in the dacite shows enrichment compared to the values given in Dereje Ayalew et al. (2002). This shows fractional crystallization dominantly affects the generation of the rhyolite magma and the dacites could be probably formed from dominant fractional crystallization plus minor addition of crustal assimilates. In addition, Dereje Ayalew et al. (2002) reported that partial melting do not explain lower values in Sr (<100ppm) and CaO (<1.23wt %). In contrast, the values of these elements/oxides in the dacites of the study area are high, suggesting the involvement of contamination. On the other hand, relatively low values in Nb and Ta are observed in the two dacite samples (MW2-G16 and MW5-5 in Table 4.1.), which is too low for felsic magmas formed by fractional crystallization only. This evidence suggests the probable involvement of small amount of crustal material in the residual liquid, as also supported by Dereje Ayalew et al. (2002). These all with the petrogenetic model given below (Fig. 6.1) explains the dominant fractional crystallization process resulting in the formation of rhyolites and Assimilation Fractional Crystallization produces the dacite samples.

To model the petrologic evolution of the felsic rocks in the study area, Zr vs V variation diagram was used due to the compatibility of V and incompatibility of Zr in Fe-Ti crystals. Hence, fractional crystallization (FC) with some degree of crustal contamination and Assimilation Fractional Crystallization processes (AFC) were considered. The most probable parent magma composition was assumed to be the LA-48 basalt sample of Trua et al (1999), as it is from the same geologic regime and generally considered as primitive magma in the rift. In addition, mineral chemistry required for mass balance calculation is from Trua et al. (1999) and composition of the assimilant is taken from Shaw et al. (1986)

and Wedepohl (1995). Besides, AFC calculation is based on Depaolo (1981), FC is calculated using Neuman et al. (1954), while partial melting is based on Wood and Fraser (1976). Besides, three of the models in figure 6.1 and mass balance calculations are conducted using Petrograph 2 beta software version 1.0.2, where the soft ware is available in the website *(http://www.unipg.it/~maurip/SOFTWARE.htm)*. The model (Fig. 6.1) together with mass balance calculation result shows the fractionating crystal phases in their order of formation were olivine (24.25%), pyroxene (undetermined chemistry), plagioclase (72.3%) and finally 3.46 wt% Fe-Ti oxides. Enrichment in LREE (7< $(La/Yb)_N$ <14) (Trua et al., 1999) or 6< $(La/Yb)_N$<14 (Dereje Ayalew et al., 2002) could indicate moderate degree of fractionation whereas partial melting could not produce Sr<100ppm. The dacites in the area (except one sample;G16) are enriched in LREE and are enriched in Sr. As the model shows and the previous studies suggest, the rhyolites were formed by fractional crystallization (85.74-90%) with minor crustal addition, and the dacites by Assimilation Fractional Crystallization. The actual calculation results are given in Appendix III.D.

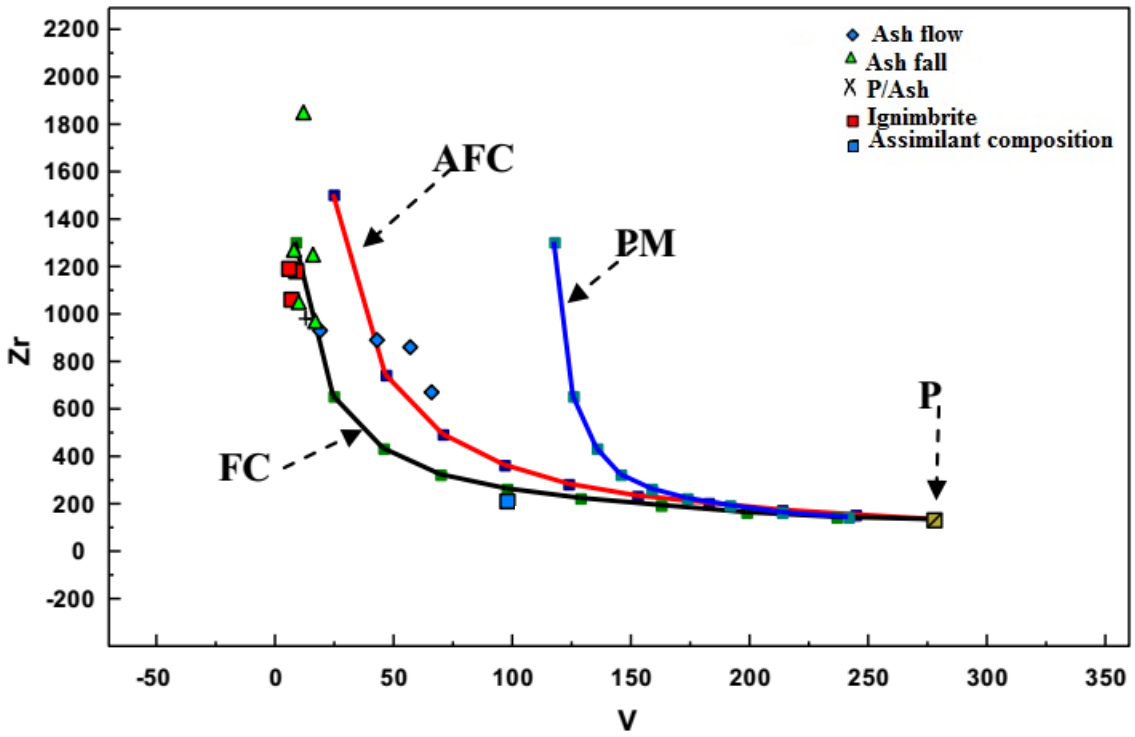

Figure 6.1. *Petrogenetic Models showing the relationship between the primitive and evolved magmas using Petrograph 2 beta version 1.0.2.The composition of the primitive magma LA 48, and mineral chemistry are taken from Trua et al. (1999); and the highly evolved magmas are those with high SiO_2 in the recalculated values (MW9-S7). Assimilant compositions (continental crust) are from Shaw et al. (1986) for major elements and Wedepohl (1995) for trace elements.*

The red line shows Assimilation Fractional Crystallization (AFC), the black line represents Fractional Crystallization (FC) and the blue line is for Partial Melting (PM) models. $D_{V\ Fe\text{-}Ti}$ *=2 and* D_{Zr}*=0 in ilmenite;* D_V *2.5 and* D_{Zr}*=0 in clinopyroxene in silica rhyolite. Ratio of assimilation rate to fractional crystallization rate(R) is 0.1;* D_V *is the partition coefficient for Vanadium; and* D_{Zr} *is for Zirconium; P is the primitive magma. The partition coefficients are from (http://www.unipg.it/~maurip/SOFTWARE.htm) for Vanadium in the ilmenite and clinopyroxene phenocrysts. In the case of Zr it is incompatible and the value of the partition coefficient in these samples is zero.*

6.3. Fluvial Sediments and Inter-volcanic Reworked Volcaniclastic Deposits

Recent survey and excavations at the MelkaWakena site indicate that the site contains significant archaeological and potentially significant anthropological records contained in fluvial and reworked volcanoclastic sediments deposited interspersed with the pyroclastic layers. The age range of the dated pyroclastic layers (1.617 to 0.696 Ma) largely coincides with the suggested period of arrival of hominids in the area (between 1.5 and 0.7 Ma; Williams et al., 1979). In one of the well dated localities of the study area, MW2 locality, the oldest ignimbrite artifacts and bones are concentrated in the conglomerates and sands deposited on top of the 1.617 Ma welded tuff and capped by the 1.337 Ma rhyolitic ash tuff layer. Younger conglomerates, sand and reworked volcaniclastics have been deposited between 1.33 and 1.227 Ma. The top layers of this section are mostly ignimbrites and reworked pyroclastic deposits with some thin layers of fluvial sediments. In another locality, MW1, sand and conglomerate layers are deposited before capping by 0.699 Ma old ash layer.

Most of the sedimentary and volcanic layers are laterally non-continuous, rather characterized by frequent pinch outs and thickening and thinning sequences. Both erosional processes (down cutting among others), which occurred at various stages, and depositional unconformity could explain the lateral variations. The pinch out relationship between the unwelded and welded tuffs towards the bottom of the section suggests an erosional process that happened during the early Pleistocene (nearly 1.617 Ma), a process that continued throughout the deposition history of both the volcanic and sedimentary rocks, as observed also on the ignimbrite layers towards the upper levels, which are eroded and dissected laterally before deposition of the youngest ash layers in the area. The conglomerate and sand deposits between the ash layers are similarly laterally non-

continuous, suggesting a complex depositional history marked by confined channel and possibly overbank slope deposits later modified by down cutting. The increasing proportion of more reworked volcaniclastic layers towards the upper levels also confirms a continuous erosional process occurring contemporaneous with the deposition of younger volcanic and sedimentary rocks.

The increase in coarse grained sediments and fining up ward lithologic packages indicates sedimentation by significantly higher energy river and tributaries capable of eroding, transporting and winnowing the sediments in higher gradient fluvial stage mainly meandering river (Campisano, 2008a; 2012 and reference therein). Accordingly, the fining upward conglomerates as well as sand layers in the Melka Wakena area could be indicators of deposition by a meandering river, while the finer reworked layers towards the top could be deposited by low energy flow. The conglomerates and sands, considering their winnowed nature and composition (mostly of volcanic origin), are most likely sourced from the nearby Bale highlands, deposited when the perennial rivers and ephemeral tributaries lost their energy in meandering courses. On the other hand, low energy streams and local network of channels could form the reworked volcaniclastic layers. Local post-deposition compaction and cementation might also be responsible for the formation of the compacted sandy conglomerate layers.

All the evidences call for a geomorphologically active area during the Early to Middle Pleistocene where overbank sedimentary sequences (conglomerates and sands) formed by a big meandering river, dotted with possible temporary ponds and ox-bow lakes, have been covered by episodic volcanic eruptions and the products thereof. A dense network of channels and streams have been subsequently down cutting through the older volcanic and sedimentary sequences before the deposition of the younger volcanic and reworked volcaniclastic rocks. Such pyroclastics and sedimentary rock successions collectively known as the Dino Formation deposited during the age range of 1.5 – 0.8 Ma (Kazmin and Seife Michael Berhe, 1981) are extensively exposed on either side of the Main Ethiopian Rift and on the shoulders draping over the older Nazareth Series pyroclastics. The archaeology bearing Melka Wakena successions could therefore be attributed to the Dino Formation, though our dates show that the bottom pyroclastic layers could also be part of the upper layers of the Nazareth Series, while the top layers could possibly be correlated to the volcanic products of the Central Rift Volcanic Complex.

CHAPTER SEVEN

CONCLUSION AND RECOMMENDATION

7.1. Conclusion

The major conclusions are:

- The ignimbrite, ash fall and pumiceous ash units are rhyolitic while the ash flow unit is dacitic in composition. The geochemical characteristics and modeling suggest that the rhyolites were formed by Fractional Crystallization of basaltic magmas involving crustal input, while Assimilation Fractional Crystallization followed by post depositional leaching of the mobile elements formed the dacites. The existence of old (up to 3.5 Ma old) xenocrysts in the younger layers together with the existence of pokioclasts in the orthoclase crystals supports some amount of crustal contamination.

- The positive correlation among highly incompatible elements in the variation diagrams reflects cogenesis of the pyroclastic materials, while the scattered distribution of the mobile elements suggests that significant post depositional alteration or weathering was likely before the deposition of the subsequent layers.

- The pyroclastic rocks and intercalated volcano-sedimentary rocks have been formed during the Early to Middle Pleistocene (1.617 and 0.696 Ma ago) in a topographically complex area resulting in non-continuous and erratically distributed layers. The Melka Wakena pyroclastic rocks form part of the Dino Formation, which are extensively exposed on either side of the Main Ethiopian Rift and on the shoulders draping over the older Nazareth Series pyroclastics.

- The Melka Wakena pyroclastic rocks and the archaeology bearing intercalated sedimentary successions could be attributed to the Dino Formation, though the older dates show that the bottom pyroclastic layers could also be part of the upper layers of the Nazareth Series, while the top layers could possibly be correlated to the volcanic products of the Central Rift Volcanic Complex.

- The Melaka Wakena archaeological site was a geomorphologically active area during the Early to Middle Pleistocene where overbank sedimentary sequences (conglomerates and sands) formed by a big meandering river have been covered by episodic volcanic eruptions and the products thereof. A dense network of channels and streams have been subsequently down cutting through the older volcanic and sedimentary sequences before the deposition of the younger volcanic and reworked volcaniclastic rocks.

- The episodic eruption of pyroclastic rocks on actively depositing and eroding sedimentary layers containing cultural sequences allow constraining the age of the archaeological remains in the area as well as their depositional history, providing a great potential for dating the cultural sequences at high resolution.

7.2. Recommendations

Better understanding of the petrogenetic evolution of the silicic pyroclastics rocks could be achieved with:

- More detailed sampling (higher number of samples) and major and trace element data as well as petrographic data thereof;
- Sampling and analysis of a more diverse compositional range (from basalts to rhyolites);
- Isotope analysis of some samples in order to trace the source of the magma and the relative contribution of magmatic and crustal contamination input; and
- Dating of all the volcanic layers in the sequence in order to better constrain the age of the archaeology containing volcano-sedimentary layers.

REFERENCES

Baker, J., Snee, L. and Menzies, M. (1996). A brief Oligocene period of flood volcanism in Yemen. *Earth and Planetary Science Letters,* **138**: 39–55.

Barberi F., Ferrara G., Santacroce R., Treuil M. and Varet J. (1975). A transitional basalt-pantellerite sequence of fractional crystallization, the Boina Centre (Afar Rift, Ethiopia). *J. Petrol.* **16**: 22–56.

Basalfew Zenebe, Mathios Agonafir, Meskerem Teshome, Mekdes Taye, Mekonen Bekele, Mohamed Edris, Getachew Burusa and Ezra Yehualashet (2012). Geology geochemistry and gravity survey of the Hosaena area. Geological survey of Ethiopia, unpublished technical report, Addis Ababa, Ethiopia, 69pp.

Bekele Abebe, Acocella V., Tesfaye Korme, Dereje Ayalew (2007). Quaternary faulting and volcanism in the Main Ethiopian Rift. *Journal of African Earth Sciences*, **48**: 115–124.

Boccaletti M., Getaneh Asefa, Mazzuoli R., Tortorici L. and Trua T. (1995). Chemical variations in a bimodal magma system: The plio Quaternary volcanism in the Dera Nazret area (Main Ethiopian Rift, Ethiopia). *Afr. Geosci. Rev.* **2**: 37–60.

Boccaletti, M., Mazzuoli, M., Bonini, R., Trua, T. and Bekele Abebe (1999). Plio- Quaternary volcano tectonic activity in northern sector of the Main Ethiopian Rift: Relationship with oblique rifting. *Journals of earth sciences*, **29**(4): 679-698.

Bonini, M., Corti, G., Innocenti, F., Manetti, P., Mazzarini, F., Tsegaye Abebe and Pecskay, Z. (2005). Evolution of the Main Ethiopian Rift in the frame of Afar and Kenya rifts propagation. *Tectonics,* **24**: TC1007. doi:10.1029/2004TC001680.

Boynton W.V. (1984). Geochemistry of rare earth elements: meteorite studies, In: Henderson P. (ed.), *rare earth element geochemistry, 63-114.*

Campisano, C.J., Feibel, C.S. (2008a). Depositional environments and stratigraphic summary of the Hadar Formation at Hadar, Afar Depression, Ethiopia. **In**: Quade, J., Wynn, J.G. (Eds.), The Geological Context of Human Evolution in the Horn of Africa. *Geological Society of America,* Boulder. (179-201). Geological summary of the Busidima Formation (Plio-Pleistocene) at the Hadar paleoanthropological site, Afar Depression, Ethiopia *Journal of Human Evolution*, **62**: 338-352.

Campisano, C. (2012). Geological summary of the Busidima Formation(Plio-pleistocene) at hadar paleoanthropological site, Afar Depression, Ethiopia. *Journal of Human evolution,* **62**: 338-352.

Corti, G. (2009). Continental rift evolution: From rift initiation to incipient break-up in the Main Ethiopian Rift. East Africa. *Earth-Science Reviews*, **96**: 1–53.

Davidson, A. and Rex, D.C. (1980). Age of volcanism and rifting in south-western Ethiopia. *Nature*, **283**: 654–658.

Deniel, C. (2000). Crustal control in the genesis of Plio-Quaternary bimodal magmatism of the Main Ethiopian Rift: geochemical and isotopic (Sr, Nd, Pb) evidence. *Chemical Geology*, **168**: 5–7.

DePaolo, D.J. (1981). Trace element and isotopic effects of combined wall rock assimilation and fractional crystallization. *Earth and Planetary Science Letters,* **53:** 189-202.

Dereje Ayalew, Gezahegn Yirgu and Pik, R. (1999). Geochemical and isotopic (Sr, Nd and Pb) characteristics of volcanic rocks from southwestern Ethiopia. *Journal of African Earth Sciences,* **29**: 381-391.

Dereje Ayalew (2000). Origin by fractional crystallization of transitional basalt for the Asela-Ziway pantellerites. Crustal control in the genesis of Plio-Quaternary bimodal magmatism of the Main Ethiopian Rift (MER): geochemical and isotopic Sr, Nd, Pb evidence by Trua et al. 1999.*Chemical Geology*, **168**: 1–3.

Dereje Ayalew, Barbey, P., Marty, B., Reisberg, L., Gezahegn Yirgu and Pik, R. (2002). Source, genesis, and timing of giant ignimbrite deposits associated with Ethiopian continental flood basalts. *Geochimica et Cosmochimica Acta*, **66**(8): 1429–1448.

Dereje Ayalew and Gezahegn Yirgu (2003). Crustal contribution to the genesis of Ethiopian plateau rhyolitic ignimbrites: Basalt and rhyolite geochemical provinciality. *Journal of the Geological Society*, **160**: 47-56. Doi: 10.1144/0016-764901-169.

Dereje Ayalew, Ebinger, C., Bourdon, E., Wolfenden, E., Gezaheng Yirgu and Grassineau, N. (2006). Temporal compositional variation of syn-rift rhyolites along the western margin of the southern Red Sea and northern Main Ethiopian Rift. In: Gezaheng Yirgu, Ebinger, C.J., Maguire, P.K.H. (Eds.), the Afar Volcanic Province within the East African Rift System: *Geological Society, London, Special Publication*, **259**: 121–130.

Dereje Ayalew (2011).The relations between felsic and mafic volcanic rocks in continental flood basalts of Ethiopia: implication for the thermal weakening of the crust. *Geological Society, London, Special Publications*, **357**: 253-264.doi:10.1144/SP357.13.

Eberz, G.W., Williams, F.M., Williams. M.A.J. and Clayton (1988). Plio-Pleistocene volcanism and sedimentary facies changes at Gadeb pre historic site, Ethiopia. *Geologische Rundschu,* 513-527.

Ebinger, C.J., Tesfaye Yemane, Gidey WoldeGabriel, Aronson, J.L. and Walter, R.C. (1993). Late Eocene Recent volcanism and faulting in the southern Main Ethiopian Rift. *Journal of the Geological Society of London*, **150**: 99–108.

Gasparon, M., Innocenti, F., Manetti, P., Peccerillo, A. and Tsegaye Abebe (1993). Genesis of the Pliocene to Recent bimodal mafic–felsic volcanism in the Debre–Zeyt area, central Ethiopia: volcanological and geochemical constraints. *Journal of African Earth Sciences*, **17**: 145–165.

George, R., Rogers, N. and Kelly, S. (1998). Earliest magmatism in Ethiopia: evidence for two mantle plumes in one flood basalt province. *Geology,* **26**: 923-926.

Gezahegn Yirgu, Maguire, C.J., Eds, P.K.H. (2006). The Afar volcanic provinces with in the East African Rift System. *Geological society special publications*, **259**: 73-75.

Gibson I. L. (1972). The chemistry and petrogenesis of a suite of pantellerite from the Ethiopian Rift. *J. Petrol.* **13**: 31–44.

Gidey WoldeGabriel, G., Aronson, J.L. and Walter, R.C. (1990). Geology, geochronology, and rift basin development in the central sector of the Main Ethiopia Rift. *Geological Society of America Bulletin,* **102**: 439–458.

Giday WoldeGabriel, Heiken, G., White, T D., Berhane Asfaw, Hart, W K. and Renne, P. R. (2000).Volcanism, tectonism, sedimentation, and the paleoanthropological record in the Ethiopian Rift System. *Geological Society of America*, Special Paper, **345**: 83-98.

Giday WoldeGabriel (2009). Renowned paleoanthropological areas in the Ethiopian Rift basins: Geological and paleo environmental contexts and chronology of hominid fossils and archaeology. **In:** *International symposium of Africa*, *Cradle of Humanity*;1-33. Recent Dis, Sedif, Algeria.

Giordano F., D'Antonio M. ,Civetta L., Tonarini S., Orsi G., Dereje Ayalew, Gezahegn Yirgu, Dell'Erba F., Di Vito M.A. and Isaia R. (2014). Genesis and evolution of mafic and felsic magmas at Quaternary volcanoes within the Main Ethiopian Rift: Insights from Gedemsa and Fanta 'Ale complexes. *Lithos,***188**: 130–144.

Hambisa Gobena, Mandefro Belayneh, Tesfaye Kebede, Samson Tesfaye and Amenti Abraham (1997). Geology of Dodola area. Geological survey of Ethiopia. Unpublished technical report, Addis Ababa, Ethiopia,150pp.

Harker A. (1909).The *Natural history of igneous rocks. Methuen, London.*

http://www. gsdkit.org

http://www.unipg.it/~maurip/SOFTWARE.htm.

Hayward, N.J. and Ebinger, C.J. (1996). Variations in the along-axis segmentation of the Afar Rift system. *Tectonics*, **15**: 244–257.

Hofmann, C., Courtillot, V., Féraud, G., Rochette, P., Gezahegn Yirgu, Endale Ketefo, and Pik, R. (1997). Timing of the Ethiopian flood basalt event and implications for plume birth and global change: *Nature*, **389**: 838–841.

Kazmin, V. and Seife Michael Berhe (1981). Geological map of the Ethiopian Rift (1:500,000). Ministry of mines, energy and water resource. *Ethiopian institutes of geological survey*.

Keranen K. and Klemperer S.L. (2008). Discontinuous and diachronous evolution of the Main Ethiopian Rift: Implications for development of continental rifts. *Earth and Planetary Science Letters*, **265**: 96–111.

Kieffer, B., Arndt, N., LaPierre, H., Bastien, F., Bosch, D., Pecher, A., Gezahegn Yirgu, Dereje Ayalew, Weis, D., Jerram, D., Keller F. and Meugniot, C. (2004). Flood and shield basalts from Ethiopia: magmas from the African Super swell. *Journal of Petrology*, **45**: 793–834.

Kurkura Kabeto, Sawnda, Y. and Roser B. (2009). Compositional differences between felsic volcanic rocks from the margin and center of the northern Main Ethiopian Rift. *MEJS*, **1**(1): 4-35.

Kurkura Kabeto (2010). Geological and geochemical variations in Mid-Tertiary Ethiopian Flood Basalt Province, Maychew, Tigray Region, Ethiopia. *MEJS, **2** (1): 4-25*.

Kurz,T., Gloaguen, R., Ebinger, C., Casey, M. and Bekele Abebe (2007). Deformation distribution and type in the Main Ethiopian Rift (MER): a remote sensing study. *Journal of African Earth Sciences*, **48**: 100–114.

Le Bas, M. J., Le Maitre, R. W., Streckeisen, A. and Zanettin, B. (1986). A chemical classification of volcanic rocks based on the total alkali–silica diagram. *Journal of Petrology*, **27**: 745–750.

Le Turdu, C., Tiercelin, J.J., Gibert, E., Travi, Y., Lezzar, K.E., Richert, J.P., Massault, M., Gasse, F., Bonnefille, R., Decobert, M., Gensous, B., Jeudy, V., Tamrat, E., Mohammed, M.U., Martens, K., Balemwal Atnafu, Tesfaye Chernet, Williamson, D. and Taieb, M. (1999). The Ziway– Shala lake basin system, Main Ethiopian Rift: influence of volcanism, tectonics and climatic forcing on basin formation and sedimentation. *Palaeogeography, Palaeoclimatology and Palaeoecology*, **150**: 135–177.

Macdonald, R. (1974). Nomenclature and petrochemistry of the peralkaline oversaturated extrusive rocks. *Bulletin Volcanologique*, **38**(2):498-516.

Mazzarini, F., Tsegaye Abebe, Innocenti, F., Manetti, P. and Pareschi, M.T. (1999). Geology of the DebreZeyt area (Ethiopia) (with a geological map at scale 1:100.000). *ActaVulcanologica*, **11:** 131–141.

Mengesha Tefera, Tadiwos Chernet and Workineh Haro (1996). Exploration of the geological map of Ethiopia (1:20,000,000). Ethiopian institutes of geological surveys. Unpublished technical report, Addis Ababa, Ethiopia, 83pp.

Merla, G., Abbate, E., Azzaroli, A., Bruni, P., Caunti, P., Fazzuoli, M., Sagri, M. and Tacconi, P. (1979). Geological map of Ethiopia and Somalia (1973):1:2,000,000 and comment with major land forms, 2-98.

Meseret Teklemariam (1996). Water rock interaction processes in the Aluto –Langano geothermal field Ethiopia. phD dissertation, University of Pisa, Italy, 245pp.

Meyer, W., Pilger, A., Rosler, A. and Stets, J. (1975). Tectonic evolution of the northern part of the Main Ethiopian Rift in Southern Ethiopia. **In**: Pilger, A., Rosler, A. _Eds.., Afar Depression of Ethiopia. *Schweizerbart, Stuttgart,* 352–362.

Mohr, P. A. (1968): The Cenozoic volcanic succession in Ethiopia. - Bull. *Volcanol*. **32**: 5-14. (1983): Ethiopian flood basalt province. *Nature,* **303**:577-584.

Mohr, P.A. (1983). Ethiopian Flood basalt provinces. *Nature*, **303**: 577-583.

Mohr, P., Zanettin, B., 1988. The Ethiopian food basalt province. **In**: Macdougall, J.D. (Ed.), Continental flood basalts. *Kluwer Academic Publishers*, 63–110.

Neispolo, E., Rutte, D., Deino, Renne, A.L. (2016). Intercalibration and age of the Alder Creek sanidine 40Ar/39Ar standard. *Quaternary geochronology*, 1-9.

Neuman, H., Mead, J. and Vitaliano, C.J. (1954). Trace-element variation during fractional crystallization as calculated from the distribution law. *Geochimica et Cosmochimica Acta*, **6**: 90-100.

O'Connor, J. T. (1965). A classification for quartz-rich igneous rocks based on feldspar ratios. **In**: *US Geological Survey Professional Paper* B525. USGS, 79–84.

Peccerillo, A. and Taylor, S. R. (1976). Geochemistry of Eocene calc-alkaline volcanic rocks from the Kastamonu area, Northern Turkey. *Contributions to Mineralogy and Petrology*, **58**: 63–81.

Peccerillo A., Gezahegn Yirgu and Dereje Ayalew (1995). Genesis of acidic volcanics along the Main Ethiopian Rift: a case history of the Gedemsa volcano. *SINET: Ethiopian J. Sci.* **18**: 23–50.

Peccerillo, A., Barberio, M.R., Gezahegn Yirgu, Dereje Ayalew, Barberi, M. and Wu, T.W. (2003). Relationships between mafic and acid peralkaline magmatism in continental rift settings: a petrological, geochemical and isotopic study of the Gedemsa volcano, central Ethiopian Rift. *Journal of Petrology*, **44**(11): 2003-2032. doi: 10.1093/petrology/egg068.

Peccerillo, A., Donati, C., Santo, A.P., Orlando, A., Gezahegn Yirgu and Dereje Ayalew (2007). Petrogenesis of silicic peralkaline rocks in the Ethiopian rift: geochemical evidence and volcanological implications. *Journal of African Earth Sciences*, **48**: 161–173.

Pik, R., Deniel, C., Coulon, C., Gezahegn Yirgu, Hofmann, C. and Dereje Ayalew (1998). The Northwest Ethiopian plateau flood basalts: classification and spatial distribution of magma types. *Journal of Volcanology and Geothermal Research*, **81**: 91–111.

Pik, R., Deniel, C., Coulon, C., Gezahegn Yirgu and Marty B. (1999). Isotopic and trace element signatures of Ethiopian flood basalts: Evidence for plume–lithosphere interactions. Geochimica et Cosmochimica Acta, **63**(15): 2263–2279.

Pik, R., Marty, B. and Hilton, D.R. (2006). How many mantle plumes in Africa? The Geochemical point of view. *Chemical Geology*, **226**:100-114.

Renne, P.R., Balco, G., Ludwing, K.R., Mundil, R.and Min, K. (2011). Response to the comment by W.H Schwarz et al. (2010) on joint determination of 40Ar- decay constants and 40Ar*/40 K for the Fish Canyon sanidine standard and improved accuracy for 40Ar/39Ar geocrronology by PR Rennene et al(2010). *Geochim.Cosmochim. Acta*, **75**: 5097-5100.

Rogers, N., Macdonald, R., Fitton, J.G., George, R., Smith, M. and Barreiro, B. (2000). Two mantle plumes beneath the East African Rift System: Sr, Nd and Pb isotope evidence from Kenya Rift basalts. *Earth and Planeta~ Science Letters*, **176**: 387-400.

Rollinson H. (1993). *Using geochemical data: evaluation, presentation, interpretation*. Pearson, prentice hall, 380pp.

Ronga, F., Lustrino, M., Marzoli A. and Melluso, L. (2010). Petrogenesis of a basalt-comendite-pantellerite rock suite: the Boseti Volcanic Complex (Main Ethiopian Rift). *Miner Petrol*, **98**: 227–243. doi 10.1007/s00710-009-0064-3.

Rooney, T., Furman, T., Bastow, I., Dereje Ayalew and Gezahegn Yirgu (2007). Lithospheric modification during crustal extension in the Main Ethiopian Rift. *Journal of Geophysical Research*, **112**: 1-21. B10201. doi:10.1029/2006JB004916.

Rooney, O.T., Hart, K.W., Hall, M.C., Dereje Ayalew, Ghiorso, S.,M., Hidalgo, P. and Gezahegn Yirgu (2012). Peralkaline magma evolution and tephra record in the Ethiopian Rift. *Contrib Mineral Petrol*, **164**: 407-426. DOI 10.1007/s00410-012-0744-6.

Seife Micahel Berhe, Berhe Desta, Nicoletti, M. and Teferra Mengesha (1987). Geology, geochronology and geodynamic implications of the Cenozoic magmatic province in W and SE Ethiopia. *Journal of the Geological Society, London*, **144**: 213- 226.

Shaw, D.M., Gramer, J.J., Higgins, M.D. and Truscott, M.G. (1986). Composition of the Canadian Precambrian shield and the continental crust of the earth. **In**: The Nature of the lower continental crust, Dawson, Vol.J.B., Hall, C.D.A.J., and Wedepohl, K.H. ed. *Oxford, Blackwell Scientific publ*, 275-282

Stromer, J.C., Nicholls, J. (1978). Program for the interactive testing of the magmatic deferentiation models. *Computers and geosciences*, **4**:143-159.

Tadiwos Chernet (1995). Petrological, geochemical and geochronological investigation of volcanism in the Northern Main Ethiopian Rift-Southern Afar transition region. Unpublished PhD. Thesis, Miami University, Ohio, USA.

Tadiwos Chernet, Hart, W.K., Aronson, J.L. and Walter, R.C. (1998). New age constraints on the timing of volcanism and tectonism in the northern Main Ethiopian Rift-southern Afar transition zone (Ethiopia). *Journal of Volcanology and Geothermal Research,* **80**: 267–280.

Tadiows Chernet and Hart W.K. (1999). Petrology and Geochemistry of volcanism in the northern Main Ethiopian Rift- southern Afar transition region. *Actavolcanologica,* **11**(1): 21-41.

Thrall, R. (1973). Gedemsa caldera. *Center for Astrophysics preprint series*, (280): 1-17.

Tesfaye Yemane. (1997). Stratigraphy and Sedimentology of the Hadar Formation. Ph.D. dissertation, Iowa State University, USA.

Trua, T., Deniel, C. and Mazzuoli, R. (1999). Crustal control in the genesis of Plio-Quaternary bimodal magmatism of the Main Ethiopian Rift (MER): Geochemical and isotopic (Sr, Nd and Pb) evidence. *Chemical Geology*, **155**: 201–231.

Tsegaye Abebe, Manetti, P., Bonini, M., Corti, G., Innocenti, F., Mazzarini, F. and Pecskay, Z. (2005). Geological map (scale 1:200000) of the northern Main Ethiopian Rift and its implication for the volcano-tectonic evolution of the rift. *Geological Society of America*, Boulder Colorado, USA, Maps and Charts series, MCH094.

Tsegaye Abebe, Balestrieri, M. and Bigazzi, G. (2010). The Central Main Ethiopian Rift is younger than 8 Ma: confirmation through apatite fission-track thermochronology. *Terra Nova, **22**:* 470–476. doi: 10.1111/j.1365-3121.2010.00968.x.

Walter R. C., Hart W. K. and Westgate J. A. (1987). Petrogenesis of a basalt-rhyolite tephra from the west-central Afar, Ethiopia. *Contrib. Mineral. Petr.* **95**: 462–480.

Wedepohl, K. H. (1995). The composition of the continental crust. *Geochim, cosmochim. Acta,* **59**: 1217-1232.

Williams, M. A. J., Williams, E M., Gasse, E, Curtis, G.H. and Adamson, D. A. (1979): Plio-Pleistocene environments at Gadeb prehistoric site, Ethiopia. *Nature*, ***282***: 29-33.

Wolfenden, E., Ebinger, C., Gezahegn Yirgu, Deino, A. and Dereje Ayalew (2004). Evolution of the northern Main Ethiopian Rift: birth of a triple junction. *Earth and Planetary Science Letters*, **224**: 213–228.

Wood, B.J., Fraser, D.G.(1976). Elementary thermodynamics for geologists. *Oxford University press, Oxford.*

Wood, D.A, Tarney J.Varct J. Saunders, A.D, Bougault, H., Joron J.L., Treuil, M. and Cann J.R. (1979). Geochemistry of basalts drilled in the North Atantic by IPOD Leg **49**: implications for mantle heterogeneity. *Earth planet. SCi. let. **42**: 77-97.*

Workineh Haro, Daba Bulto, Mekonen Bekele, Desalegn Debelo, Muluken Kebede and Mohamed Edris (2014). Geology, geochemistry, and gravity survey of Asela area. Geological survey of Ethiopia, basic geo science mapping directorate. Un published technical report, Memoir, **38**: 87pp.

www.goldensoftware.com/guidespurch/st4ugpd.shtml

Wynn, J.G., Roman, D.C., Zerasenay Alemseged, , Reed, D.N., Geraads, D. and Munro, S. (2008).Stratigraphy, depositional environments, and basin structure of the Hadar and Busidima Formations at Dikika, Ethiopia. **In**: Quade, J., Wynn, J.G. (Eds.), the Geology of Early Humans in the Horn of Africa. *Geological Society of America*, Boulder, 87-118.

Zanettin, B., Justin-Visentin, E., Nicoletti, M. and Petrucciani, C. (1978). Evolution of the Chencha escarpment and the Ganjiuli graben (Lake Abaya) in the southern Ethiopian rift. *Neues Jahrbuch fur Geologie und Palaontologie. Monatshefte*, **8:** 473–490.

Appendix

Appendix I

Location Data

Sampling and Stratigraphic Log Section locations

Locality name	Easting	Northing	Elevation (m)	Accuracy(m)
MW11	0528783	0782093	2325	1
MW12	0528667	0782148	2326	0.8
MW13	0528655	0782172	2327	0.8
MW2	0528885	0782535	2326	2.9
MW5-E	0529904	0783250	2322	0.8
MW5-N	0529673	0783275	2323	0.8
MW5-N1	0529640	0783267	2329	1.5
MW5N3	0529569	0783561	2329	1
MW7	0529759	0783741	2325	1.1
MW7-S	0529695	0783700	2326	0.8
MW8	0528722	0782419	2323	0.8
MW9	0528644	0782300	2325	0.8
MW9-S	0528624	0782220	2328	0.9
MWD1	0528232	0780845	2324	0.9
MWD2A	0527615	0780707	2349	1
MWD2B	0527394	0780607	2380	1.5
MWNS1	0524714	0783411	2330	2.8
MWNS2	0524389	0783080	2330	0.8
MW1	0528972	0782975	2341	3
MW3	0528979	0782900	2336	4

- Elevation is above the mean sea level.

Appendix II

Petrographic Data

Sample and minerals	**Field of view and mineral proportion in weight percentage**									
MW7-91										
	1	2	3	4	5	6	7	8	Total	Average
Quartz	10	10	5	10	3	15	5	10	68	8.5
Orthoclase	0	20	25	15	25	0	10	0	95	11.8
Ground mass	75	50	60	60	50	60	75	60	490	61.25
Fiames	10	10	4	10	10	10	10	10	74	9.25
Rock fragment	2	2	1	3	1	10	1	10	30	3.75
Zeolite	0	0	0	0	8	0	0	0	8	1
Plagioclase	1	3	0	3	3	0	4	3	17	2.83
Opaque	1	0	1	2	2	5	5	10	26	3.25
Sanidine	0		0	0	0	0	0	1	1	0.125
Total	98	97	96	100	99	100	106	101	797	99.625
MW7-92										
Quartz	10	10	10	15	10	5	5	5	70	8.75
Orthoclase	3	3	1	3	2	0	2	1	15	1.875
Ground mass/glass	70	40	70	65	75	75	65	50	510	63.75
Fiames	3	0	1	1	1	1	1	1	9	1.125
Rock fragment	10	45	20	15	5	15	24	40	174	21.75
Plagioclase	5	0	0	5		4	3	1	18	3
Muscovite	0	0	0	0	0	0			0	0
Opaque	4	2	2	1	3	2	2	2	18	2.25
Clino pyroxene	0	0	0	1	2		1		4	0.666
Total	100	100	104	101	96	98	99	99	797	99.625
MWNS-2										
Quartz	10	15	20	15	15	15	20	25	135	16.875
Orthoclase	25	10	5				5		45	5.625
Ground mass	50	65	65	60	75	65	65	60	505	63.125
Fiames	0	0	3	0	0	0	0	0	5	0.625
Rock fragment	20	10	5	5	5	15	5	10	75	9.375
Plagioclase	1	0	0	0	0	3	0	0	4	0.66
Muscovite	0	0	2	0	0	0	0	0	2	0.25
Opaque	1	2	5	4	4	5	3	5	29	3.625
Sanidine	0	3	0	15	0	5	3	0	25	3.125
Total	106	105	105	99	99	105	101	100	796	99.5
MWNS-1										

Quartz	10	20	15	10	15	15	10	15	110	13.75
Orthoclase	0	5	5	10	10	15	10	20	75	9.375
Ground mass/glass	85	60	70	60	60	55	65	50	505	63.125
Fiames	0	10	5	10	3	5	5	3	41	5.125
Rock fragment	0	0	0	5	0	5	0	5	15	1.875
Muscovite				2		5			7	0.875
Opaque	4	5	5	3	10		3	3	33	4.125
Sanidine							5	3	8	1
Total	99	100	100	100	98	100	98	99	794	99.25
MW5-N7										
Quartz	35	5	10	15	10	15	20	15	125	15.625
Orthoclase	15	5			5			15	40	5
Ground mass/glass	40	75	75	75	65	70	55	55	510	63.75
Plagioclase	0	0	0	0	3	0	0		3	0.5
Rock fragment					15	10	20	15	60	7.5
Muscovite	10	10	10	5	3	2	4	1	45	5.625
Opaque	1	3	3	3	1	1	1	2	15	1.875
Total	101	98	98	98	99	98	100	103	795	99.375
MW9S-5										
Quartz	10	7	3	5	3	7	5	7	47	5.875
Orthoclase	2	5	2	3	2	5	5	5	29	3.625
Ground mass/glass	70	70	80	70	75	70	75	65	575	71.875
Fiames	1	1	1	1				2	6	0.75
Rock fragment	10	15	10	15	15	15	10	15	105	13.125
Muscovite		0		5	3				8	1
Opaque	2	2	3	1	1	1	3	5	18	2.25
Sanidine	5								5	0.625
Total	100	100	99	100	99	98	98	99	793	99.125
MW7-9										
Quartz	10	5	5	5	5	5	5	5	45	5.625
Orthoclase	5	10	5	10	3	15	13	5	66	8.25
Ground mass/glass	65	80	80	80	80	75	75	85	620	77.5
Fiames	1	0						2	3	0.375
Rock fragment		3	4		5	3	0	2	17	2.125
Clino pyroxene		5	2	0	0	0	2		9	1.5
Opaque	3	1	5	5	3	2	2	1	22	2.75
Sanidine	15								15	1.875

Total	99	99	99	100	99	100	95	100	791	98.875
MW2-G19										
Quartz	5	10	5	3	5	5	5	5	43	5.375
Microcline	0	5	0	5	0	0	10	20	40	5
Ground mass/glass	80	65	70	75	70	80	80	70	590	73.75
Fiames	1	0						0	1	0.125
Rock fragment	10	15	20	15	20	15	0	3	98	12.25
Opaque	2	5	3	2	3	1	2	1	19	2.375
Total	98	100	98	100	98	101	97	99	791	98.875
MW9-S10										
Quartz	3	3	3	5	5	5	5	3	32	4
Orthoclase	20	10	3	20	20	5	15	5	98	12.25
Ground mass/glass	75	85	75	65	60	55	65	72	552	69
Rock fragment	0	0	20	10	15	35	15	20	115	14.375
Opaque	1	0	1	1	1	1	1	1	7	0.875
Total	99	98	102	101	101	101	101	101	804	100.5

Appendix III

Geochemical Data

A. CIPW Norm Calculation Results

Sample	Normative minerals (wt%)			
	Quartz	Plagioclase	Orthoclase	Hematite
MW2-G16	43.83	15.85	16.13	8.06
MW2-G19	37.39	26.38	30.32	4.11
MW2-G10	32.83	33.39	24.97	5.5
MW3-G3	44.69	18.97	27.87	6
MW3-G7	46.5	16.25	27.7	7.78
MW5-5	41.98	24.48	18.55	6.3
MW5-7B	34.91	29.72	21.4	5.97
MW7-4	33.27	21.26	37.33	5.47
MW9-S7	27.24	31.83	34.21	4
MW9-S9	39.07	20.08	32.81	6.42
MWD2-D	30.5	27.16	27.62	1.87
MWNS-1	30.69	24.6	29.74	1.98
MWNS-5	34.3	26.81	32.18	5.09

B. Normalized Values of Selected Elements

	Er	Tm	Yb	Lu	Eu/Eu*	La/Yb
MWG-16	33.05	33.33	32.78	34.16	0.47	7.63
MW2-G19	56.16	51.54	52.15	52.48	0.28	6.18
MW2G10	43.67	40.12	38.95	39.75	0.54	10.81
MW3-G3	56.9	56.79	52.15	50.62	0.49	7.45
MW3-G7	94.29	93.21	88.04	84.78	0.5	6.91
MW5-5	39.62	39.51	37.42	36.96	0.55	7.79
MW5-7B	38.57	38.27	36.39	37.27	0.56	9.03
MW7-4	59.05	61.42	55.5	56.83	0.29	7.82
MW9-S7	57.62	59.26	55.74	55.9	0.55	7.06
MW9-S9	57.86	57.1	55.5	55.28	0.47	7.93
MWD2-D	65.48	60.8	59.81	57.76	0.45	7.2
MWNS-1	66.9	67.28	59.81	61.18	0.47	7.17
MWNS-5	54..29	54.32	53.35	53.42	0.41	7.98

C. Agpaitic values for Peralkaline/subalkaline classification as a function of silica

Sample code	Al_2O_3	Na_2O	K_2O	Na_2O+K_2O	Al_2O_3/Na_2O+K_2O
MW2-G16	0.14025	0.01597	0.02399	0.03996	3.50976
MW2-G7	0.11034	0.04501	0.05223	0.09724	1.13472
MW2-G10	0.12064	0.04776	0.04151	0.08927	1.35141
MW3-G3	0.09759	0.03066	0.04735	0.07801	1.25099
MW3-G7	0.08013	0.0221	0.04554	0.06764	1.18465
MW5-5	0.12701	0.03356	0.02994	0.0635	2.00016
MW5-7B	0.13584	0.04534	0.03514	0.08048	1.68787
MW7-4	0.11034	0.03195	0.06285	0.0948	1.16392
MW9-S7	0.09337	0.03356	0.0552	0.08876	1.05194
MW9-S9	0.12946	0.04534	0.05722	0.10256	1.26229
MWD2-D	0.10102	0.07535	0.04915	0.1245	0.81141
MWNS-1	0.09572	0.06793	0.05085	0.11878	0.80586
MWNS-5	0.10249	0.04501	0.05308	0.09809	1.04486

D. Peralkaline (Comendite –pantlleretic) classification data

Sample code	Fe_2O3	Al_2O_3	L1	L2
MW2-G16	6.81	16.92	1.2	0
MW2-G10	3.94	13.01	10	10
MW5-5	5.2	14.18	6	17.2
MW5-7	5.71	14.89	18	10
MW2-G19	7.25	11.74		
MW3-G3	5.78	10.34		
MW3-G7B	5.55	10.23		
MW7-4	5.92	10.45		
MW9-S7	6.02	8.86		
MWD2-D	3.79	11.94		
MWNS-1	5.66	10.15		
MWNS-5	5.58	11.32		
MW9-S9	4.7	13.94		

E. Mass balance calculation results

RECAL.	**ANALYSES**	**(WT.%)**	**TO 100%**		
Oxide	Initial	Final	Ol	Pl	Fe-To
SiO_2	53.9451	78.3631	48	53.13	0.46
TiO_2	2.23158	0.22856	0	0	80.39
Al_2O_3	18.5472	12.2442	0	30.09	9.1
MnO	0.19356	0.15237	0.35	0	2.11
MgO	10.304	0.20679	51.28	0	7.48
CaO	10.6114	0.39182	0.37	12.35	0.46
Na_2O	2.99442	3.03657	0	4.23	0
K2O	0.81977	5.35481	0	0.2	0
P_2O_5	0.35295	2.18E-02	0	0	0
TOT	100	100	100	100	100

RESULTS

OXIDE	BULK COMP. OR ADDED OR SUBTR.MATL.	OBS.DIFF. BETWEEN MAGMAS	CALC.DIFF. BETWEEN MAGMAS	OBS.-CALC. RESIDUALS
SiO2	50.063	24.418	24.266	0.152
TiO2	2.781	-2.003	-2.188	0.185
Al2O3	22.069	-6.303	-8.424	2.121
MnO	0.159	-0.041	-0.006	-0.036
MgO	12.693	-10.097	-10.706	0.609
CaO	9.036	-10.22	-7.412	-2.808
Na2O	3.055	0.042	-0.016	0.058
K2O	0.145	4.535	4.467	0.068
P2O5	0	-0.331	0.019	-0.35
			TOTAL	0

SUM OF THE SQUARES OF THE RESIDUALS 12.9413

PHASE NAME	AMOUNT AS WT.% OF INIT. MAGMA	AMOUNT AS WT.% OF ALL PHASES	AMOUNT AS WT.% OF ADDED PHS.	AMOUNT AS WT.% OF SUBTRD.PHS.
Ol	-20.79	24.25	0	24.25
PL	-61.99	72.3	0	72.3
FE-TI	-2.97	3.46	0	3.46
TOTAL REL.	TO INITIAL	MAGMA	0	**85.74**